Welding Research

SPONSORED BY THE WELDING RESEARCH COUNCIL
OF THE ENGINEERING FOUNDATION

W. SPRARAGEN, DIRECTOR

SUPPLEMENT TO THE WELDING JOURNAL, MARCH, 1956

EFFECT OF INDIVIDUAL COATING INGREDIENTS ON SURFACE TENSION OF IRON ELECTRODES

Coating materials found to reduce the surface tension considerably below the value for bare electrode

BY THOMAS H. HAZLETT AND EARL R. PARKER

Introduction

It is well known that arc characteristics are markedly affected by the composition of the electrode coating. However, the effects of the individual ingredients, while generally understood, are not entirely clear. In an attempt to isolate and study some of the fundamental factors which influence arc welding characteristics and the properties of the resulting bead, a fundamental program on arc welding has been undertaken at the University of California. One phase of this program has been concerned with a study of the effects of some of the individual electrode coating ingredients upon the surface tension of low-carbon steel. It is believed that surface tension affects the metal droplet size and thus is one factor which has a pronounced influence upon arc characteristics.

High-speed motion pictures of welding arcs have shown that the metal is transferred from the electrode to the work primarily as a spray of molten metal droplets. Observations that the droplet size varies with different electrode types and atmospheres is the basis for the hypothesis that the surface tension is one of the important factors in determining the arc characteristics.

It was decided that the surface tension should be measured under conditions that approximated welding conditions as closely as possible. Two major differences existed, however, namely that the metal was at a much lower temperature (just above the melting point) in these studies, and that the disturbing force of the arc was not present; the droplet forming merely by the force of gravity. Even with these differences, the results obtained are considered significant.

Experimental Procedure

The surface tension was measured by the drop geometry method as described and utilized by Andreas, Hauser, and Tucker[1] and modified by Davis and Bartell.[2] The absolute limits of accuracy of this method are not clearly defined for the case of molten metals but they appear to be well within a range of $\pm 5\%$ if all conditions approach ideality.

Most of the experimental results reported were obtained by melting the end of a $^{3}/_{32}$-in. diam low-carbon steel wire in the apparatus shown schematically in Fig. 1. This consists of a $2^{1}/_{2}$-in. diam pyrex tube equipped with a gas inlet and outlet at the top and bottom to permit the use of controlled atmospheres, and a single turn RF transformer located in the center. The wire under test was heated by means of a commercial electronic RF oscillator with the primary coil located around the outside of the glass tube. Heating was concentrated at the end of the wire by the geometry of the single turn transformer which, in cross section, narrowed down to approximately $^{1}/_{8}$ in. at the center. A ceramic sleeve was inserted in the central hole of the transformer to

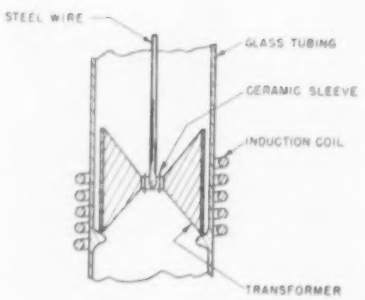

Fig. 1 Schematic cross section of drop formation equipment

Thomas H. Hazlett is Research Engineer, and **Earl R. Parker** is Professor of Metallurgy, Minerals Research Laboratory, University of California, Berkeley, Calif.

Presented at AWS 1955 National Fall Meeting held in Philadelphia, Pennsylvania, Oct. 17-21.

prevent the wire from touching the transformer core. The wire was held vertically and centered in the apparatus so that a drop could form freely at the end.

The wire was prepared by giving it a quick dip in nitric acid and a thorough rinsing in distilled water. It was used immediately after drying so that there was virtually no oxidation. In some cases the surfaces were protected immediately after drying with a thin film of kerosene but it was found that this did not alter the surface tension values obtained.

In addition to the bare wire tests, experiments were made with wires coated with SiO_2, TiO_2, $NaCO_3$, MgO, Fe_2O_3, and Al_2O_3. The powders were dusted on to the wires after cleaning and oiling. This produced a very fine layer of the ingredient under test. Considerable skill was required to form the drop and yet have it cooled at the proper moment without running off the end of the wire. Only uniform symmetrical drops such as that shown in Fig. 2 were used in obtaining the reported data.

Method of Analysis

As mentioned previously, the data were analyzed by the method of Davis and Bartell. Their equation for the surface tension is

$$S = \rho_c^2/_3\rho^1/_3 g\, De^2(1/H)$$

S = surface tension
ρ_c = cold density difference between metal and atmosphere
ρ = hot density difference between metal and atmosphere
g = density (dynes)
De = diameter of drop at equator
Ds = diameter of drop at selected plane at distance De from end of drop
$1/H$ = function of ratio Ds/De

Fig. 2 MgO coated rod in helium atmosphere

It may be noted that the factors (ρ_c), (ρ) and (g) may be treated as constant for any given system. The values of (De) and (Ds) were obtained by photographing the drops, tracing the silhouette outline, finding the axis of symmetry and measuring the values as indicated in the sketch of Fig. 3. In all cases, a scale was placed in the photograph so that the magnification is precisely known. Values of $(1/H)$ are those given by Andreas, Hauser and Tucker.

Experimental Results

Values of surface tension as determined in this investigation are given in Table 1. In general, these are averages obtained from four to six individual determinations which differed by not more than ±50 dynes per centimeter. Unfortunately, data from other laboratories were not available for comparison except the one value for electrolytic iron in an atomic hydrogen arc. This was determined by Davis and Bartell who reported 840 dynes per centimeter. This compares favorably with the values reported herein for bare rod in atmospheres of nitrogen, argon and helium. Average surface tension values in these atmospheres were 829, 829 and 836 dyne per centimeter, respectively.

Analysis of Results

A study of Table 1 reveals that the surrounding atmosphere may produce differences in surface tension of 50% as, for example, the rods with TiO_2 coating in nitrogen and in helium. It may also be seen that the atmospheres do not always affect surface tension. For example, measurements made on Fe_2O_3 coated rods were not materially different in the three atmospheres used. It is also interesting to observe that even argon and helium produced quite different results, although both are considered inert gases.

Table 1—Average Surface Tension Values (Dynes per Centimeter)

	N_2	A	He	Air
SiO_2	632	746	539	..
TiO_2	818	603	524	..
$NaCO_3$	624	496	579	..
MgO	533	776	526	..
Fe_2O_3	595	595	517	..
Al_2O_3	578	697	438	..
Bare	829	829	836	724

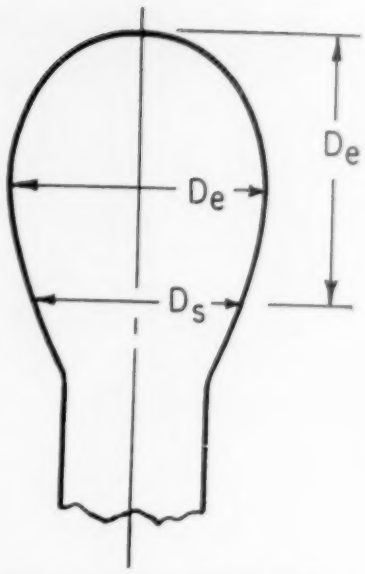

Fig. 3 Geometry of drop. D_e = diameter at equator; D_s = diameter at selected plane

All of the coating materials reduced the surface tension considerably below the value for bare rod. It may be seen that although the surface tension of bare rod in the three gases is essentially the same, the value obtained in air was significantly lower. Probably the most surprising observation was the large influence of Al_2O_3 upon the surface tension. No explanation for this result is available at the present time.

The results reported herein must be considered as a progress report only. Further studies are in progress with other materials and with combinations of materials. Additional results will be forthcoming in the near future.

Acknowledgment

The authors wish to thank the Office of Ordnance Research whose support has made this research program possible. They also want to acknowledge the contributions of Ruel Williams and Pierre Pellissier in carrying out much of the experimental program.

References

1. Andreas, J. M., Hauser, E. H., and Tucker, W. B. "Boundary Tension in Pendant Drops," *J. Phys. Chem.*, **42**, 1001 (1938).
2. Davis, J. K., and Bartell, F. E., "Determination of Surface Tension of Molten Materials," *Analyt. Chem.*, **20**, 1182 (1948).

THE PERFORMANCE OF HIGH-STRENGTH PRESSURE-VESSEL STEELS

Six representative high-strength steels are given extensive mechanical tests to aid in determining their applicability to pressure vessels. They are found to compare favorably with the conventional, plain carbon A201 steel

BY J. H. GROSS AND R. D. STOUT

FOREWORD. The report herein contained was sponsored by the Pressure Vessel Research Committee, F. L. Plummer, Chairman. The initial program was conceived by the Materials Division, PVRC, T. N. Armstrong, Chairman, and was guided by the Subcommittee on Research on High-Strength Steels, Dr. F. Eberle, Chairman.

Introduction

Modern day applications of pressure vessels have resulted in marked increases in operating pressures. The required increase in section thickness of conventional plain carbon steel vessels presents many additional problems in the manufacture, forming, welding, heat treatment and transportation of the steel. Should the trend continue and with the same steels, it is quite possible that thicknesses in excess of 12 in. would be employed. The Pressure Vessel Research Committee recognized this problem and initiated a twofold attack. First, it was to examine and improve methods of design with a view toward an increase in allowable design stresses, and second, it was to investigate the use of steels with strengths considerably in excess of those currently employed in pressure vessel construction.

Although several steels with tensile strengths greater than the 60,000 psi typical of A201 have been approved for pressure vessel construction, very little service information is available and with present code restrictions is not likely to become available in the near future. Therefore a program of laboratory testing was undertaken to compare the high-strength steels to A201 steel, whose service performance is well known. It was hoped to substitute these new laboratory data for long time service experience in order to place the higher strength steels into service at an early date.

The use of higher strength steels not only permits construction of vessels of practical thicknesses under increased operating pressures, but also may permit substantial reduction in thickness in conventional vessels. However the increased strength of these new steels is much greater with respect to yield strength than tensile strength. Quenched and tempered steels with a tensile strength double that of A201 usually have a yield strength (0.2% offset) as much as three times the A201 yield strength. Thus if design pressures could be based on yield rather than tensile strength it would greatly increase the attractiveness of higher strength steels.

The Experimental Program

The Materials Division of the Pressure Vessel Research Committee selected six steels—two each of 50, 70 and 90 thousand psi specified yield strength—for investigation by laboratory tests to determine their suitability for pressure vessel applications. Similar tests were performed on A201 for comparative purposes. Approximately 60 sq ft of each steel was obtained as a single plate in 1-in. thickness. The plate was subdivided into 18 in. squares from which the test specimens were taken on a deliberately random basis.

The laboratory tests were designed to provide information as to the probable service performance of the steels in pressure vessels. Two general areas of interest were investigated. First, the general mechanical and related properties of the base plate were compared to A201, and second, the effect of various fabrication operations upon these steels.

In a separate investigation,[1] Bunk developed qualified welding procedures in accordance with Section IX, ASME Boiler and Pressure Vessel Code. The recommended procedures were employed throughout this investigation.

The possibility of failure due to fatigue at increased design stresses was also examined. Results of these investigations[2-3] have been previously reported in detail.

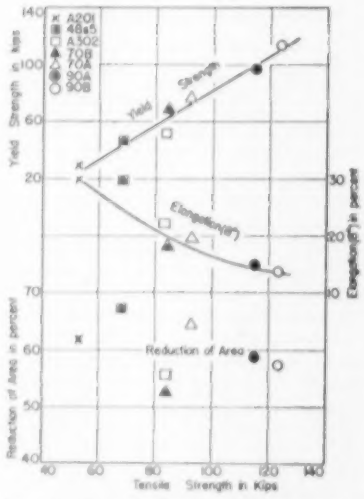

Fig. 1 Full section tensile properties of the high-strength steels

Experimental Results and Discussion

All steels were received and tested in the condition recommended for service use. The condition, the chemical analysis, and full section tension properties of each steel are listed in Table 1.

Base Metal Properties

In order to determine the basic strength and ductility characteristics of the new steels, full section strip tension and standard 0.505-in. tests in duplicate were performed. The behavior of the

J. H. Gross is Assistant Professor and R. D. Stout is Professor of Metallurgy, Lehigh University, Bethlehem, Pa.

Presented at AWS 1955 National Fall Meeting held in Philadelphia, Pa., Oct. 17-21.

Table 1

(A) Chemical analysis of steels

Steel	% C	Mn	P	S	Si	Ni	Cr	Mo	V	Ti	Cu	B
A201	0.11	0.44	0.014	0.030	0.16	..	..	..	..	..	..	..
48s5HT	0.15	1.09	0.033	0.028	0.18	0.06	0.06	0.02	0.09	0.009	0.11	..
A302	0.20	1.32	0.022	0.030	0.25	..	..	0.42	..	..	..	..
70B	0.16	0.63	0.012	0.037	0.05	1.47	0.04	0.23	..	..	1.02	..
70A	0.12	0.48	0.013	0.032	0.21	2.16	0.06	0.39	0.11	..	0.70	..
90A	0.30	1.49	0.013	0.020	0.22	0.06	..	0.12	..	..	..	Yes
90B	0.15	0.93	0.015	0.022	0.27	0.89	0.48	0.44	0.06	..	..	0.0031

(B) As received—Condition and Strip Tensile Properties*

Steel	Condition	Yield strength (0.2% Offset), psi	Tensile strength, psi	Elongation (8 in.), %	Reduction of area, %
A201	Hot rolled	29,700	54,800	33.8	65.8
48s5HT	Normalized	47,300	68,300	29.8	67.2
A302	Normalized	52,000	83,300	22.1	55.8
70B	As rolled and tempered 4 hr at 1100° F	68,700	84,600	18.1	52.9
70A	Normalized and tempered 1 hr at 1250° F	76,700	92,800	19.5	64.6
90A	Quenched and tempered	97,500	115,000	14.8	58.8
90B	Quenched and tempered	114,000	123,600	13.9	57.5

* Tensile properties determined parallel to rolling.

full section tests at room temperature is shown in Fig. 1. The 90A and 90B specimens had approximately twice the ultimate tensile strength, three times the yield strength and half the elongation compared to A201. The yield strength increased linearly with tensile strength, while elongation decreased with increasing strength. The strength increase is certainly desirable since it permits substantially increased design stresses particularly on the basis of yield strength. This presupposes no dangerous sacrifice in other significant properties. The importance of the decrease in elongation is not apparent since no minimum values for successful fabrication and service performance have been established. Nor has elongation been established as a more useful criterion of ductility than reduction of area, which shows relatively little change with variation in strength.

Tensile properties at elevated temperatures are also important since most codes permit service operation to 650° F without reduction of room temperature design values. The performance of the various steels up to 750° F is shown in Figs. 2 and 3. The tensile strength rises slightly in the range 450 to 650° F with a corresponding decrease in ductility. This "blue brittle" behavior is characteristic of most steels. Above 650° F all of the steels tested showed susceptibility to softening and loss of ultimate tensile strength. The yield strength, in general, decreased continuously with increasing temperature. At 750° F the decrease ranged from 14 to 40%, averaging 21%. With the exception of 48s5, all of the high-strength steels decreased less than the plain carbon A201.

Notch toughness is important in pressure vessel steels operated at atmos-

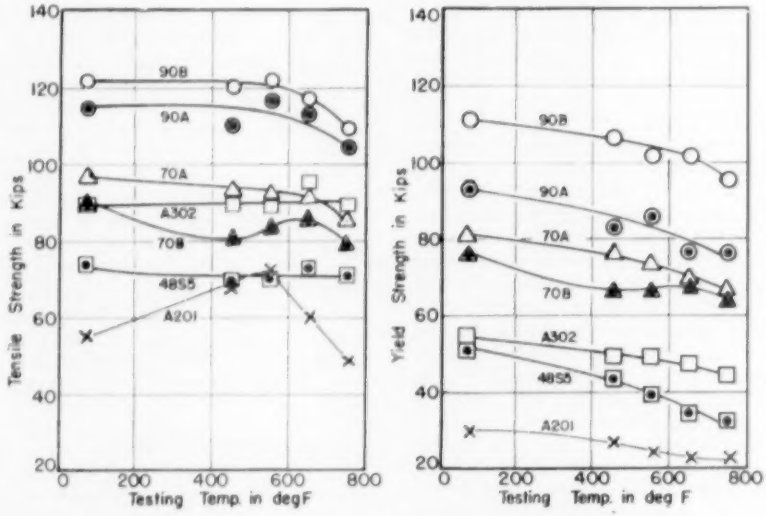

Fig. 2 Strength characteristics of the high-strength steels at elevated temperatures

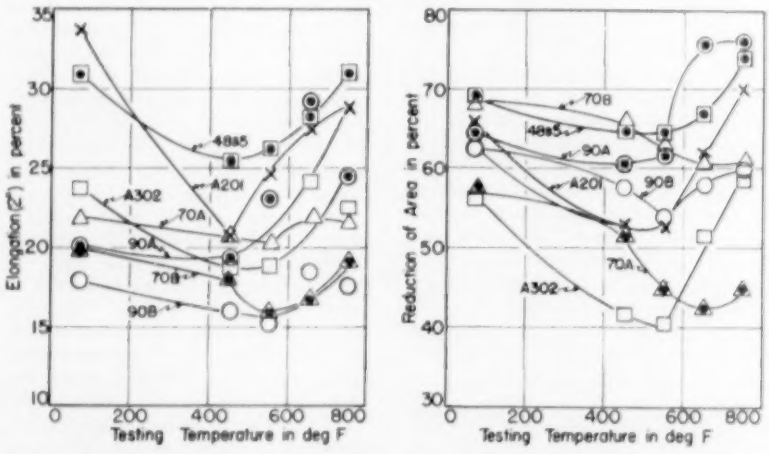

Fig. 3 Ductility characteristics of the high-strength steels at elevated temperatures

Table 2—Notch Toughness Properties of High-Strength Steels

(A) 15 ft-lb Charpy transition temperature in ° F

Steel	*Condition*	*V-notch*	*Keyhole*
A201	As-received	+30	..
	Strain aged*	+110	..
	Single stress relief—1 hr at 1150° F	+40	..
	Quadruple stress relief	+35	..
	24-hr stress relief	+50	..
4825HT	As-received	−55	−95
	Strain aged*	+20	−40
	Single stress relief—1 hr at 1150° F	−30	..
	Quadruple stress relief	−10	..
	24-hr stress relief	+10	..
A302	As-received	−15	−80
	Strain aged*	+65	0
	Single stress relief	−60	..
	Quadruple stress relief—1 hr at 1150° F	−40	..
	24-hr stress relief	−30	..
70B	As-received	+50	−40
	Strain aged*	+100	+60
	Single stress relief—1 hr at 1100° F	+50	..
	Quadruple Stress Relief	+20	..
	24-hr stress relief	+50	..
70A	As-received	−80	−120
	Strain aged*	+10	−50
	Single stress relief—1 hr at 1150° F	−40	..
	Quadruple stress relief	−40	..
	24-hr stress relief	−20	..
90A	As-received	−175	−215
	Strain aged*	−150	−180
	Single stress relief—1 hr at 1150° F	−160	..
	Quadruple stress relief	−125	..
90B	As-received	−195	−215
	Strain aged*	−160	−205
	Single stress relief—10 hr at 900° F	−190	..
	Quadruple stress relief	−195	..
	24-hr stress relief	−180	..

(B) Kinzel transition temperature at 1% lateral contraction in ° F

Steel	*Electrode*	*As-received*	*As-welded*	*Welded at 300° F preheat*	*Welded and postheated Single*	*Welded and postheated Quadruple*
A201	E7016	−120	−30	−30	−30	−20
48s5HT	E7016	−175	−10	−20	+30	−20
A302	E7016	−80	+20	+30	−95	−115
70B	E9015	−120	+95	+5	−50	−50
70A	E10015	−210	−50	−70	0	−5
90A	E12015	−180	−20†	−80	−65†	−55†
90B	E12015	−225	−80	−105	−90	−120

* 5% parallel tensile prestrain plus 1 hr at 550° F.

† Welded at 200° F preheat. Postheat cycles same as stress relief cycles in (A) above.

Table 3—Results of Lehigh Restraint Test

Steel	*Electrode*	*Restraint cracking level, in.*
A201	E7016*	>8
	E9015	>8
48s5HT	E7016*	>8
	E9015	3½
A302	E7016*	6½
	E9015	4½
70B	E9015*	5
70A	E10015*	3½
	E9015	5½
90A	E12015*	6
	E9015	3
90B	E12015*	>8
	E9015	4½

* Qualified electrode.

Table 4—Results of Longitudinal-Bead-Weld Cracking Test*

Steel	*Cracking, %*
A201	0
48s5HT	0
A302	58
70B	0
70A	2
90A	76
90B	39

* Average of five specimens.

pheric or subatmospheric temperatures. Table 2 summarizes all of the notch toughness tests. In Fig. 4 the Charpy V-notch toughness of the high-strength steels is compared to A201. The quenched and tempered steels in particular show exceptional notch toughness. This behavior is to be expected, since quenched and tempered microstructures generally exhibit excellent notch toughness.

During fabrication, high-quality pressure vessels normally undergo one or more stress-relieving treatments. It is noted from the notch-toughness data in Fig. 4 that the high-strength alloy steels responded more to thermal stress relieving than the A201 carbon steel. Stress relieving is commonly employed to restore notch toughness after welding. However, the notch toughness of the base plate may be seriously impaired by continued stress relieving as noted in the 48s5, 70A and 90A steels. With the exception of 70B, all of the steels including A201 lost notch toughness upon prolonged stress relieving. Only A302 improved with a single stress relief and this advantage was markedly reduced by subsequent treatments. 90B steel showed only a minor loss and still retained excellent notch toughness. 70B steel had relatively poor notch toughness initially and remained essentially unchanged. These effects have not been previously reported and no explanation is offered, except to say that an aging action is possibly responsible. However, further investigation of the origin and magnitude of the phenomenon appears desirable.

Fabrication Properties

Fabrication of pressure vessels normally by plastic deformation of the steel plate. Subsequent aging at slightly elevated temperatures for short times or at room temperature for longer times produces "strain aging." Figure 5 depicts the loss in notch toughness resulting from 5% plastic elongation followed by aging at 550° F for 1 hr. The quenched and tempered steels have only a minor susceptibility to strain aging compared to the lower strength steels. A201 steel has equal or greater susceptibility than the high-strength steels in general.

As previously cited, satisfactory welding of the high-strength steels, as measured by the standard weld qualification tests, can be accomplished by proper choice of welding techniques. Additional tests were performed to establish the relative susceptibility of the steels to weld metal cracking and underbead cracking. Results are reported in Tables 3 and 4. In the restraint tests the qualified electrode and a comparative E9015 electrode were employed to determine the maximum specimen width at which cracking would begin. A201, 48s5 and 90B showed no cracking at the maximum specimen width of 8 in. for the qualified electrode. Only A201 resisted cracking at maximum restraint with

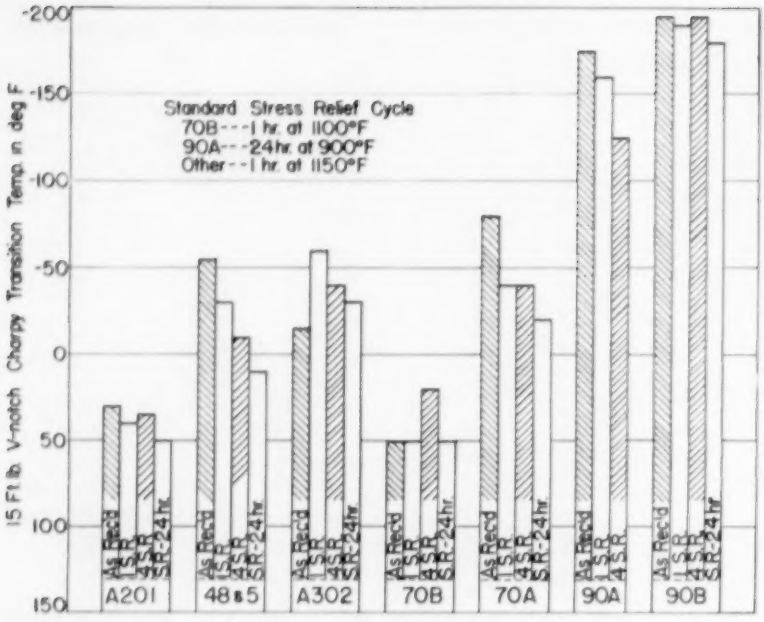

Fig. 4 The effect of stress relieving on the base metal notch toughness of the high-strength steels

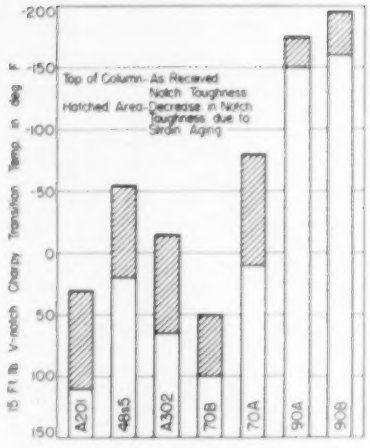

Fig. 5 The effect of strain aging on the notch toughness of the high-strength steels

the comparative E9015 electrode. Although cracking in the restraint test is a complex process, the increased sensitivity of the weld metal deposited in the high-strength steels is due principally to dilution of the weld metal by the alloy base plate.

Underbead cracking can occur in the heated zone when it is hardened by the rapid heating and cooling cycle during welding. A201 exhibited no underbead cracking since its low hardenability prevents the formation of brittle constituents in sufficient amount to cause cracking. The alloy content of all the high-strength steels and high-carbon content of A302 and 90A contributed substantially to reduced resistance to underbead cracking (See Table 4).

Adequate notch toughness in a weldment as well as in the base plate is essential to satisfactory pressure vessel operation. The marked decrease due to welding in the notch toughness of A201 as well as in the high-strength steels is depicted in Fig. 6. Preheat is

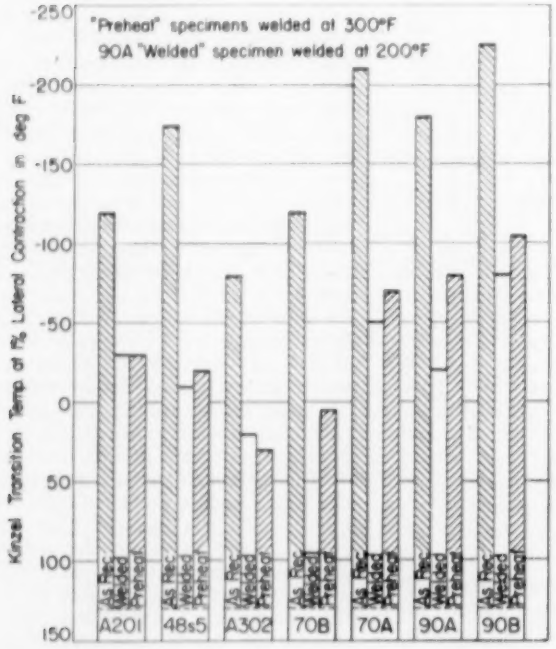

Fig. 6 The effect of welding on the notch toughness of the high-strength steels

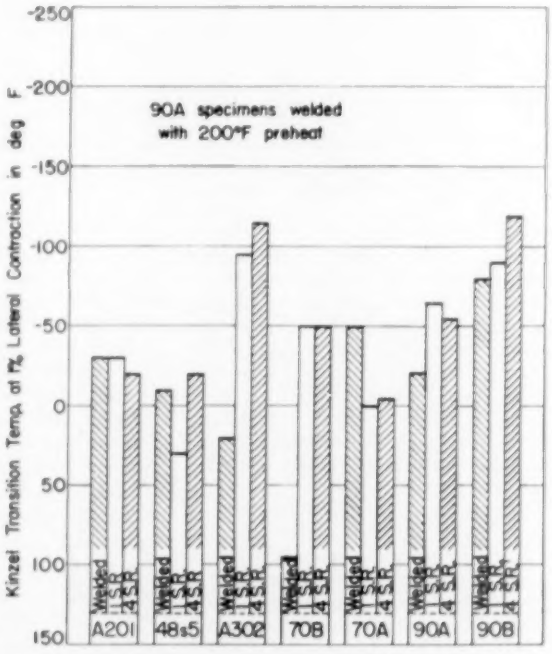

Fig. 7 The effect of postheating on the welded notch toughness of the high-strength steels

commonly used to reduce this effect particularly in the more hardenable steels. However, no substantial recovery in notch toughness was noted in any of the steels other than 70B. Since 70B showed by far the largest decrease in welded notch toughness, the benefit from preheating represented only partial restoration.

Welded notch toughness is usually improved substantially by postheating. Improvement was not uniformly obtained as evidenced in Fig. 7. The A201 was not hardened in the weld zone and therefore showed no response to postheating. Those high-strength steels which were not sensitive to postheating embrittlement in the base metal benefited substantially from postheating, namely A302 and 70B. The rather large sensitivity to embrittlement in 48s5 and 70A base plate resulted in a further loss in the welded notch toughness from stress relieving.

Conclusions

In the laboratory tests performed the high-strength steels compared favorably with the conventional, plain carbon, A201 steel. As expected, their strength both at room temperature and elevated temperatures is considerably greater than that of A201 with a correspondingly lower elongation. Whereas the strength increase is particularly desirable, no estimate of the undesirability of the decreased elongation can be made. The loss in yield strength at elevated temperatures may require some reduction in design stress for elevated temperature operation if design is based on the yield strength.

Satisfactory welding procedures for high-strength steels have been developed. Somewhat greater cracking tendency is generally noted and more careful control of the welding variables is necessary for the high-strength steels.

Notch toughness is generally equal to or better than that of A201 in all conditions tested. However the embrittlement occurring in the high-strength steels when stress relieved is not normally encountered in carbon steels and requires special precautions in fabrication.

Of the steels investigated, 90B shows the greatest promise. Compared to A201, it shows (1) twice the tensile strength, three times the yield strength and half the ductility; (2) equally satisfactory elevated temperature tensile behavior; (3) only slightly greater tendency to cracking in standard cracking tests; (4) substantially superior notch toughness in all conditions; and (5) minimum susceptibility to base metal embrittlement.

The results reported above were obtained solely from laboratory tests and therefore do not reproduce service conditions. They were not intended as a basis for design computations. However, some indication of the service performance of the six high-strength steels for the simulated conditions investigated can be inferred from a comparison with laboratory tests on A201 and a knowledge of the service behavior of A201.

Bibliography

1. Bunk, A. P., "Welding Procedure Qualification Tests for Six High Yield Strength Steels," THE WELDING JOURNAL, **34** (4), Research Suppl., 197-s to 206-s (1955).
2. Tor, S. S., Rozek, J. M., and Stout, R. D., "Repeated Load Tests on Welded and Prestrained Steels," *Ibid.*, **31** (5), Research Suppl., 238-s to 246-s (1952).
3. Gross, J. H., Tsang, S., and Stout, R. D., "Factors Affecting Resistance of Pressure Vessel Steels to Repeated Overloading," *Ibid.*, **32** (1), Research Suppl., 23-s to 30-s (1953).
4. Bowman, C. E., and Dolan, T. J., "Biaxial Fatigue Properties of Pressure Vessel Steels," *Ibid.*, **32** (11), Research Suppl., 529-s to 537-s (1953).
5. Gross, J. H., Guest, D. E., and Stout, R. D., "The Plastic Fatigue Strength of Pressure Vessel Steels," *Ibid.*, **33** (1), Research Suppl., 31-s to 39-s (1954).
6. Gross, J. H., and Stout, R. D., "Plastic Fatigue Properties of High-Strength Pressure-Vessel Steels," *Ibid.*, **34** (4), Research Suppl., 161-s to 166-s (1955).
7. Bowman, C. E., and Dolan, T. J., "Biaxial Fatigue Properties of Pressure Vessel Steels," *Ibid.*, **34** (1), Research Suppl., 51-s to 59-s (1955).
8. Bowman, C. E., and Dolan, T. J., "Resistance of Low-Alloy Steel Plates to Biaxial Fatigue," *Ibid.*, **35**, (2) Research Suppl., 102-s to 109-s (1956).

WELDING PROCEDURES

The Welding Research Council, through several of its Committees, has been conducting fundamental research on the factors affecting weldability for a decade or more. This basic information has been utilized by industry. Nevertheless, in many critical applications engineers and code-writing bodies are loathe to accept the results of this fundamental research work carried out for the most part on small specimens under carefully controlled laboratory conditions unless such results are checked with full scale prototype or actual structures.

One of the most controversial subjects that has plagued engineers and code-writing bodies is when to require "stress relieving." Laboratory tests have demonstrated the value of thermal stress-relieving treatments in improving metallurgical conditions surrounding welded joints. For the most part it has not been possible to separate the beneficial effects due to reduction of residual stresses from the metallurgical improvements. Ordinarily the engineer would not be too much concerned as to this differentiation providing he could know at all times that such treatment was beneficial and worthy of the expense involved. This has not been adequately demonstrated and perhaps cannot be with small specimens. Therefore, a newly organized research committee under the Welding Research Council with the general title of Welding Procedures Committee has undertaken this task.

It proposes to fabricate and test some 20 good-sized pressure vessels 1 in. thick, 36 in. diam, 5 ft long made of a commonly used pressure vessel steel A212 Grade B. Some of these vessels will be stress relieved, others will not. In both conditions some will have notches and others not. A preliminary program on small scale tests made of steel from the same heat it is hoped will aid the Committee in carefully selecting temperatures where conditions will be critical. However, it is proposed to use a range of temperatures varying from $-40°$ to room temperature. Later on, the effects of preheating and a number of other conditions will be studied. Industry will be invited to cooperate in this program and assist in its financing. The Committee will select a suitable fabricator and testing laboratory to carry out its work.

Some of the other conditions that will be investigated by the Committee within the next few years will include effects of porosity and the best procedures for welding a number of low-alloy steels for low, intermediate and high temperature service.

Anyone interested in these programs should communicate with W. Spraragen, Director, Welding Research Council, 29 W. 39th St., New York 18, N. Y.

V NOTCH CHARPY IMPACT TESTING OF WELD METAL AND HEAT-AFFECTED ZONE SIMULTANEOUSLY

Composite test provides, at least in part, a method for evaluating the relative notch-toughness characteristics of weld metal and heat-affected base metal in a natural environment

BY WILLIAM P. HATCH, JR., AND CARL E. HARTBOWER

SUMMARY. This paper introduces a method for evaluating *simultaneously* the notch toughness of weld metal and heat-affected base metal in a multiple bead-on-plate weld using the standard V notch Charpy impact specimen. The test specimen was machined from the bead-on-plate weldment in such a way that the cross section under the notch, which the fracture traversed, consisted of equal areas of weld metal and heat-affected base metal. Such specimens taken from a single weldment were tested over a range of temperature encompassing the ductile-to-brittle transition.

The plots of impact energy versus testing temperature obtained with this specimen provided an integration of the notch toughness of the weld metal and heat-affected base metal structures. The relative notch toughness of weld metal and heat-affected base metal was determined by a comparison between the impact-energy transition curves obtained with the composite specimen and those obtained with an all-weld-metal specimen. If the composite-specimen transition curve was located at a higher temperature than that of the all-weld metal, the heat-affected base metal was indicated to be more notch sensitive than the deposited weld metal.

Because of the simple relationship that exists between lateral deformation and energy absorbed in fracturing the test specimen, it was possible to substitute lateral deformation for energy in plotting transition curves. Separate measurements of lateral deformation in weld metal and heat-affected base metal provided two distinct transition curves from a single set of test specimens. The transition curves so obtained indicated the relative notch toughness of the weld metal and heat-affected base metal structures.

Introduction

In metal-arc welding, the heat of the arc is used to melt the base metal and at the same time melt the electrode to provide filler for the weld joint. Since the heat required to obtain fusion between the weld and base metals is applied by the arc in a highly localized area, the flow of heat to the surrounding base metal occurs as a complex thermal cycle involving rapid rates of heating and peaks of temperature and cooling rates depending upon location in the heat-affected zone. Thus, the heat-affected zone consists of a steep gradient of metallurgical structures and attendant mechanical properties.

For as many years as fusion welding has been in practice, welding engineers have been confronted with the problem of evaluating the properties of a weld joint. Welding researchers have sought suitable test methods for evaluating the mechanical properties of weld joints as a whole and of their separate components, i.e., deposited weld metal and heat-affected zone. As a result of these studies, some investigators have concluded that the heat-affected base metal is a controlling factor in determining the performance of a weld joint; others have concluded that the deposited weld metal dominates. Nevertheless, most investigators agree on the basis of the present state of knowledge with respect to fracture initiation and propagation, that notch toughness is a highly desirable characteristic in both weld metal and the surrounding heat-affected base metal.

In spite of the many indications in welding research that notch toughness of the weld heat-affected zone should be one of the prime considerations in evaluating weldability, insufficient attention has been given to this problem because of the difficulties of evaluation. Many investigators have attempted to single out the most notch-sensitive structure of a weld heat-affected zone by locating the apex of a notch in a particular microstructure. There are two major difficulties involved in such an approach. The first arises from the practical problem of accurately and reproducibly locating the notch in a single predetermined structure within the steep gradient of the heat-affected zone. The second arises from the fact that fracture, once initiated, traverses a gradient of structures involving variable resistance to crack propagation.

Another method of attack has been the reproduction, by controlled heat treatment of test specimens, of microstructures simulating those found in weld heat-affected zones. A synthetic-specimen technique which appears to be the most successful yet found for evaluating the notch toughness of a specific heat-affected zone structure is that developed at Rensselaer Polytechnic Institute.* By this technique the thermal cycle associated with the microstructure at any desired location in a weld heat-affected zone is reproduced in a Charpy blank. Several series of V notch Charpy impact specimens, each series containing a single heat-affected zone structure, are tested in impact over a range of temperature in order to obtain conventional impact-transition curves for each particular microstructure under investigation. This approach has the disadvantages of requiring special equipment to reproduce the weld thermal cycles and a large number of test specimens to establish the transition curves for the many structures of the weld heat-affected zone. Also, there is the possible criticism that testing a single structure of uniform cross section is an over simplified situation: i.e., adjacent structures of different strengths, due-

William P. Hatch, Jr., is a Welding Engineer, and Carl E. Hartbower is a Physical Metallurgist, Watertown Arsenal.

Presented at the 1954 AWS National Fall Meeting in Chicago, Ill., November 1-5.

* Nippes, E. F., and Savage, W. F., "Development of Specimen Simulating Weld Heat-Affected Zones," THE WELDING JOURNAL, 28 (11), Research Suppl., 534-s to 546-s (1949).

Table 1—Welding Details

Base metal	Electrode class	First pass: Preheat temp., ° F	First pass: Electrode size, in.	First pass: Amp	First pass: Volts	Second pass: Interpass temp., ° F	Second pass: Electrode size, in.	Second pass: Amp	Second pass: Volts
A	E12015	200	5/32	185	23*	...	5/32	185	23*
B	E12015	200	5/32	150	70†	200	5/16	170	70†
B	E10016	200	5/16	200	70†	200	5/16	200	70†
B	E9016	200	5/32	150	70†	200	5/16	200	70†
B	EL-307	200	5/32	150	70†	200	5/16	200	70†
B	EL-307	R. T.	5/32	150	70†	200	5/16	170	70†
B	E12015	R. T.	5/32	150	70†	200	5/16	200	70†
B	E9016	R. T.	5/32	150	70†	200	5/16	200	70†
B	E7016	R. T.	5/16	200	70†	200	5/16	200	70†

* Motor generator power source, closed-circuit voltage.
† Rectifier power source, open-circuit voltage.

tility and toughness are not present to exert their influence on the behavior of the structure under investigation.

It is the purpose of this paper to present a method using the standard V notch Charpy impact specimen for evaluating simultaneously the notch toughness of weld metal and heat-affected base metal in a multiple bead-on-plate weld.

Experimental Procedure

Materials

Two alloy steel base metals were used in this investigation. The chemical analyses of these steels follow:

Steel	C	Mn	Si	S	P	Ni	Cr	Mo	V	BHN
	%									
A	0.46	0.70	0.24	0.018	0.020	0.15	1.13	0.67	0.26	363
B	0.25	1.58	0.16	0.013	0.021	..	..	0.45	..	340

Steel B contained an undetermined amount of boron. Both steels were welded in the quenched-and-tempered condition. Steel A had been heat treated under carefully controlled conditions to obtain a 100% tempered martensitic structure with an acceptable level of notch toughness at temperatures as low as −80° C. Steel B had been used in an extensive research program conducted under Ordnance Corps sponsorship at an industrial test facility.* The latter material was obtained from a large production heat which was representative of its composition type as a quenched-and-tempered alloy steel.

The electrodes used in this investigation were commercial low-hydrogen ferritic and austenitic types currently employed in the welding of high-strength alloy steel.

Welding Procedure

The details of welding procedure are presented in Table 1. All welds were made manually in a flat position using d-c reverse-polarity. The first series of weldments was prepared using a 200° F preheat for the first pass. The second pass in all weldments was deposited with the weld joint area at 200° F (interpass temperature). No preheat was used in the second series of weldments. Thus, for all practical purposes the only difference in welding procedure between the several weldments was the temperature of the base metal in depositing the first pass and the kind of electrode used. Prior to welding, all electrodes were baked in an oven for 2 hr at 450° F to minimize the moisture content in the electrode coating.

The Test Specimen

Standard ASTM V notched Charpy impact specimens were sectioned from each weldment as shown in Fig. 1. The test weldment consisted of a multiple (2-pass) bead-on-plate weld deposit in a longitudinal groove machined in the surface of the test plate. Charpy specimens were machined transversely to the weld, with the notch centered on the weld and perpendicular to the plate surface. The specimens were so located with respect to the weld deposit that the path of fracture traversed equal portions of weld metal and heat-affected base metal; i.e., the cross section under the notch consisted of approximately one-half weld metal and one-half heat-affected base metal. Thus, all components of the weld joint were subjected simultaneously to the triaxial stress state occurring under the standard Charpy V notch. With this orientation of notch relative to test specimen, the cross section under the notch had a uniform microstructure at its intersection with any plane perpendicular to the notch. On the weld-metal side of the test specimen, all planes were of the same microstructure; on the heat-affected zone side, the planes were all different, each representing

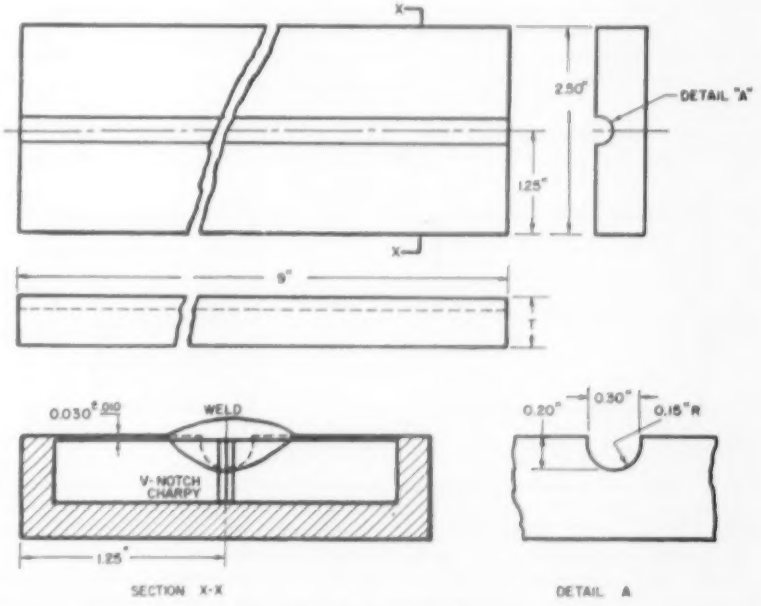

Fig. 1 The test plate and orientation of test specimen

* Ordnance Contract No. DA-33-019-ORD-1132, Battelle Memorial Institute.

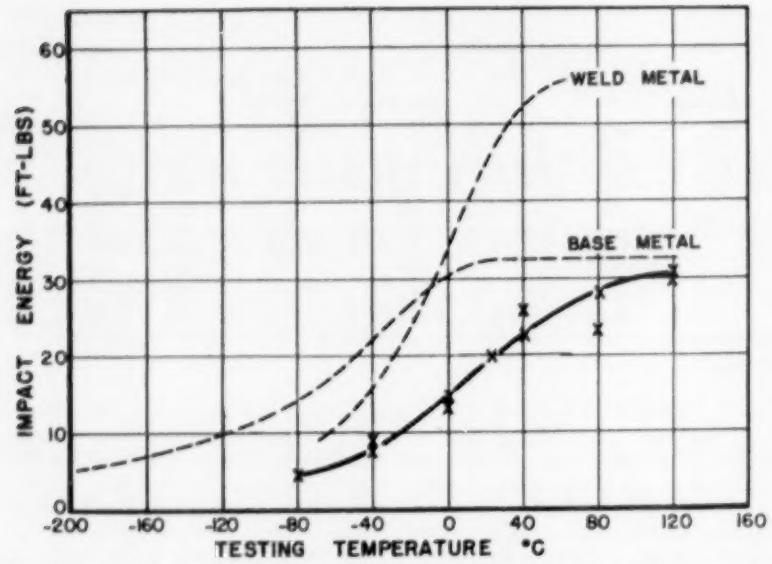

Fig. 2 Transition curves for base metal A, E12015 weld metal and the composite weld joint

one of the gamut of different microstructures occurring in the weld heat-affected zone.

Discussion of Results

Tests and Measurements

The composite specimens were broken in a standard impact-testing machine over a range of temperature encompassing the transition from ductile to brittle behavior. The data from preliminary tests using base metal A welded with an E12015-type electrode were plotted in Fig. 2 in the usual manner for determining the impact-energy transition curve. Also shown on Fig. 2 are the transition curves for deposited E12015 weld metal and the unwelded base material as determined separately. Both the weld metal and base metal are shown to have lower transition temperatures than the composite structure. The higher transition temperature for the composite specimen was taken to indicate that some structure in the weld joint was embrittled.

At this point, the meaning and measurement of transition criteria for the composite specimen require discussion. The transition curve for the composite specimen represents an integration of the toughness of the deposited weld metal and the toughness of the gamut of structures contained in the heat-affected zone. Thus, in Fig. 2 the position of the composite transition curve relative to the positions of the transition curves for unwelded base metal and all-weld metal indicates that the notch toughness of the weld joint was influenced by some structure which was more notch sensitive than either the deposited weld metal or the base metal. In other words, it is assumed that the displacement of the composite transition curve is the result of notch sensitivity in one or more of the structures of the weld heat-affected zone.

Since the plot of impact energy versus testing temperature obtained with the composite specimen provided an integration of the notch toughness of the various components of the weld joint, it was apparent that the usefulness of the test would be greatly increased if some method could be found to determine the structure in which fracture was initiated and the extent to which the two major components (weld metal and heat-affected base metal) resisted crack propagation. Patterns occurring in the fracture face of the Charpy test specimens (the herringbone) indicated that the site of first separation could be determined. Measurement of lateral deformation (expansion or contraction) in each side of the composite test specimen provided a method for separately determining resistance to crack propagation in the weld metal and heat-affected base metal.

For pearlitic steels it has been shown* that a simple linear relationship exists between lateral deformation and the energy expended in fracturing the Charpy specimen. In quenched and tempered steel, the relationship may not be linear but, nevertheless, a simple relationship does exist which permits substitution of lateral deformation for energy in plotting transition curves. In that the cross section under the notch in the composite specimen consists of one-half weld metal and one-half heat-affected base metal, the deformation occurring in the two sides of a given test specimen is not the same. In fact, at certain testing temperatures the difference in lateral deformation between the two sides is so pronounced as to be plainly visible on casual observation. This suggested that separate measurements of lateral deformation occurring at either side of the composite test specimen might provide information as to the relative ductility of the two major components of the weld joint, namely, the weld metal and the heat-affected base metal.

Measurement of lateral deformation was accomplished easily with an optical comparator. The measurements were made on each half of the broken specimen by lining up the cross-hair of the comparator with the profile (30 × magnification) of the undeformed back of the specimen and, then, by moving the calibrated cross slide until the cross hair was tangent to the point of maxi-

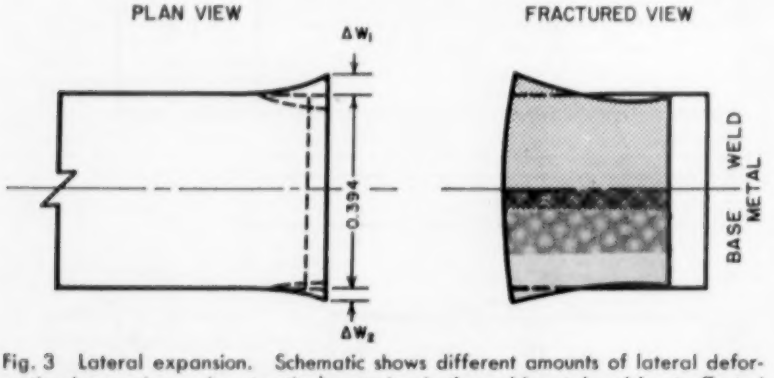

Fig. 3 Lateral expansion. Schematic shows different amounts of lateral deformation (expansion and contraction) occurring in the weld metal and heat-affected base metal sides of a fractured V notch Charpy impact specimen. The undeformed sides of the test specimen are used for reference in setting the cross hair of a comparator used in measuring the deformation; the cross hair is then moved by means of a calibrated slide to determine the maximum expansion (see dimension lines for dw_1 and dw_2).

* Hartbower, C. E., "Poisson Effect in the Charpy Test" presented at the 57th Annual Meeting of ASTM; scheduled for Publication in the *Proceedings*, Vol. 54, 1954.

mum lateral expansion, deformation was measured to the nearest ten thousandth of an inch (see Fig. 3). Thus, separate measurements of lateral expansion in the weld metal and heat-affected base metal sides of the specimens made it possible to plot two distinct transition curves from a single set of test specimens.

In connection with the plots of lateral deformation versus testing temperature, study was made of the relationship between energy expended in fracturing the composite test specimen, lateral expansion occurring across the entire width of specimen (*total* deformation) and lateral expansion occurring in either side of the test specimen (*partial* deformation). When *total* lateral deformation was measured, the ductilities of the weld metal and heat-affected base metal were integrated; when *partial* lateral deformation was measured on each side of the specimen, one of the measurements indicated the ductility of weld metal and the other provided an integration of the ductilities of the heat-affected base metal structures. The relationship between *total* lateral deformation and impact energy for the composite V notch Charpy impact specimen with the austenitic or ferritic welds in Steel B is shown in the upper block of Fig. 4. This figure indicates that in the case of the ferritic welds a relationship similar to that found in pearlitic steel exists, but the slope of the line is less because of the higher flow strength of the heat-affected zone structures in the alloy base metal. In other words, alloy steel requires a greater amount of energy (work) to produce an equivalent amount of plastic deformation (as compared to pearlitic steel). Note that the specimens welded with austenitic electrode showed appreciably greater *total* deformation than those welded with ferritic electrode at a given fracture-energy level. This difference is attributed to the markedly greater ductility of the deposited austenitic weld metal. The lower block of Fig. 4 indicates a similar relationship for the *partial* deformation occurring in the heat-affected base-metal half of the composite specimen. Note that in the case of the heat-affected base metal of austenitic welds, it is indicated that appreciably less plastic deformation is produced at a given energy level (as compared to that of ferritic welds). This is explained by the fact that austenitic weld metal does not undergo the usual transition from ductile to brittle fracture that occurs in the case of ferritic weld metal; even at temperatures as low as −196° C, austenitic metal presents a relatively high degree of toughness. Thus, in the lower portion of Fig. 4, at a given energy level the data for the austenitic welds represent the results of tests conducted at much lower temperatures than in the case of ferritic welds. At these lower temperatures, the heat-affected base metal had lost much of its ductility as shown in the illustration. The ferritic data were obtained from five weldments involving E120, E100 and E90 electrodes, prepared both with and without preheat of the first weld pass; and the austenitic data were obtained from two weldments, one with and one

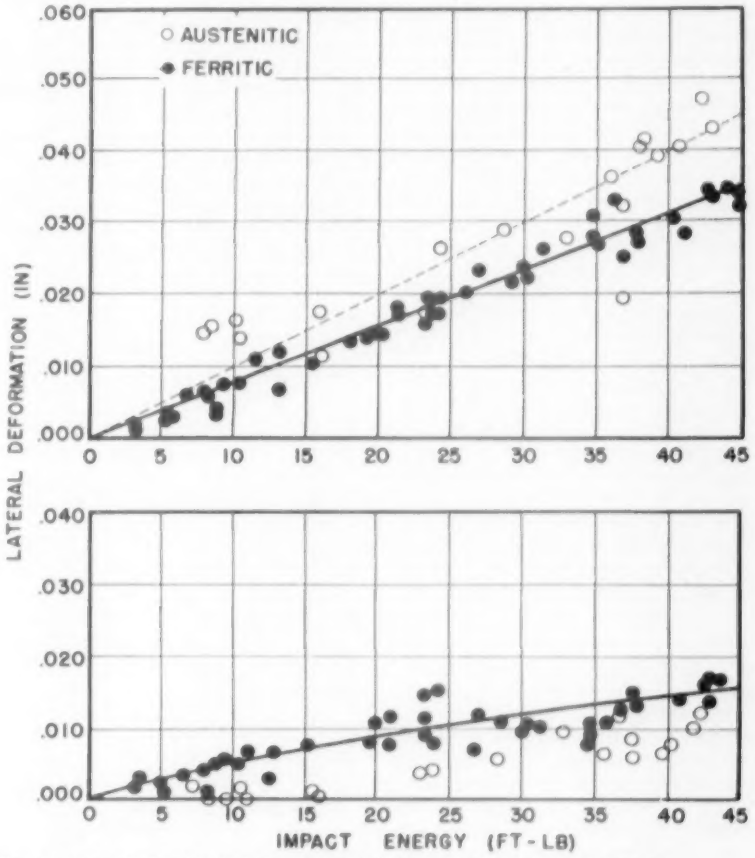

Fig. 4 The relationship between lateral deformation and impact energy

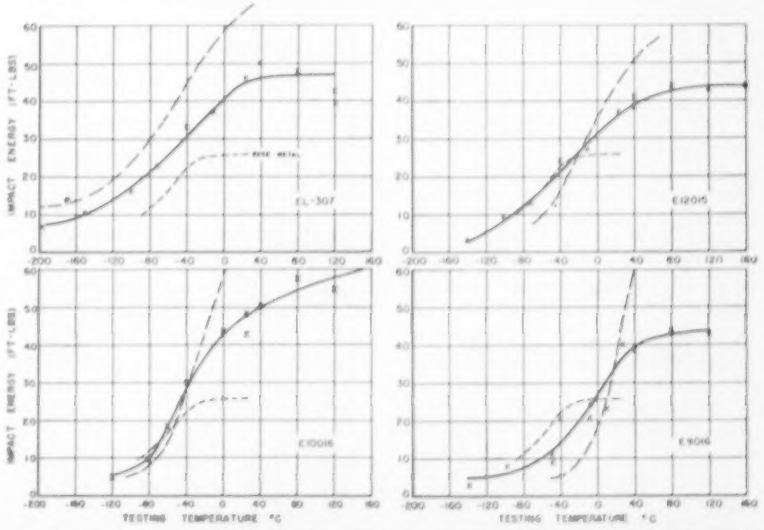

Fig. 5 Transition curves for base metal B, various weld metals and composite joints welded with 200° F preheat

without preheat of the first weld pass.

Test Results

In connection with the discussion of test results further on, attention is invited to the fact that the performance indicated by the composite specimen is not necessarily indicative of over-all performance in an actual weld joint. The performance of a weldment involves numerous factors such as joint geometry, mechanical notches and load and residual stress conditions which cannot be reproduced in a laboratory test specimen. Failure in a *weld joint* occurs by (1) fracture initiation at points of stress concentration (mechanical) and points of high notch sensitivity (metallurgical), and by (2) fracture propagation in the structure of least toughness. Although the path of fracture propagation is predetermined by the orientation of V notch in the composite specimen, the site of first separation (fracture initiation) will occur in the most notch sensitive of the weld and heat-affected base metal structures. By means of the low-blow technique (see Fig. 11), it is possible to determine the structure initiating fracture because all of the structures just below the apex of the V notch (except those in the areas immediately adjacent to the free surfaces) are subjected to essentially the same triaxial stress field.

The impact-energy testing-temperature curves for the composite specimen in Steel B are shown in Fig. 5. Impact-energy transition curves separately determined for the base metal and similar AWS types of weld metals are also included in Fig. 5 to indicate their relative positions with respect to the composite test curves.

A comparison between the relative positions of the composite curves and the base-metal curves with respect to the temperature axis was taken to indicate the combined toughness of the weld metal and heat-affected base metal relative to that of the unwelded base metal. In rating the various welds on this basis, the austenitic EL307 was indicated to be superior, the ferritic classes E100 and E120 about equal, and the Class E90 weld inferior to the base-metal performance. The comparative weld ratings obtained from the composite specimen tests confirm the general findings of past Ordnance research.

The relative position of the weld metal and composite transition curves of Fig. 5 was taken as an indication of the relative notch toughness of the two major components of the weld. For example, in the case of the EL307 weld, the composite curve being to the right of the austenitic weld-metal curve was taken as an indication that the heat-affected base metal was more notch sensitive than the weld metal; and conversely, in the case of the E90 weld the composite curve being left of the weld-metal curve was taken as an indication that the heat-affected base metal was tougher than the weld metal. Measurement of the lateral deformation occurring at the two sides of the composite specimen testify to the validity of these observations.

Separate measurements of lateral deformation occurring in the sides of the test specimen made it possible to plot two distinct transition curves from a single set of test specimens. Thus, the two curves in each block of Fig. 6 were obtained from the same series of test specimens which provided the data plotted in Fig. 5. Figure 6 shows the variations in performance of the weld deposits ranging from the very superior austenitic EL307 weld metal to the markedly more notch-sensitive Class E90 ferritic weld metal. Note that in spite of the wide variations in weld-metal toughness, the heat-affected base metal curves remained essentially constant.

A second group of plates (Table 1) was welded using a procedure identical to that used for the previous group except that preheat of the *first* pass was eliminated. In both groups, an interpass temperature of 200° F was maintained. The results obtained in these tests are presented in Fig. 7. In general the curves of Fig. 7 indicate that a higher impact-energy level, i.e., greater resistance to crack propagation, was obtained by preheating. Figure 8 presents the curves of lateral deforma-

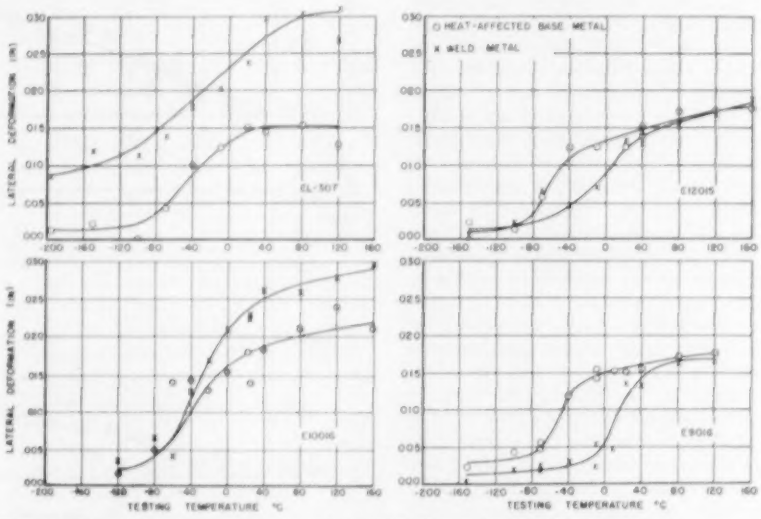

Fig. 6 Transition curves based on lateral deformation (200° F preheat)

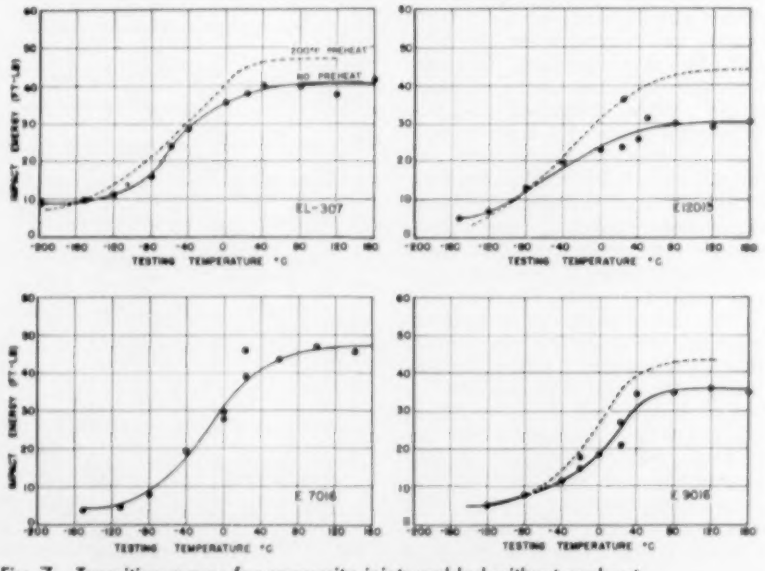

Fig. 7 Transition curves for composite joints welded without preheat

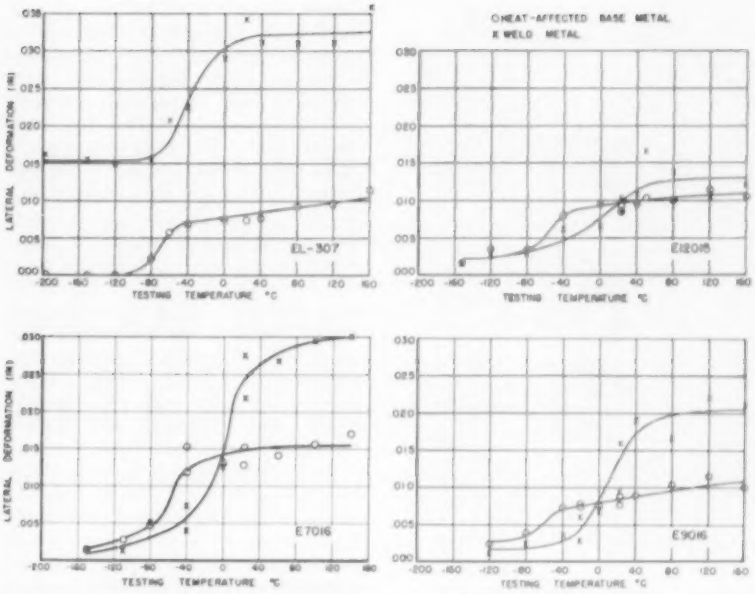

Fig. 8 Transition based on lateral deformations (without preheat)

tion versus temperature corresponding to Fig. 7. It is interesting to note in comparing the curves of Fig. 8 with those of Fig. 6 that in the case of the austenitic EL307 weld, the range of temperature over which the transitions from ductile to brittle occurred was much narrower without preheat, and that for all welds preheating the first pass resulted in greater ductility at temperatures corresponding to the upper portion of the transition curves.

The latter observation is easily made from Figs. 9 and 10. In Fig. 9, individual measurements of heat-affected base-metal deformation on all specimens from both series of tests, except for the E70 type electrode, have been plotted against testing temperature (the E70 results are discussed later in connection with Fig. 10). Figure 9 illustrates that, for all practical purposes, the transition data for heat-affected base metal associated with the E120, E100, E90 and EL307 type electrodes fall on two transition curves, one for the preheated weldments and one for weldments prepared without preheat. Although the range of temperature over which the transition occurred is the same in both cases and the curves coincide at the lower end of the transition range, preheating the first weld pass had a marked effect on the upper portion of the transition curve.

The microstructures of single pass welds deposited to reproduce the first pass procedures of the composite test welds were examined for indications of differences which might explain the higher impact levels for the preheated welds. It was noted that, when the preheated and nonpreheated specimens were etched together using a 4% picral etchant, the heat-affected area of the preheated specimen appeared slightly darker than the corresponding area of the nonpreheated specimen. The only difference visible in the microstructures at a magnification of $\times$ 1000 was a little greater precipitation of carbides in the heat-affected zone of the preheated specimens. The increased precipitation of carbides is undoubtedly associated with slower cooling rates effected by preheating.

The curves of Fig. 9 indicated that regardless of the relative notch toughness of the weld metals, a single transition curve for heat-affected base metal was obtained for a given plate composition and welding procedure. However, an anomaly appeared in the case of welds produced with E70 type electrodes. The lateral deformation occurring in the heat-affected base metal involving three E70 type weldments (two manufacturers' brands investigated) welded without preheat but with a 212° F interpass temperature are presented in Fig. 10. The broken-line curves are those from Fig. 9. The data for all three E70 weldments *prepared without preheat* fall on the curves for preheated heat-affected base metal of the E120, E100, E90 and EL307 weldments. The explanation for this anomaly has to date not been found.

Future Work

As a continuation of this investigation (aimed at a more thorough evaluation of the mechanics of flow and fracture in the composite test specimen), a method is proposed which promises to make the composite test still more useful. The method consists of a modification of the "low-blow" testing procedure described by Harris, Rinebolt and Raring.* The procedure consists of delivering a low blow by

* Harris, W. E., Rinebolt, J., and Raring, R., "Upper and Lower Transitions in Charpy Test," The Welding Journal, 30 (9), Research Suppl., 417-s to 422-s (1951).

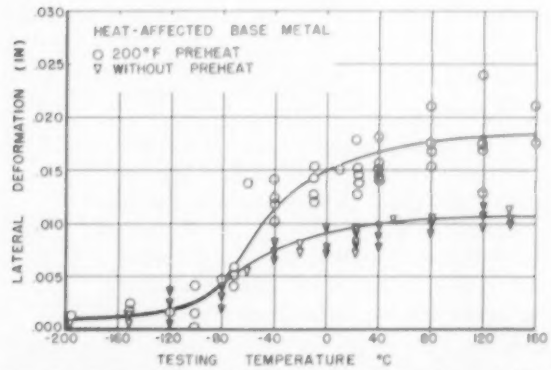

Fig. 9 Comparison of transition curves based on lateral deformation in heat-affected base metal with and without preheat

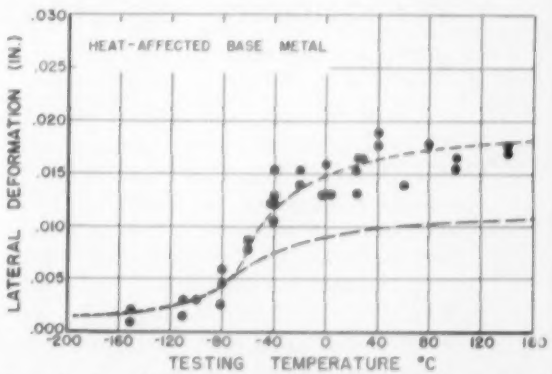

Fig. 10 Transition curve based on lateral deformation in heat-affected base metal of E7016 welds without preheat

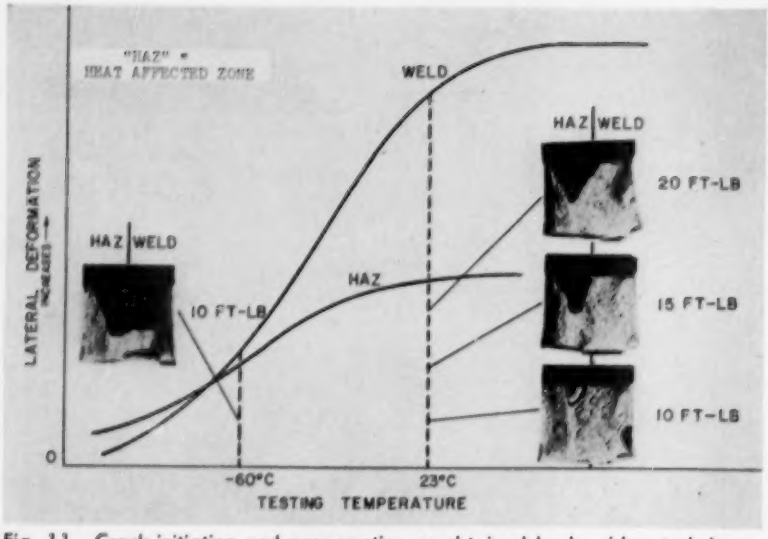

Fig. 11 Crack initiation and propagation as obtained by low-blow technique

releasing the pendulum of a standard impact-testing machine from a calculated intermediate height. After the specimen is struck the low blow, India ink containing a wetting agent is placed in the notch; the ink flows by capillary action into any crack that may have occurred as a result of the blow. The specimen is then fractured at the same testing temperature using the full capacity of the impact-testing machine. The location and extent of the initiated crack developed by the low blow is indicated by the stain on the fracture surface. A series of such tests conducted over a range of temperature promises to provide valuable information on the process of fracture initiation and propagation in the composite specimen. An attempt will be made to correlate such results with the lateral-deformation curves obtained from the composite test.

Some very interesting results have been obtained from the initial experiments using this procedure. Figure 11 shows the results of a series of composite specimens delivered 10, 15 and 20 ft-lb blows at room temperature, then stained with India ink, and fracture completed at room temperature. The specimens consisted of an E100-type weld deposit in a base metal similar in composition to Steel B. The lateral-deformation transition curves for weld metal and heat-affected base metal are shown schematically with the fracture surfaces. Note from the transition curves that at room temperature there is a considerable difference between the ductilities of weld metal and heat-affected base metal and that, from the fractured specimens tested at room temperature, crack initiation and propagation occurred in a narrow band within the heat-affected zone. The structures contiguous to the band in which fracture initiated retained their ability to resist fracture in the presence of the propagating crack. Note also from the curve that at a testing temperature of −60° C both weld metal and heat-affected zone had nearly the same ductility. When a test specimen was delivered a crack-initiating blow of 10 ft-lb at −60° C, fracture progressed a considerable distance across the test specimen with an essentially square front although still slightly leading in the more notch-sensitive band of heat-affected zone. In other words, the leading front of the fracture occurred in the heat-affected zone in the same location as in the room-temperature test but the fracture extended across the weld metal as well as the heat-affected zone. Thus, it was indicated that at −60° C the weld metal had little ability to resist the propagating crack.

The low-blow technique as described above will occupy a position of considerable importance in the continuing investigation of the composite specimen test.

Conclusions

The composite test is sensitive to variations in weld metal and heat-affected zone toughness, and to a seemingly minor variation in welding procedure. Therefore, the test provides, at least in part, a method for evaluating the relative notch-toughness characteristics of weld metal and heat-affected base metal in a natural environment.

Weldability of Steels

Copies of the monograph entitled "WELDABILITY OF STEELS" by Robert D. Stout and W. D'O. Doty, who were commissioned by the Weldability Committee of the WELDING RESEARCH COUNCIL to prepare this book, are still available for distribution. This monograph consists of 381 pages, handsomely bound and copiously illustrated. A limited edition of this book has been published. The list price is $6.50. Special arrangements with the American Welding Society are such that Members of the Council and the American Welding Society receive a 20% discount from the list price. The distribution of four or more copies will be handled by the WELDING RESEARCH COUNCIL. Less than four copies may be ordered from the American Welding Society, 33 West 39th Street, New York 18, N. Y.

OPTIMUM SPOT AND SEAM WELDING CONDITIONS FOR INCONEL "W"

Results of research investigation indicate that the optimum conditions for spot and seam welding Inconel W are much the same as those for Inconel X

BY ERNEST F. NIPPES, WARREN F. SAVAGE, AND KHOSROW L. MOAZED

ABSTRACT. This research defines recommended conditions for spot and seam welding Inconel "W" sheets of 0.010-, 0.015-, 0.021-, 0.031- and 0.062-in. thicknesses. The RWMA criteria for spot and seam welding in conjunction with the previously determined conditions for spot and seam welding Inconel "X" are used in this determination. A comparison of the spot and seam welding conditions for Inconel "W" is made with those previously determined for Inconel "X" and other high-nickel alloys. The strength-current relationships are shown and discussed for spot and seam welds made at the optimum conditions. The relationship of interdependent welding variables is pointed out, and an outlined procedure for this type of investigation is presented. The results indicate that the optimum conditions for spot and seam welding Inconel "W" are much the same as those previously determined for Inconel "X."

Object and Scope

The research reported in this paper was instituted to investigate the spot- and seam-welding conditions for Inconel "W." The investigation was limited to include five thicknesses of Inconel "W," ranging from 0.010-to 0.062-in. A comparative analysis was to be made of the results of this investigation of Inconel "W" and those previously determined in this laboratory for Inconel "X."

Ernest F. Nippes, Warren F. Savage, and **Khosrow L. Moazed** are associated with the Department of Metallurgical Engineering, Rensselaer Polytechnic Institute, Troy, N. Y.

Introduction

Since 1939 there has been sponsored a program of research at the Welding Laboratory of Rensselaer Polytechnic Institute for the determination of welding conditions for high-nickel alloys. The research reported in this paper is the latest addition to the compilation of information which includes the spot- and seam-welding conditions for Inconel "X,"[1] the seam welding of Monel,[2] the seam welding of Monel metal to steel,[3] and the spot welding of nickel, Monel and Inconel.[4]

Because of the similarity of the chemical and mechanical properties of Inconel "W" with those of Inconel "X," equipment, instrumentation, testing and procedure were designed to parallel the investigation of Inconel "X."

Careful comparative analyses were made between Inconel "X" and Inconel "W" and the differences defined were interpreted toward the establishing of welding conditions for Inconel "W."

The recommendations of the Resistance Welding Manufacturers Association as presented in the Resistance Welding Manual[5] were considered as preliminary criteria for acceptable welds. The RWMA recommends:

1. A fusion zone which is porosity-free and contains no cracks.
2. Less than 10% separation of the sheets welded.
3. Less than 5% electrode indentation into the sheet.
4. Fusion-zone penetration of 30–80% of the total thickness of the sheets.
5. Fusion-zone overlap of 10–25% for pressure-tight seam welds.
6. A wide and reproducible current range.

Material

The material used in this investigation was Inconel "W" strips cut from sheets with thicknesses of 0.010-,0.015-, 0.021-,0.031- and 0.062-in. The sheets were supplied cold rolled to size and solution treated to obtain the soft-tempered condition. Tables 1 and 2 list, respectively, the chemical analyses and mechanical properties of Inconel "W" and Inconel "X."

Equipment

The electrical energy was produced by using a 125-hp, 350-kva motor-generator set operating from a 3-phase, 60-cycle, 4160-v line. The generator output was adjustable in the range of 275 to 550 volts. "On-time"–"off-time" sequences of $^1/_2$ to 30 cycles were available as well as phase control and slope control; the slope control was not used in this investigation, since acceptable welds could

Table 1—Chemical Analysis of Inconel "W" and Inconel "X"

Melt	*C*	*Mn*	*Fe*	*S*	*Si*	*Cu*	*Ni*	*Cr*	*Al*	*Ti*	*Cb*
Chemical analysis of Iconel "W"											
Y6971W	0.03	0.56	6.48	0.007	0.18	0.08	74.57	14.96	0.71	2.40	..
Y6530W	0.03	0.52	6.58	0.007	0.29	0.09	74.52	14.79	0.60	2.55	..
Chemical analysis of Inconel "X"											
Y3576X	0.05	0.54	6.75	0.007	0.41	0.03	73.59	14.35	0.78	2.43	1.04
Y3400X	0.04	0.40	6.17	0.007	0.41	0.01	74.34	14.39	0.71	2.48	1.01
Y3402X	0.04	0.42	6.58	0.007	0.41	0.02	73.46	14.89	0.64	2.54	1.00
Y3401X	0.04	0.41	6.42	0.007	0.33	0.01	73.78	14.72	0.69	2.48	1.05

Table 2—Mechanical Properties of Inconel "W" and Inconel "X"

Gage, in.	Melt	Yield strength, psi	Tensile strength, psi	Elongation, %	Hardness Rb
		Mechanical properties of Inconel "W"			
0.010	Y6530W	41,000	99,500	32	81–82
0.015	Y6530W	40,000	102,500	36	74–76
0.021	Y6530W	41,000	107,000	47	74
0.031	Y6971W	38,000	104,000	60	77
0.062	Y6971W	43,000	109,000	52	77–79
		Mechanical properties of Inconel "X"			
0.010	Y3576X	54,000	128,700	38	
0.015	Y3576X	54,400	127,000	45	
0.021	Y3400X	48,200	108,800	47	
0.031	Y3402X	45,000	109,100	61	
0.062	Y3401X	63,100	126,000	52	

be made without its utilization. The secondary current was varied by changing the primary voltage, the transformer tap setting, or the phase control setting.

A 200-kva press-type spot welder with a maximum electrode force of 5000 lb was used for the spot welding part of this investigation. Three transformer tap settings were available with this spot welder, giving transformer ratios of 36:1, 72:1 and 144:1.

A 175-kva seam welder having a maximum electrode force of 4000 lb was used for the seam-welding portion of this investigation. The seam welder had a transformer ratio of 50.7:1 and feed speeds ranging from 5 to 200 ipm.

Instrumentation

Two main types of instrumentation were used in this investigation, electrical and nonelectrical.

1. Instrumentation for electrical measurements:

The surface contact resistance of the material, which is a measure of the surface condition, was determined with a modified Kelvin double-bridge circuit.

The spot-welding currents were measured by the use of an ampere-squared-second indicator.[5] The seam-welding currents were measured by a recording ammeter and by a pointer-stop ammeter. The seam-welding currents were evaluated for the various "on-time" and "off-time" sequences by the use of a cathode-ray oscilloscope and a camera.

2. Instrumentation for nonelectrical measurements:

The electrode force was measured with a deflection-type force indicator which was calibrated with the aid of a Universal testing machine.

The welding times were measured and recorded with a direct-inking recording oscillograph. Welding speeds in ipm were calculated from the product of wheel speed in rpm and circumference of the wheel in inches. The weld spacing was determined by direct counting of the number of welds per inch or by using the following relationship:

$$(\text{weld spacing}) \times (\text{welding speed}) \times (\text{total time per spot}) = K$$

The value of the constant, K, depends on the choice of the dimensions for the three interdependent variables. If weld spacing is taken in spots/in., the welding speed in ipm and the total time in cycles/spot, then K will have the value of 3600.

Penetration and width of the fusion zone were measured with a Filar eyepiece and a low-power binocular microscope.

Electrode indentation was measured at the center of the weld zone with a ball-end micrometer. Sheet separation was measured with this micrometer at a distance equal to the overlap distance required by the RWMA standards.

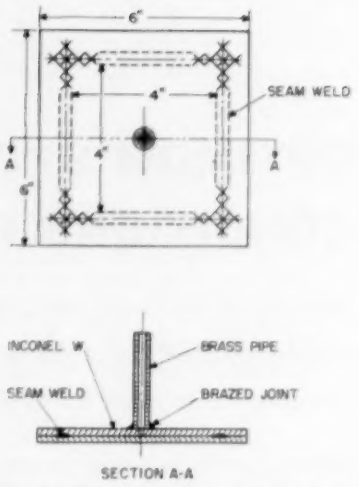

Fig. 1 Details of pillow-test specimen

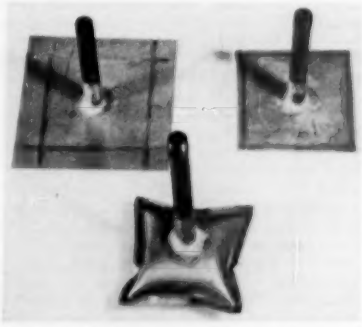

Fig. 2 Various stages in making and testing of a pillow sample

(a) Upper left—as-welded; (b) upper right—after trimming; (c) lower center—after testing.

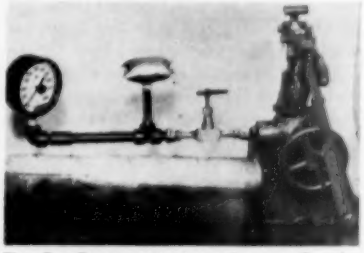

Fig. 3 Pressure test equipment for the pillow samples

Table 3—Conditions for Radiography

Film: Eastman Kodak Type M X-ray film
Exposure: 40 ma min
Tube-film distance: 36 in.

Gage, in.	Voltage, kv
0.010	40
0.015	50
0.021	60
0.031	80
0.062	100

Table 4—Composition of Etchants

Macro-etch	
$FeCl_3$	25 gm
$(NH_4)_2SO_4$	1.5 gm
HCl (conc.)	10 cc
HNO_3 (conc.)	3 cc
H_2O	7.5 cc
Micro-etch	
$CuSO_4$	4 gm
HCl	20 cc
C_2H_5OH	10 cc
H_2O	10 cc

Table 5—Specimen Size for Various Tests

Gage, in.	Tensile-shear test for spot weld, in.	Cross-tension test for spot weld, in.	Pillow tests for seam welds, in.
0.010	1 x 3	2 x 6	6 x 6
0.015	1 x 3	2 x 6	6 x 6
0.021	1 x 3	2 x 6	6 x 6
0.031	1 x 4	2 x 6	6 x 6
0.062	1½ x 5	2 x 6	6 x 6

Table 6—Recommended Spot-Welding Conditions for Inconel "W"

Gage, in.	Electrode size, in. Diam	Radius	Weld time, cycles	Weld force, lb	Weld current, amp	Fusion zone, diam, in	Penetration, %
0.010	5/32	6	2 (2–4)*	300 (270–330)	6400 (6000–7000)	0.11 (0.10–0.12)	60
0.015	5/32	6	4 (2–6)	450 (425–475)	7000 (6500–7500)	0.10 (0.10–0.11)	40
0.021	3/16	6	6 (6–8)	850 (800–900)	9000 (8500–9500)	0.13 (0.12–0.14)	35
0.031	7/32	6	8 (6–10)	1750 (1600–1900)	9200 (8800–9400)	0.17 (0.16–0.18)	40
0.062	5/16	10	14 (12–16)	4400 (4200–4400)	16,800 (16,000–17,000)	0.31 (0.30–0.32)	55

* The values within parentheses are the range of variables which are satisfactory for good welds. Since these variables are interdependent, they cannot be independently varied over the range without adjusting other variables to compensate.

RWMA Class II electrodes were used for all gages.

Procedure

Because the chemical analysis and the mechanical properties of Inconel "W" were similar to those of Inconel "X," the most efficient approach to the determination of spot- and seam-welding conditions for Inconel "W" seemed to be the use of conditions previously determined for Inconel "X."

Material Preparation

The material as it was received had contact resistance values ranging from 200–400 microhms. After degreasing in acetone, the contact resistance was lowered to the range of 150–250 microhms.

In resistance welding, it is usually desirable, and in some cases imperative, to pickle the material to be welded. The pickling operation should bring about not only a *low* contact resistance but also *uniform* contact resistance by the removal of any oxide film present on the sheet. In the case of high-nickel alloys, this operation is particularly necessary, because of the tenacious oxide film which is introduced on the surface of the material during processing. Therefore, after the degreasing operation, the sheets were pickled for a period of from 20 to 30 min in a solution of 10 parts concentrated nitric acid, 10 parts water, and 1.5 parts hydrofluoric acid by volume. The pickling time depended on the age of the bath. The contact resistance after the pickling operation was lowered to the range of 30–70 microhms.

Examination of Welds

The examination of the welds included both destructive and nondestructive methods, the latter method in-

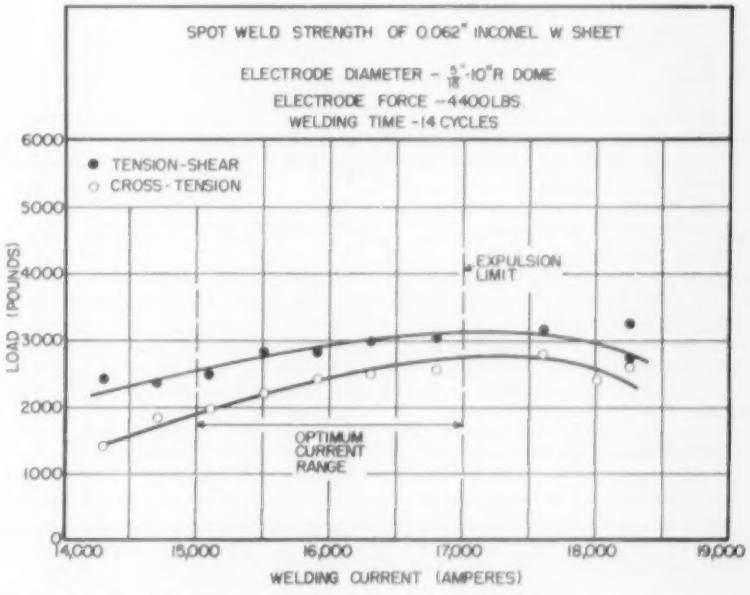

Fig. 4 Spot weld strength of 0.062-in. Inconel "W" sheet

Table 7—Recommended Spot-Welding Conditions for Inconel X

Gage, in.	Electrode size, in. Diam	Radius	Weld time, cycles	Weld force, lb	Weld current, amp	Fusion zone, diam, in.	Penetration, %
0.010	5/32	6	2 (2–4)*	300 (270–330)	7300 (7000–7750)	0.11 (0.11–0.12)	45
0.015	5/32	6	4 (2–6)	400 (350–450)	7400 (7000–7800)	0.11 (0.10–0.12)	45
0.021	3/16	6	6 (6–8)	750 (650–850)	7500 (7100–7900)	0.14 (0.12–0.14)	35
0.031	7/32	6	8 (6–10)	1750 (1600–1900)	9900 (9500–10,200)	0.17 (0.14–0.18)	35
0.062	5/16	10	14 (10–16)	4400 (4200–4700)	16,350 (15,500–17,250)	0.29 (0.27–0.30)	45

* The values within parentheses are the range of variables which are satisfactory for good welds. Since these variables are interdependent, they cannot be independently varied over the range without adjusting other variables to compensate.

volving the use of radiographs of the welds to detect porosity in the fusion zone. Table 3 lists the conditions used for radiography.

Representative samples of both spot and seam welds were also sectioned, polished, and etched for metallographic examination. In seam welds both longitudinal and transverse sections were made to determine the penetration, the fusion-zone width and the weld overlap. Table 4 lists the composition of micro- and macro-etchants used in this investigation.

Testing of Welds

All spot welds were tested in tensile-shear and normal-tension. Table 5 lists the RWMA recommendations for the specimen sizes used in the destructive testing of the various sheet thicknesses.

The peel test was used as a qualitative test for the seam welds, and the pillow test was used to determine the strength of pressure-tight welds.[6] Pillow-test specimens for all gages were made of 6- x 6-in. sheets. One sheet of this test specimen was drilled at the center and a brass pipe brazed to the sheet so that the axis of the hole and the pipe were coincident. If the inside diameter of the pipe was about the same size as the diameter of the drilled hole, the brazed joint tended to crack. This cracking was due to the stresses produced around the hole during the drilling operation. Therefore, the inside diameter of the pipe had to be larger than the diameter of the drilled hole so that the brazed joint would not be in the region where the stress concentration was great enough to cause cracking. The brazing alloy used for making the joint was a proprietary alloy composed of 65% Ag, 28% Cu, 5% Mn, 2% Ni. The use of this alloy was necessary because ordinary Cd-bearing silver brazing alloy wet the grain boundaries near the drilled hole and caused stress-corrosion cracking.

The sheet with the brass pipe attached was seam welded to a 6- x 6-in. flat sheet. The welds were made so that a 4- x 4-in. area was bounded by the seam welds, as shown in Figs. 1 and 2. Following seam welding, the excess metal was sheared to within $^1/_8$ in. of the welds. The pipe

Table 8—Results of Mechanical Tests on Inconel "W" Spot Welds

Gage, in.	*Shear-tensile strength, lb*	*Normal-tensile strength, lb*	*Ratio normal to shear, %*
0.010	230 (210–240)	200 (175–220)	87
0.015	400 (350–420)	380 (350–400)	95
0.021	670 (600–720)	630 (580–670)	94
0.031	1350 (1250–1370)	1280 (1150–1300)	95
0.062	3040 (3000–3200)	2580 (2200–2700)	85

Table 9—Recommended Seam-Welding Conditions for Inconel "W"

Gage, in.	*Wheel geometry*	*Speed, ipm*	*Force, lb*	*Current, amp*	*Timing Cycles "on"*	*Timing Cycles "off"*	*Spacing, spots/in.*	*Penetration, %*	*Fusion zone width, in.*
0.010	RWMA Class II, $^1/_4$ in., 3-in., radius 9-in. wheel diam	45 (28–63)*	400 (350–450)	4900 (4500–5500)	1 ($^1/_2$–1$^1/_2$)	3 (2–5)	20 (19–22)	(30–60)	0.11
0.015	RWMA Class II, $^1/_4$ in., 3-in., radius 9-in. wheel diam	36 (21–56)	700 (625–775)	6400 (6100–6700)	2 (1–2)	4 (3–6)	17 (16–19)	(30–60)	0.12
0.021	RWMA Class II, $^5/_{32}$ in., 3-in., radius 9-in. wheel diam	30 (20–43)	1400 (1250–1550)	7600 (6700–8400)	3 (2–4)	6 (5–8)	14 (12–16)	(30–60)	0.14
0.031	RWMA Class III, $^3/_{16}$ in., 3-in., radius 9-in. wheel diam	30 (19–40)	2300 (2100–2500)	9700 (8500–10,800)	4 (3–5)	8 (5–10)	10 (9–12)	(30–60)	0.17
0.062	RWMA Class III, $^1/_4$ in., 6-in., radius 8-in. wheel diam	12.5† (8–15)†	4000† min	14,400† (12,500–16,500)†	8† (7–9)†	16† (15–28)†	12† (11–13)†	(30–60)	0.24

* The values within parentheses are the range of variables which are satisfactory for good welds. Since these variables are interdependent, they cannot be independently varied over the range without adjusting other variables to compensate.

† Not optimum conditions, but satisfactory when sufficient force is not available.

Table 10—Recommended Seam-Welding Conditions for Inconel "X"

Gage, in.	*Wheel geometry*	*Speed, ipm*	*Force, lb*	*Current, amp*	*Timing Cycles "on"*	*Timing Cycles "off"*	*Spots/in.*	*Penetration, %*	*Fusion zone width, in.*
0.010	RWMA Class II, $^1/_4$ in., 3-in., radius 9-in. wheel diam	45 (28–63)*	400 (350–450)	3600 (3200–4000)	1 ($^1/_2$–1$^1/_2$)	3 (2–5)	20 (19–22)	(30–45)	0.11
0.015	RWMA Class II, $^1/_4$ in., 3-in., radius 9-in. wheel diam	36 (21–56)	700 (625–775)	3900 (3600–4200)	2 (1–2)	4 (3–6)	17 (16–19)	(30–45)	0.12
0.021	RWMA Class II, $^5/_{32}$ in., 3-in., radius 9-in. wheel diam	30 (20–43)	1400 (1250–1550)	8000 (7700–8400)	3 (2–4)	6 (5–8)	14 (12–16)	(30–50)	0.14
0.031	RWMA Class III, $^3/_{16}$ in., 3-in., radius 9-in. wheel diam	30 (19–40)	2300 (2100–2500)	8500 (8100–8900)	4 (3–5)	8 (5–10)	10 (9–12)	(30–50)	0.17
0.062	RWMA Class III, $^3/_{16}$ in., 6-in., radius 8-in. wheel diam	12.5 (8–15)†	4000† min	10,300 (10,000–10,600)†	8 (7–9)†	16 (15–28)†	12 (11–13)†	(30–65)	0.18

* The values within parentheses are the range of variables which are satisfactory for good welds. Since these variables are interdependent, they cannot be varied independently over the range without adjusting other variables to compensate.

† Not optimum conditions, but satisfactory when sufficient force is not available.

was connected to a hand-operated hydraulic pump and water was pumped into the specimen until it ruptured. The rupture-strength was recorded on a pointer-stop hydrostatic pressure gage. Figure 3 shows a photograph of the pillow-testing equipment.

Investigative Procedure

In all determinations the welding current was varied from a value just sufficient to produce sticking to a magnitude great enough to cause expulsion.

The investigative procedure followed has been outlined below:

1. Welds were made using the optimum conditions as previously determined for Inconel "X" for all variables.

2. Welds were made using the optimum conditions as determined for Inconel "X" for all but one variable, this variable being assigned values between the upper and the lower limits of the range as determined previously for Inconel "X."

3. Step 2 was repeated until each variable had been considered individually.

4. The conditions determined as optimum for Inconel "X" were considered optimum for Inconel "W" if acceptable welds were made throughout the range for all the variables.

5. The conditions were adjusted until acceptable welds were made on Inconel "W" if the optimum conditions as determined for Inconel "X" did not prove satisfactory.

The variables investigated were electrode geometry, electrode force, electrode speed, welding time and welding current. The values of the variables which gave the best results according to the RWMA criteria were reported as optimum.

Electrode geometry and electrode force were considered together since their combined effect determined the pressure requirements for good welds. In the investigation of electrode geometry for welding of Inconel "W," the minimum electrode diameter for spot welding and the minimum electrode width for seam welding were chosen as $(0.1 \text{ in.} + 2t)$ where t was the single-sheet thickness, in inches, of the material being welded. The value of $(0.1 \text{ in.} + 2t)$ was increased 10% to compensate for the curvature machined on the contact surface of the electrode.

The electrode force range was determined so that porosity, electrode indentation and sheet separation met RWMA requirements. First, the force was lowered from the optimum force value for welding Inconel "X" to the minimum value at which porosity did not appear. This value was taken as the lower limit of the optimum force range for welding Inconel "W." Then the force was increased to a value where both indentation and sheet separation were just below the allowable RWMA limits. This value was taken as the upper limit of the electrode force range. The value within the determined range which gave the best results was taken as the optimum value.

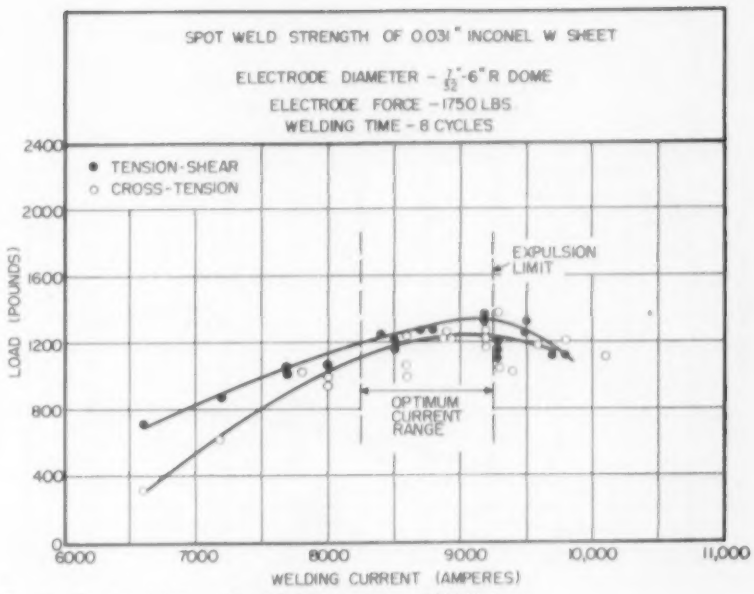

Fig. 5 Spot weld strength of 0.031-in. Inconel "W" sheet

Rapid electrode deterioration resulted from the use of either insufficient or excess electrode force. In addition the electrodes deteriorated much more rapidly with current values near or greater than the expulsion limit. The use of deteriorated electrodes resulted in uneven current and pressure distribution and in poor, irregularly shaped welds. The problem of electrode deterioration was not considered separately in this investigation.

The problem of maintaining electrode alignment was of major importance. With excellent electrode alignment the value of the welding current at which expulsion occurred was much greater than when poor electrode alignment was used. Good alignment also decreased deterioration of the electrodes considerably. Poor electrode alignment, on the other hand, caused early expulsion, surface spitting, increased sheet separation and indentation, and influenced the shape of the fusion zone.

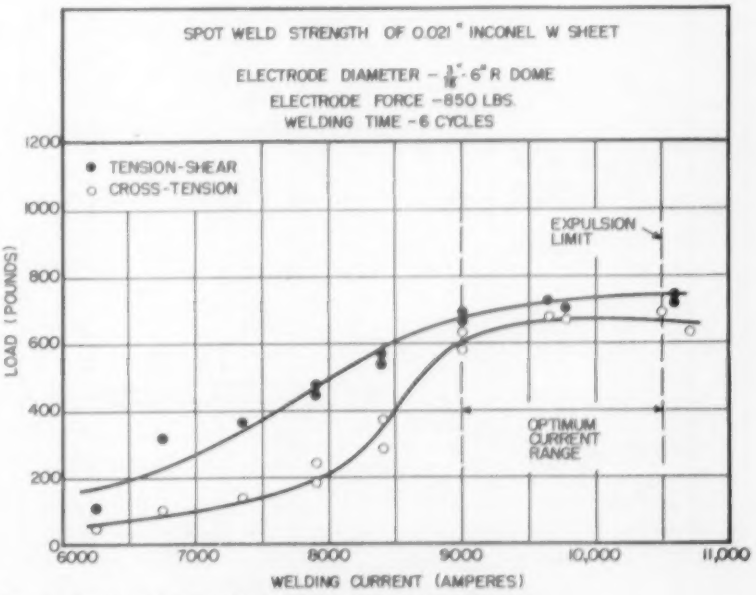

Fig. 6 Spot weld strength of 0.021-in. Inconel "W" sheet

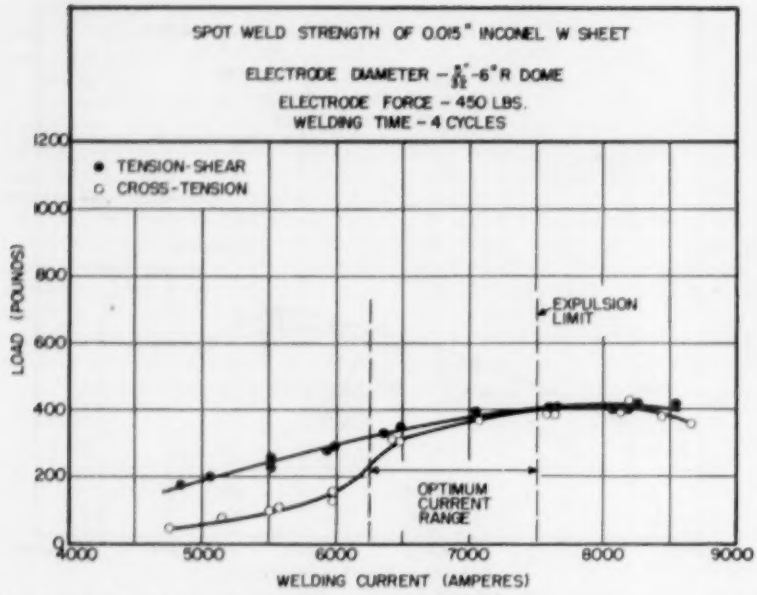

Fig. 7 Spot weld strength of 0.015-in. Inconel "W" sheet

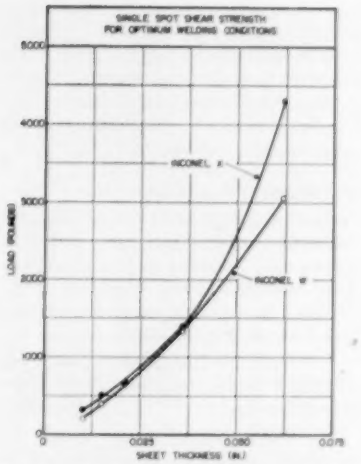

Fig. 9 Single spot shear strength for optimum welding conditions

Because of the importance of the electrode alignment, which is very critical in the thin gages, much time was spent to secure proper alignment. To decrease the set up time in spot welding and to maintain good alignment, a jig was made which held both the top and bottom electrodes simultaneously in such a position that the cylindrical axis of the electrode were coincident. The necessary adjustments were then made on the electrode holders to maintain these axes in coincidence during the welding operation. In addition the axis of the dome machined on the electrode face had to be coincident with the cylindrical axis of the electrode.

The problem of alignment during seam welding was more difficult to solve because of the unpredictable nature of the deflection of the axle and bearing assemblies. Therefore, trial-and-error adjustment of the electrodes was required each time a change was made in wheel geometry or electrode force.

As shown previously, the product of the weld time, the weld spacing and the welding speed is a constant. Therefore, for a given value of one of these variables, only one of the remaining two variables can be considered to be independent and, hence, varied. In order to produce satisfactory pressure-tight seam welds, the following conditions must be satisfied simultaneously for the above variables:

1. The "on-time" must be long enough to produce a fusion zone with 30 to 70% penetration.
2. The "off-time" must be long enough to eliminate porosity and cracking in the fusion zone.
3. The weld spacing must provide sufficient overlap to produce a pressure-tight seam.
4. The wheel speed must be sufficient to allow a practical fabrication rate.

In this part of the research the optimum value determined for Inconel "X" was chosen and kept constant for one of the variables while the other two were varied so that their product was constant. The effect on the welds was noted, and the optimum condition and the range were determined for the three variables.

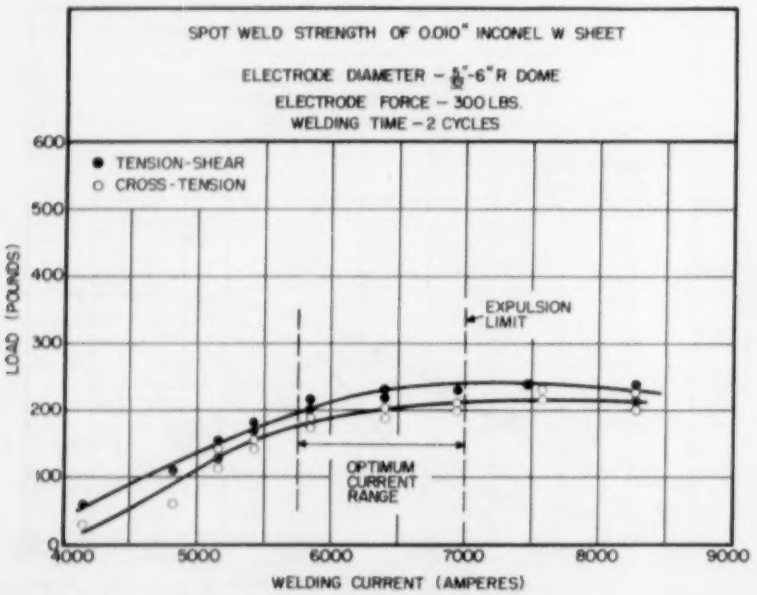

Fig. 8 Spot weld strength of 0.010-in. Inconel "W" sheet

Results

In general the results obtained from this investigation paralleled closely those obtained previously for Inconel "X."

Spot Welding

In spot welding Inconel "W," both the optimum welding time and electrode geometry were found to be the same as those for Inconel "X." As may be seen from a comparison of Tables 6 and 7, the electrode force required for spot welding Inconel "W" was the same as that for Inconel "X" except for the 0.015- and 0.021-in. sheets. For 0.015-in. sheets the recommended value of electrode force for Inconel "W" was 450 lb, whereas for Inconel "X," the recommended value was 400 lb. For

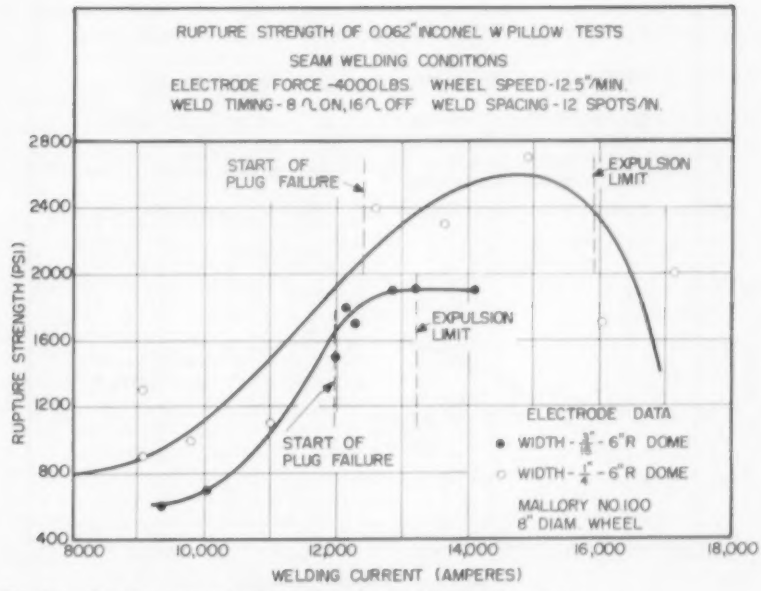

Fig. 10 Rupture strength of 0.062-in. Inconel "W" pillow tests

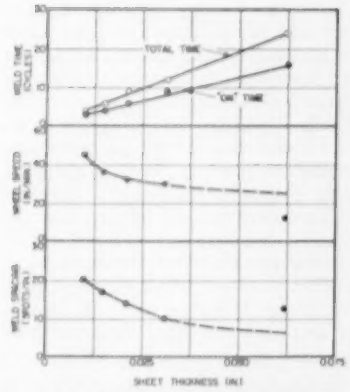

Fig. 11 Plot of weld spacing, wheel speed and weld time vs. sheet thickness

Fig. 12 Photomacrograph of a longitudinal section of a seam weld showing porosity, X 15

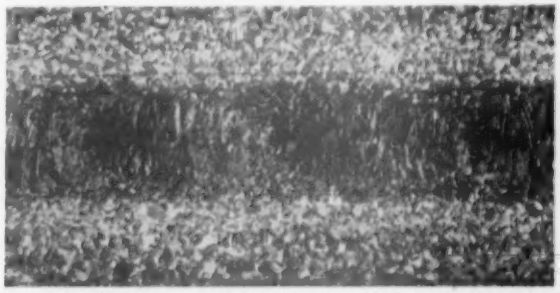

Fig. 13 Photomacrograph of a longitudinal section of a seam weld showing good overlap and elimination of porosity, X 15

the 0.021-in. sheet the optimum value of 750 lb previously determined for Inconel "X" was changed to a value of 850 lb for Inconel "W."

The optimum current ranges for the two alloys were slightly different for all gages investigated. Tables 6 and 7 indicate the spot-welding conditions for Inconel "W" and Inconel "X," respectively.

The strengths of the spot welds made at the optimum conditions measured by tensile-shear and normal-tension tests (see Table 8), were generally slightly lower than those of Inconel "X." This difference was predicted because the mechanical properties of Inconel "W," as-received, indicated that its strength was lower than that of Inconel "X." The strength-current relationships for both tensile-shear and normal-tension tests for the various thicknesses of Inconel "W" are shown in Figs. 4–8. Figure 9 is a plot of single spot shear strength of Inconel "X" and Inconel "W" as a function of sheet thickness.

Seam Welding

In seam welding, the optimum values

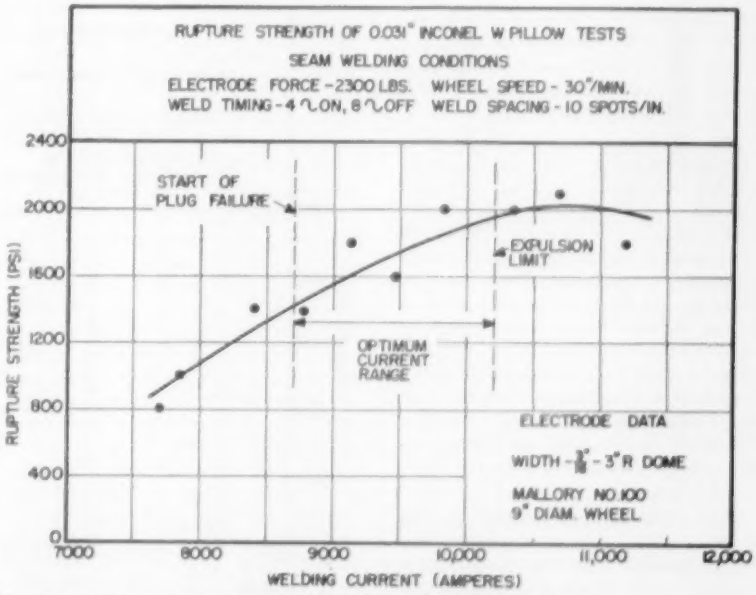

Fig. 14 Rupture strength of 0.031-in. Inconel "W" pillow tests

of weld spacing, welding speed, welding time, and electrode force were found to be the same as those recommended for Inconel "X." The electrode geometry was the same for all thicknesses except the 0.062-in. stock.

In seam welding 0.062-in. Inconel "W" with the conditions as determined for Inconel "X," excessive indentations and sheet separations were experienced. Increasing the electrode width from $^{5}/_{16}$ in. which was the recommended width for Inconel "X," to $^{1}/_{4}$ in., and maintaining the electrode force at the same value of 4000 lb decreased the electrode pressure and thereby eliminated the excessive indentation and sheet separation for Inconel "W." The results of rupture tests of pillow samples made with electrode widths of $^{5}/_{16}$ in. and $^{1}/_{4}$ in. and with all other variables kept constant, are shown in Fig. 10.

It is to be noted that although the $^{1}/_{4}$-in. electrode geometry is considered optimum for the welds made on 0.062-in. Inconel "W," the recommended values of the welding speed and the weld spacing were changed from their estimated optimum values. This change was made to compensate for the maximum obtainable electrode force of 4000 lb, which is approximately 25% less than optimum value of 5500 lb. The force of 5500 lb. was estimated by considering the electrode force requirement for spot welding and by comparing the electrode force requirements for seam welding the other thicknesses. Figure 11 shows the relationships between welding time, wheel speed and weld spacing as a function of sheet thickness. In this figure the dashed lines, extrapolations of the smooth curves, may be used to estimate the optimum conditions for welding thicker sheets. Note that for the 0.062-in. material the wheel speed and weld-spacing values studied do not fall on the curves since the estimated optimum welding force of 5500 lb was not attainable.

Figures 12 and 13 show the effect of varying the wheel speed and the weld spacing in seam welding 0.062-in. Inconel "W." Figure 12 shows a longitudinal section at ×15 of the seam weld using the estimated optimum conditions for all variables except the electrode force. In this case the weld is porous because the estimated optimum electrode force of 5500 lb was not attainable. Figure 13 shows a longitudinal section of a sound seam weld made at the recommended conditions. Note the change in weld spacing to compensate for a lower than optimum electrode force.

The optimum current ranges for the various thicknesses of Inconel "W" were somewhat different and generally broader than those determined for Inconel "X."

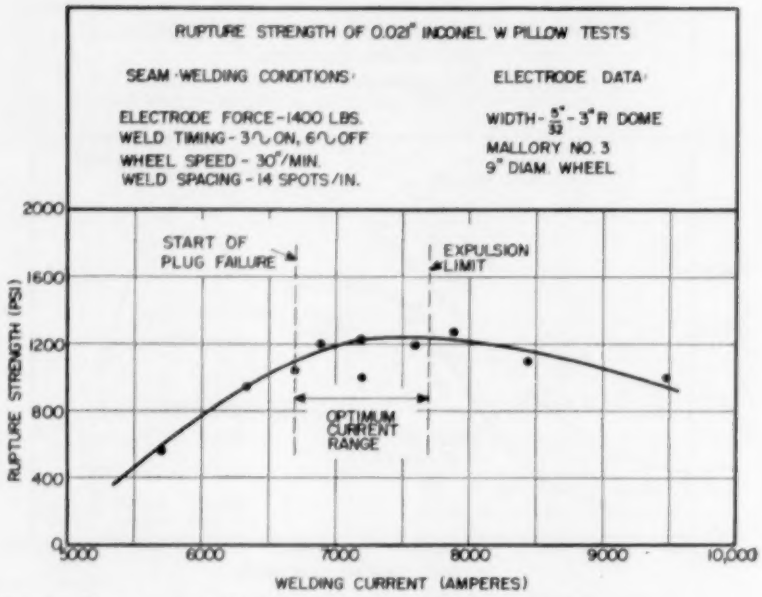

Fig. 15 Rupture strength of 0.021-in. Inconel "W" pillow tests

The pillow-test results indicated that the rupture strengths of the specimens made of Inconel "W" were in general slightly below those of Inconel "X." As mentioned previously this was expected in consideration of parent metal strengths. Figures 10 and 14–17 show the relationship between the rupture strength of pillow specimens and current for the various sheet thicknesses investigated. Tables 9 and 10 indicate the seam-welding conditions for Inconel "W" and Inconel "X," respectively.

Figure 18 is a photomacrograph of a transverse section of a sound seam weld produced with the recommended conditions for 0.062-in. Inconel "W." Figure 19 is a photomacrograph of a similar seam weld taken from the ruptured area of a pillow-test specimen, showing fracture along the edge of the fusion zone.

Figure 20 is a plot of maximum rupture strengths of the pillow specimens vs. sheet thickness for Inconel "W," Inconel "X" and Monel seam welds. It was originally hypothesized that each of the three alloys should have

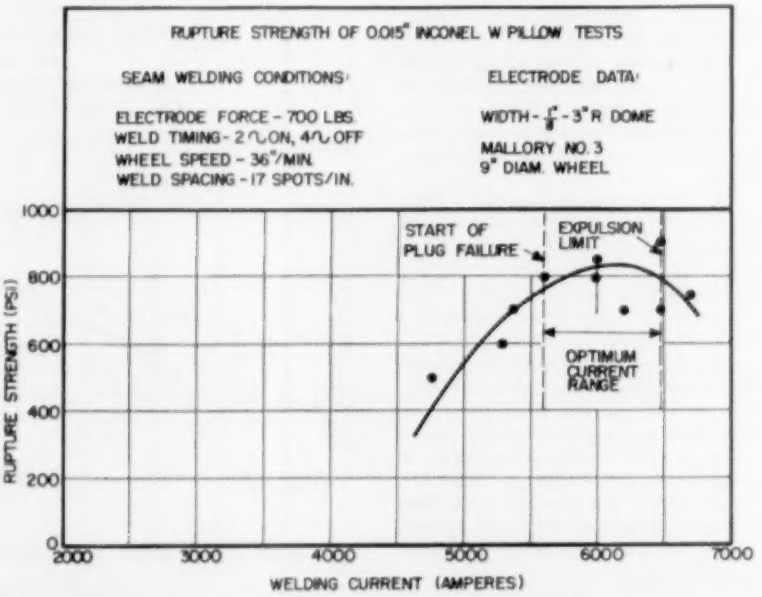

Fig. 16 Rupture strength of 0.015-in. Inconel "W" pillow tests

a linear relationship between the maximum rupture strength of its pillow samples vs. sheet thickness. This hypothesis, however, must be qualified by stating that such a relationship exists for the thinner gages, but as the sheet thickness increases the relationship is no longer linear.

However, with more ductile materials the initial linear relationship of the curve extends through thicker gages. Therefore, 0.062-in. Monel is still in the linear rage, whereas the same thickness for Inconel "X" or Inconel "W" is well out of the linear range.

The cause of this behavior is the stress concentrations introduced when testing the pillow samples. In a test of a pillow sample made of thin material the loading produces a diaphragm action and failure occurs under biaxial stress. This same type of stress concentration is also evident in thicker gages for more ductile material. However, for less ductile material, besides the diaphragm-action

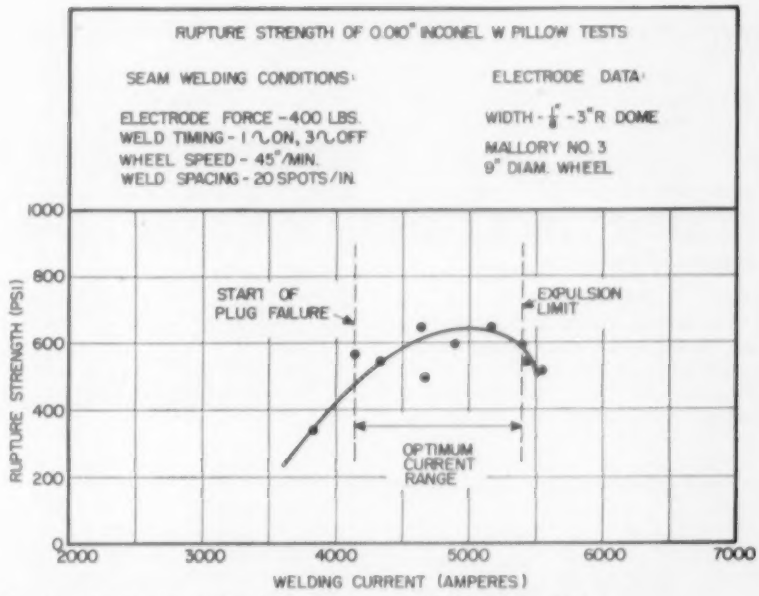

Fig. 17 Rupture strength of 0.010-in. Inconel "W" pillow tests

Fig. 18 Photomacrograph of a transverse section of a sound seam weld. ×13 (The areas along the grain boundaries in the heat-affected zone are not cracks, but "intergranular rivers." "Intergranular rivers" result from incipient fusion at the grain boundaries [5])

Fig. 19 Photomacrograph of a transverse section of a seam weld from a ruptured pillow sample showing the fracture outside the fusion zone, ×10

a beam-action is introduced, and hence the pillow sample is under triaxial stress causing earlier failure than would be expected under diaphragm-action

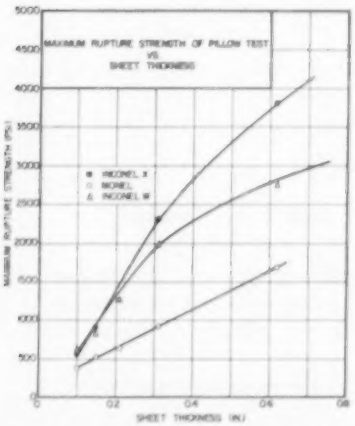

Fig. 20 Maximum rupture strength of pillow test vs. sheet thickness

alone. Figure 21 illustrates the relative amount of deformation in two pillow samples, the one on the right made of 0.062-in. Inconel "W," the one on the left 0.015-in. Inconel "W."

It is believed that if compensation were to be made in size of the pillow specimen as the thickness of the sheet to be tested was increased, this anomaly would be overcome. It should be noted in Fig. 20 that the values associated with 0.062-in. Inconel "W" and Inconel "X" probably have lower rupture strengths than those which would be obtained had the conditions used for welding these samples been optimum. This implies that the divergence of the curves from linearity is due partly to the compromise welding conditions used for welding 0.062-in. Inconel "W" and Inconel "X," and partly to the nature of the test itself.

Conclusions

1. The optimum conditions for spot and seam welding Inconel "W" were found to be similar to those previously determined for Inconel "X."

2. The strengths of the welds made on Inconel "W" under the prescribed conditions were comparable to the strengths attained for Inconel "X" of the same thickness.

3. The optimum current ranges in most cases were larger for Inconel "W" than those found for Inconel "X."

4. The welds made within the recom-

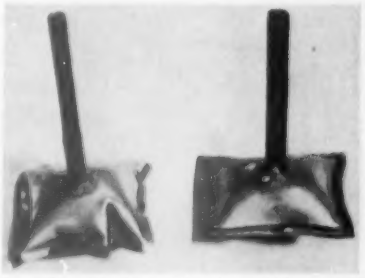

Fig. 21 Deformation in a thin gage (*left*) and a heavy gage (*right*) pillow sample

mended range satisfied the RWMA standards.

5. Before spot and seam welding of such alloys as Inconel "W" and Inconel "X," degreasing and pickling are essential.

6. Electrode alignment in spot and seam welding Inconel "W" especially in welding thin gages, is an important consideration. This was found previously to be true for Inconel "X."

Acknowledgments

The authors wish to acknowledge the sponsorship of this experimental investigation by the International Nickel Co., Inc., and to thank Dr. William A. Mudge and Robert M. Wilson, Jr., of that company for their advice and cooperation.

Bibliography

1. Nippes, E. F., and Fishman, H. B., "Optimum Spot and Seam Welding Conditions for Inconel "X." The Welding Journal, **34** (1), Research Suppl., 1-s to 14-s (1954).
2. Nippes, E. F., and Slaughter, G. M., "Seam Welding of Monel Metal," *Ibid.*, **30** (11), Research Suppl., 537-s to 543-s (1951).
3. Nippes, E. F., Pfluger, A. R., and Slaughter, G. M., "Seam Welding Monel Metal to Steel," *Ibid.*, **29** (3), Research Suppl., 134-s to 140-s (1950).
4. Hess, W. F., and Muller, A., "The Spot Welding of Nickel, Monel and Inconel," *Ibid.*, **20** (10), Research Suppl., 417-s to 426-s (1941).
5. "Resistance Welding Manual," Resistance Welder Manufacturers Assn., 1948.
6. Millar, N. P., and Kavalisuskas, A. A., "An Ampere-Squared-Second Indicator for Resistance Welding," *Elec. Engr.*, **69** (4), 362 (1950).
7. "Resistance Welding of Nickel and High-Nickel Alloys," Tech. Bull. T-33, International Nickel Co., Inc.

Correction:

"Stresses from Radial Loads and External Moments in Cylindrical Pressure Vessels"

by P. P. Bijlaard

•

In the December 1955 issue of THE WELDING JOURNAL RESEARCH SUPPLEMENT, *page 609-s, third column, sixth line, "Fig. 11b" should read "Fig. 11c". Also, page 613-s, Table 6, "β_1/β_2" should read "β_2/β_1".*

The Editor

REVIEWS
OF NEW BOOKS

Hütte, the German Engineer's Handbook. Vol. 1. Theoretical Foundations; published by Wilhelm Ernst & Sohn, Berlin, 1955, 1668 pages, 1409 illustrations, 28th edition. 36 German marks.

This is the first volume of eight comprising this comprehensive handbook for engineers of all fields. It is divided into nine sections. Section I on Mathematics contains tables of powers, roots and logarithms, and brief summaries of important practical results in such fields as algebra, calculus, and differential equations. Sections II to V deal with physics, heat, vibrations and mechanics. Section VI on strength of materials contains short sections on residual stresses and the notch strength of welds. Section VII is a materials handbook in itself, describing practically every engineering material. Section VIII describes methods of measurement.

The first edition of Hütte was issued in 1857 for students at the Royal Vocational Institute, now the Technical University of Berlin. The editors of the handbook then endeavored to combine scientific principles and practical experience to the exclusion of rigid doctrine and rambling theory. The tradition has been maintained in the present volume.

•

Welding with Electrodes Buried under Flux, by P. Berthet. Abstract of "Le soudage avec électrodes couchées sous flux," published in Soudage et Techniques Connexes, 9, 323–324 (1955). The author is an engineer at the French Institute of Welding. (Abstracted by Dr. G. E. Claussen.)

A simple process has been developed whereby firecracker welding has been made more foolproof. In this process a covered electrode of the type used for manual welding is laid along the joint to be welded. The electrode is connected to a source of dc or ac and is covered with flux to a depth of $^3/_8$ to $1^3/_{16}$ inches. A number of materials have been satisfactory as fluxes, such as powdered glass, blast furnace slag and foundry sand. A particularly simple, cheap and effective flux consists of river sand to which 5 to 8% by weight of potassium silicate (31° Bé) has been added. The flux may be used as a granular powder or as a paste.

During the fusion of the electrode, white smoke is evolved and a small blue flame burns above the weld zone. Slag is porous and easy to remove. The deposit is smooth and uniform. There is no spatter. Bare wire has been added to increase the deposit rate 25 to 31%. For surfacing applications several electrodes can be deposited in parallel. All standard types of coated electrodes have been deposited successfully.

The mechanical properties of the deposited metal were excellent. In one test with a $^1/_4$-in. 6013 electrode at 400 amp the tensile strength was 54,000 psi, elongation 27% and Charpy value 10 mkg/cm^2. The rate of deposit was about 5% slower than in firecracker welding under a copper mold.

WELDING RESEARCH COUNCIL BULLETIN No. 25

Bibliography of The Welding of Stainless Steels, 1926–1955 with Author Index

The Welding Research Council has just issued Bulletin No. 25 which is a Bibliography on The Welding of Stainless Steels covering the years 1926–1955, with Author Index. This bibliography was prepared by Mrs. Katherine Janis, Assistant Librarian, Development and Research Technical Library of the International Nickel Company, 67 Wall Street, New York 5, N. Y.

This Bulletin is priced at $1.00 a copy. Copies may be ordered through the American Welding Society, 33 West 39th Street, New York 18, N. Y.

WELDING OF HIGH-STRENGTH STAINLESS STEELS FOR ELEVATED-TEMPERATURE USE

Several high-strength stainless steels found to be weldable under conditions of high restraint using the inert-gas-shielded tungsten-arc process

BY J. J. VAGI AND D. C. MARTIN

ABSTRACT. Welding tests on stainless steels indicate that AMS 5643, AMS 5528, and AMS 5616 stainless can be welded under conditions of high restraint, using the inert-gas-shielded tungsten-arc process. Yield strengths of 100,000 psi or higher in weldments in AMS 5616, AMS 5643, and AMS 5528 were obtained by using postwelding heat treatments. However, to obtain reasonable elongations, it is necessary to solution anneal as part of the postwelding heat treatment (1700° F to 1900° F, depending on the alloy).

Preliminary tests on AMS 5735 stainless steel showed that this steel is extremely sensitive to hot cracking. X-ray diffraction and metallographic studies show the presence of a low-melting grain-boundary film.

Introduction

The welding characteristics of several high-strength stainless steels, considered for use as a pressure vessel to operate at high pressures at 800° F, have been determined. A survey of high-strength alloys indicated that those tabulated below were most likely to possess the desired properties.

AMS 5735 stainless steel
AMS 5616 stainless steel
AMS 5643 stainless steel
AMS 5528 stainless steel

Preliminary tungsten-arc welding tests were made to select the materials most readily weldable. An extensive study was made to develop sound welding procedures and to determine the effect of heat treatment on the properties of welded joints in the weldable alloys.

J. J. Vagi is Engineer and D. C. Martin is Assistant Chief, Battelle Memorial Institute, Columbus, Ohio.

Work performed under AEC Contract W-7405-eng-92.

Materials

The compositions of the high-strength steels investigated are given in Table 1.

Most of the material for the welding tests was received in the soft or solution-annealed condition in bars 6 in. wide and 2 in. nominal thickness. AMS 5528 plate was 8 in. wide. Heat treatments used for obtaining high strengths are given in the tables which report the results of tensile tests.

Test Procedures

All welding tests were made using the inert-gas-shielded tungsten-arc process. A standard 500-amp inert-gas-shielded tungsten-arc manual torch was used with a $^1/_8$-in.-diam Zirtung electrode. Commercial-grade welding argon was used as the shielding gas for welding all the materials. Straight-polarity direct current was used for all welding and was supplied by a 400-amp d-c generator.

The single-U groove-joint design shown in Fig. 1 was employed in all welding tests. A backup bar with a $^1/_{16}$-in.-deep groove machined in it was used to prevent excessive burn-through while making the root pass.

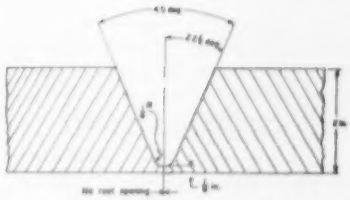

Fig. 1 Weld-joint design used for 2-in.-thick plates

In early tests of all materials except AMS 5528, the weldments were 2 in. thick and had 6-in.-long welds in them; welds in AMS 5528 were 8 in. long.

The machined plates were held in a restraining jig in such a position that the U-groove had no root opening. Runoff tabs were then tack welded in position. Welding was started and finished on the runoff tabs in each weld pass to remove any crater cracks from the actual weld specimen. The direction of welding was alternated each pass.

Most of the test weldments were made using filler metal of the same nominal composition as the base plate. One sample of AMS 5735 was welded with AMS 5528 filler metal. This special case is discussed in a later section.

The filler wire was first wiped clean with carbon tetrachloride, and then abrasion cleaned using No. 00 emery

Table 1—Typical Chemical Compositions of Alloys Studied

Alloy designation	*Composition, w/o**							
	C	*Cr*	*Ni*	*Al*	*Mn*	*Si*	*Fe*	*Other*
AMS 5616	0.15	13.00	2.00	0.15 max	0.50 max	0.5 max	Balance	0.05 max Sn, 3.00 W
AMS 5643	0.04	16.50	3.75	...	...	...	Balance	3.75 Cu
AMS 5528	0.07	17.00	7.00	1.10	...	...	Balance	...
AMS 5735	0.045	15.52	26.06	0.20	1.35	0.95	Balance	0.32 V, 1.95 Ti

* w/o = weight per cent.

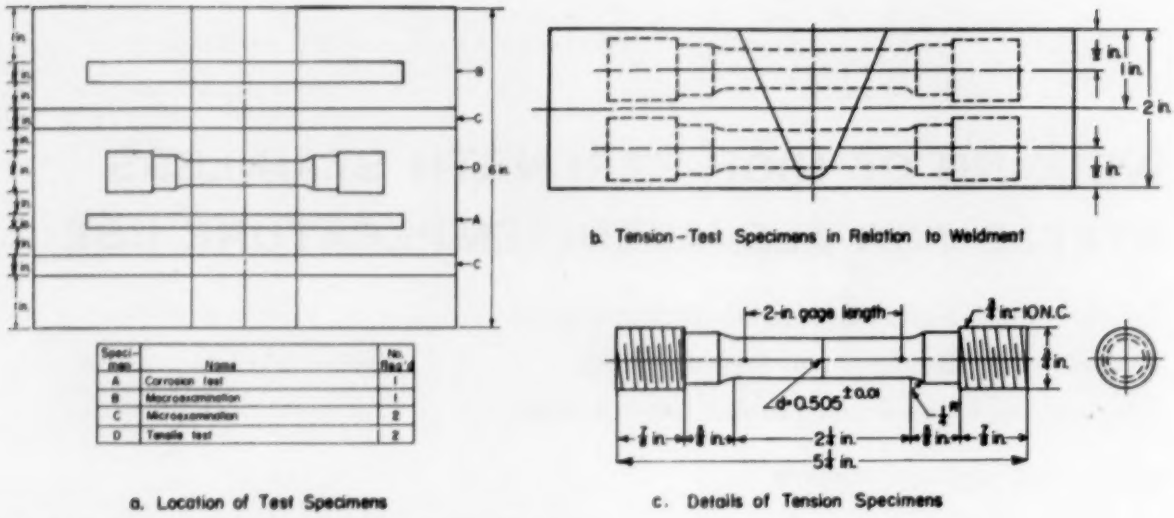

a. Location of Test Specimens

b. Tension-Test Specimens in Relation to Weldment

c. Details of Tension Specimens

Fig. 2 Test specimens from 2-in.-thick, 6-in.-long weldments

paper. This was followed by wiping again with carbon tetrachloride.

Completed welds were X-rayed to inspect for defects not observed during welding. Conditions used for radiography were: SOD, 36 in.; 350 kv; 5 ma; 10 min. The back sides of the welds were ground flush before X-ray inspection.

Following radiographic inspection, some weldments were heat treated, depending on the condition desired for testing. Then samples for mechanical tests and metallographic studies were machined from the weldments as shown in Fig. 2. Where defects were noted in radiographs of the welds, the specimens were rearranged so as to avoid incorporating the defect in one of the tension specimens.

Strength tests were made at 800° F, and values of ultimate strength, yield strength, reduction of area, and elongation in 2 in. were obtained.

Weldments of 24-in. length were made in only two of the materials. The tests made and specimens used are discussed in later sections.

Tests of AMS 5616 Stainless Steel

Welding Tests

Conditions used for welding are given in Table 2. All welds were made using $^1/_8$-in.-diam AMS 5616 filler wire of the same nominal composition as the base metal. The use of $^1/_8$-in.-diam wire was entirely satisfactory, but it was evident that a larger diameter wire would have decreased the total welding time considerably. With the exception of the first three passes and the reinforcing passes, all passes were peened with a round-nosed peening tool and an 8-lb chipping hammer. Peening was performed in an attempt to reduce warpage and to prevent cracking that might result from shrinkage stresses. No cracking was observed in any of the weldments during welding.

The weldments were radiographed prior to heat treatment in order to locate subsurface defects that could not be detected during welding. The radiographs revealed small amounts of porosity in all welds. The welds in B and D contained particles of heavy density that apparently were tungsten particles inadvertently spattered into the weld. To confirm the presence of porosity, the machined tension-test specimens were inspected with a dye penetrant. In general, failures in the tensile specimens did not appear to be related to specimen surface defects as shown by the dye.

Strength Tests of Small Weldments

Tension tests at 800° F were made on specimens machined from weldments treated as follows:

Weldment	*Treatment*
B and D	As-welded
A and C	1800° F, 2 hr, air cooled to room temperature; tempered at 1000° F, 2 hr, air cooled to room temperature

The specimens were machined from the welds, as shown in Fig. 2.

Results of short-time tension tests at 800° F are given in Table 3. The data indicated that considerable increase in strength could be obtained from post-welding heat treatment.

Table 2—Conditions Used for Welding 2-in.-Thick Plates of AMS 5616 Stainless Steel

	Weldment				
	A	*B*	*C*	*D*	*E*
Thickness, in.	2	2	2	2	2
Length, in.	6	6	6	6	24
Joint type	Single U-groove	Single U-groove	Single U-groove	Single U-groove	Single U-groove
Included angle, deg	45	45	45	45	45
Root radius, in.	$^1/_4$	$^1/_4$	$^1/_4$	$^1/_4$	$^1/_4$
Root land, in.	$^1/_8$	$^1/_8$	$^1/_8$	$^1/_8$	$^1/_8$
Root opening	0	0	0	0	0
Shielding gas	Argon	Argon	Argon	Argon	Argon
Flow rate, cfh	30	30	30	30	30
Electrode	Zirtung	Zirtung	Zirtung	Zirtung	Zirtung
Electrode diameter, in.	$^1/_8$	$^1/_8$	$^1/_8$	$^1/_8$	$^1/_8$
Filler—wire diameter, in.	$^1/_8$	$^1/_8$	$^1/_8$	$^1/_8$	$^1/_8$
Welding current, amp					
Root pass	315–320	315–320	360–365	300–305	300–305
Remaining passes	360–365	360–365	300–305	300–305	300–305
Preheat temp, F	500	500	500	70	70
Interpass temp, F	500	500	500	300	300
Welding speed, ipm	2–4	$1^1/_2$–3	2–$2^1/_2$	2–$2^1/_2$	$1^1/_2$–$3^1/_2$

Table 3—Results of Tension Tests at 800° F on Weldments of 2-in.-Thick AMS 5616 Stainless Steel

Condition	Specimen[a]	0.2% offset yield strength, psi	Tensile strength, psi	Elongation in 2 in., %	Reduction of area, %	Location of fracture
As-welded	B-U	84,000[b]	105,500	7.5	40	Heat-affected zone and base metal
	B-L	72,000	93,600	12.7	53	Heat-affected zone and base metal
	D-U	85,200	110,000	6.5	16	Heat-affected zone and base metal
	D-L	73,000	95,700	13.3	51	Heat-affected zone and base metal
Welded and heat treated at 1800° F, 2 hr, air cooled to room temperature; tempered at 1000° F, 2 hr, air cooled to room temperature	A-U	119,500	154,600	12.5	32	Weld
	A-L	112,000[c]	159,300	13.5	53	Base metal
	C-U	124,200	164,000	9.5	25	Heat-affected zone and base metal
	C-L	130,400	169,500	13	49	Weld

[a] Specimen machined from upper or lower portion of weldment designated by U or L, respectively.
[b] Extensometer slipped prior to 0.2% offset yield strength.
[c] Grip broke at 0.006 strain; specimen was rerun.

Hardness surveys on as-welded and on welded and heat-treated AMS 5616 alloy indicated that the weld-metal hardness in the as-welded condition was slightly higher than the hardness of the base metal. A fairly uniform hardness was obtained in the weld joints after they were heat treated. Results of hardness surveys on two sections are summarized below.

	Hardness range, Rockwell C	
	Unaffected base metal	Weld
As-welded	20.5–23.8	26.0–33.0
Welded and fully heat treated	39.3–43.0	39.0–43.0

In tension tests, weldments which were not heat treated would be expected to fail in the base metal because of the higher hardness and correspondingly increased strength of the weld metal. This was borne out by tension-test results shown in Table 3. The scatter in the location of failure and uniformity of hardness obtained with fully heat-treated specimens indicates that there is no particular zone of weakness in heat-treated weld joints in AMS 5616.

Strength Tests of 24-in. Weldment

As the results obtained in the welding tests on 6-in.-long samples appeared promising, a 24-in.-long weldment in 2-in.-thick plate, Weldment E, was made to determine whether such lengths were weldable, and to determine the properties of the weld. X-rays of this weldment revealed porosity in the weld. Several particles of tungsten inclusions from the welding electrode also were noted. The weldment was heat treated using the same treatment as was used for the small weldments. After heat treatment, tension-test specimens were machined from one portion of the weld, and the remaining portion was reserved for stress-rupture tests. The manner

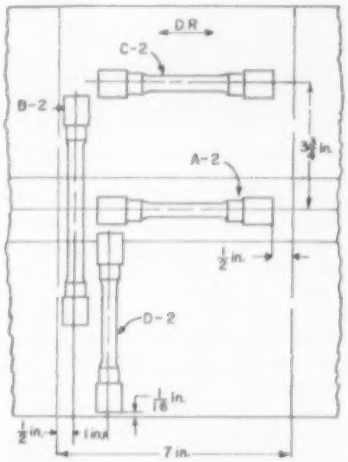

Fig. 3 Location of specimens machined from 24-in.-long weldments

in which the tension specimens were machined from the weldment is shown in Fig. 3. Tension-test results obtained at 800° F on the heat-treated tension specimens are summarized in Table 4.

It is obvious from the data in this table that weldments in AMS 5616 have excellent strengths at 800° F. However, the weld itself had rather low ductility. To determine whether this might affect the behavior of AMS 5616 weldments in service will require tests other than short-time tension tests.

Tests of AMS 5643 Stainless Steel

Welding Tests

Six 6-in.-long samples were made for the welding tests; these were designated as Weldments F, G, H, I, J and K. One sample 24 in. long, Weldment L, was also prepared. During welding, the plates were held in the restraining jig, in a position such that there was no root opening. Conditions used for welding are given in Table 5.

In Weldments F through J, 1/8-in.-diam filler wire was used; 5/16-in.-diam filler wire was used on Weldments K and L. The size of filler wire did not appear to have much effect on the behavior of the alloy during welding. The welding speeds were about the same with the two sizes of wire.

During the welding tests on Sample F, the root pass was made using 295- to

Table 4—Results of Tension Tests at 800° F on Specimens Machined from 24-in.-Long Weldment of 2-in.-Thick AMS 5616 Stainless Steel

Condition	Specimen[a]	0.2% offset yield strength, psi	Tensile strength, psi	Elongation,[b] %	Reduction of area, %
Welded and heat treated at 1800° F, 2 hr, cooled to room temperature with an air blast, tempered at 1000° F, 2 hr, air cooled to room temperature	EA-2U	141,000	187,800	11.6	28.4
	EA-2L	139,500	190,300	4.1	7.7[c]
	EB-2U	137,000	177,700	3.8	11.0[d]
	EB-2L	137,000	184,200	4.5	8.8[d]
	EC-2U	126,700	166,000	12.5	38.4
	EC-2L	125,600	171,700	13.5	40.6
	ED-2U	134,500	182,000	5.0	7.0
	ED-2L	135,800	180,200	6.8	9.5

[a] U and L represent samples from the upper and lower portions of the weld, respectively.
[b] Transverse tension specimens had 3-in. gage length; remaining specimens had 2-in. gage length.
[c] Defect found at fractured surfaces.
[d] Failed outside of weld.

Table 5—Conditions Used for Welding 2-in.-Thick Plates of AMS 5643 Stainless Steel

	Weldment F	G	H	I	J	K	L
Thickness, in.	2	2	2	2	2	2	2
Length, in.	6	6	6	6	6	6	24
Joint Type	Single-U groove	Single-U groove	Single-U groove	Single-U groove	Single-U groove	Single-U groove	Single-U groove
Included angle, degrees	45	45	45	45	45	45	45
Root radius, in.	1/4	1/4	1/4	1/4	1/4	1/4	1/4
Root land, in.	1/8	1/8	1/8	1/8	1/8	1/8	1/8
Root opening	0	0	0	0	0	0	0
Shielding gas	Argon	Argon	Argon	Argon	Argon	Argon	Argon
Flow rate, cfh	30	30	30	30	30	30	30
Electrode	Zirtung	Zirtung	Zirtung	Zirtung	Zirtung	Zirtung	Zirtung
Electrode							
Diameter, in.	1/8	1/8	1/8	1/8	1/8	1/8	1/8
Filler-wire							
Diameter, in.	1/8	1/8	1/8	1/8	1/8	3/16	3/16
Welding current, amp							
Root pass	360–365	295–300	295–300	360–365	300–305	315–300	295–300
Remaining passes	295–300	Varied	295–300	295–300	300–305	310–315	295–300
Preheat temp, F	300	70	300	300	300	200–250	200–250
Interpass temp, F	300	70–300	300	250–300	300	200–250	200–250
Welding speed, ipm	2–6	2–6	1 1/2–4 1/2	2–4 1/2	1 1/2–4	1 1/2–4 1/2	1 1/2–5

300-amp straight-polarity direct current; no cracks were observed. Passes 2 to 15 were made using 275 to 288 amp; no cracks were observed. Passes 16 to 19 also were crack free and were made using 355 to 360 amp. Passes 20, 21, and 22 were made using 415 to 420 amp. A 1/2-in.-long longitudinal crack was observed near the middle of the weld in Pass 21. The welding current was lowered to 400–405 amp for the five succeeding passes. On Pass 26, a 1/2-in.-long longitudinal crack developed at the end of the weld. Again, the welding current was reduced, this time to 295–300 amp. Welding was continued at that welding current until the weld was completed. No further cracking was observed in the total of 81 passes required to make the weld. The cracking observed occurred only in weld passes made with welding currents of 400 amp or more. Consequently, the remaining weldments were made with welding currents below 400 amp, as shown in Table 5. In addition, each pass after the third pass, except the reinforcing passes, was peened to reduce warpage.

After radiographic inspection, the weldments were heat treated and then machined into specimens for strength tests, metallographic studies, and hardness surveys.

Table 6 shows the hardness data obtained on both as-welded and heat-treated weldments of AMS 5643 alloy.

Photomacrographs of polished and etched sections from Weldments F to J are shown in Fig. 4. Weldment I contains cracks in the heat-affected zone on each side of the weld. Figure 5 shows part of a crack at a higher magnification and shows that the crack is aligned with the ferrite stringers. Figure 6 shows another part of the same crack, in which the failure follows along a series of ferrite stringers. Hardness tests made with a Knoop hardness tester showed that hardnesses of the ferrite stringers ranged from 263 to 282. The heat-treated matrix near the stringers had a Knoop hardness range of 419 to 458. Examination indicated that the crack started in the high-temperature edge of the heat-affected zone and propagated through the low-temperature edge and on into the material that was solution treated when the weld was made. Whether cracking occurred during welding due to the high restraint or during subsequent heat treatment was not determined. However, it appears that the cracking was related in some way to the ferrite stringers.

Examination of the section shown in Fig. 4 indicated that as-welded and welded-and-aged samples contained zones where some precipitation occurred near the low-temperature edge of the heat-affected zone. On approaching the fusion line from the low-temperature edge of the weld joint, areas of precipitation-hardened, overaged, and solution-treated structures were observed in these samples. On solution treatment, the precipitate was redissolved in the matrix, and uniform precipitation was obtained on reaging, as shown in sections from Weldments I and J.

Table 6—Heat Treatment and Hardness of AMS 5643 Weldments

Weldment	Heat treatment	Hardness, Rockwell C: Unaffected base metal	Weld
F	As-welded	32.0–37.0	35.0–37.0
G	Welded and aged at 875° F, 1 hr, air cooled to room temperature	41.9–45.0	37.8–43.1
H	Welded and aged at 1100° F, 1 hr, air cooled to room temperature	35.9–37.3	33.0–38.0
I	Welded and solution treated at 1900° F, 1 hr, air cooled to room temperature, water cooled to below 60° F; aged at 875° F, 1 hr, air cooled to room temperature	41.8–44.9	41.0–43.3
J	Welded and solution treated at 1900° F, 1 hr, air cooled to room temperature, water cooled to below 60° F; aged at 1100° F, 1 hr, air cooled to room temperature	35.5–37.9	35.3–37.0
L	Welded and solution treated at 1700° F, 1 hr, cooled to room temperature with an air blast; aged at 1100° F, 2 hr, air cooled to room temperature	.....	.....

Strength Tests of Small Weldments

Strength tests were made at 800° F on transverse tension-test specimens, 0.505-in.-diam, 2 1/2-in. reduced section, shown in Fig. 2. Results of the strength tests on as-welded and welded and heat-treated samples are given in Table 7. It is apparent that considerable improvement in strength can be obtained by solution treating and aging at 875° F after welding. However, there was no

Weldment F: as-welded; X1.

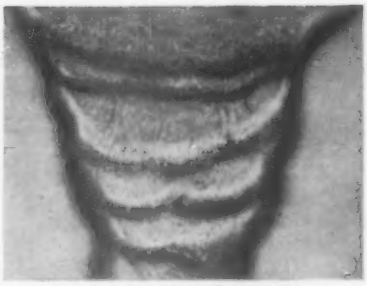

Weldment G: aged at 875° F; X1

Fig. 4 Sections of as-welded, welded and aged, and welded, solution-treated, and aged AMS 5643 weldments. (Reduced by 1/4 upon reproduction)

Weldment H: aged at 1100° F; X1.

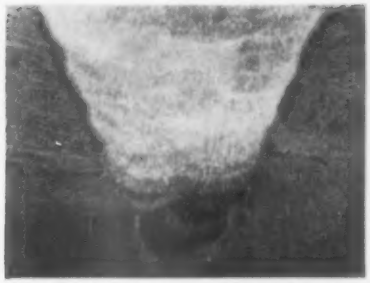

Weldment I: solution treated and aged at 875° F; X1

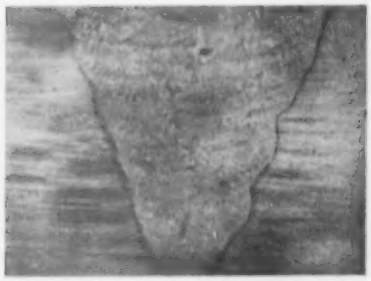

Weldment J: solution treated and aged at 1100° F; X1.

improvement in elongation and reduction of area. When 1100° F is used as the aging temperature, some improvement in elongation is obtained with only a small sacrifice in strength.

Strength Tests of 24-In. Weldment

After determining satisfactory welding procedures in the earlier tests, a weldment was made in 2-in.-thick AMS 5643 plate, 24 in. long. This sample was designated L, and the conditions for welding are given in Table 5. A total of 57 passes were required to make the weld. No cracking was observed in any of the passes during welding.

Radiographic inspection of Weldment L disclosed only a slight amount of porosity in the weld; no cracks, tungsten inclusions, or other defects were noted. Weldment L was solution treated at 1700° F, rather than 1900° F. The reason for this change in solution-treating temperature was the rather low ductility obtained in the strength tests of the small weldments. Aging at 1100° F also promotes higher ductility than aging at lower temperatures.

After heat treatment, tension specimens were machined from the weldment as shown in Fig. 3. Results of strength tests at 800° F on the tension specimens machined from the 24-in.-long weldment are given in Table 8.

Welding and Strength Tests of AMS 5528 Stainless Steel

As there was some delay in obtaining this material for welding tests, only one sample was welded. The welding test was made on highly restrained 2-in.-thick AMS 5528 plate with an 8-in.-long single-U groove machined in it.

Root-pass welding was done using 195- to 200-amp straight-polarity direct current. The remaining passes were made using 300- to 305-amp straight-polarity direct current, and 250° F interpass temperature. AMS 5528 filler wire, 3/16-in.-diam, was used in making all weld passes. Welding speed was 3 to 5 ipm. With the exception of the first three and the last five passes, all weld passes were peened to reduce warpage. A total of 43 weld passes were required to make the joint. No cracks were visible at any time during welding.

A radiograph of the weld showed some scattered porosity and a small amount of tungsten. The weldment was cut into two parts. Tension-test specimens and metallographic samples were machined from one part for use in the as-welded condition. The remaining piece was heat treated as follows: 1400° F, 1 1/2 hr, air cooled to room temperature, water cooled to 60° F; aged at 1050° F, 1 1/2 hr, air cooled to room temperature.

The hardness of the unaffected base metal increased from 83 R_B before heat

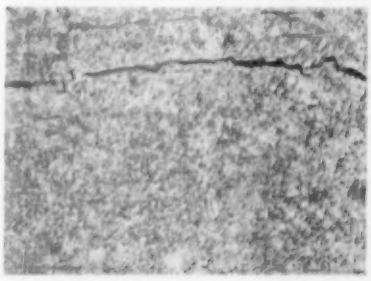

Picral etch; X100.

Fig. 6 Another part of the crack shown in Fig. 5, showing the tendency of the crack to follow along the ferrite stringers. (Reduced by 1/2 upon reproduction)

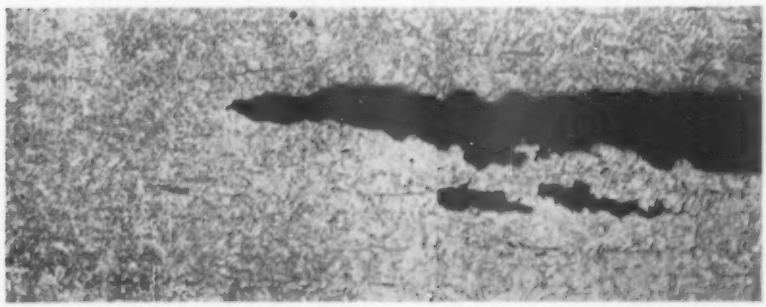

Picral etch; X100

Fig. 5 Crack on left side of weld in Weldment I showing start of crack adjacent to the weld. (Reduced by 1/2 upon reproduction)

Table 7—Results of Tension Tests at 800° F on Weldments of 2-in.-Thick AMS 5643 Stainless Steel

Condition	Specimen[a]	0.2% offset yield strength, psi	Tensile strength, psi	Elongation in 2 in., %	Reduction of area, %	Location of fracture
As-welded	F-U	105,000	136,700	5.3	8	Weld and heat-affected zone
	F-L	103,500	131,200	4.6	[b]	Weld and heat-affected zone
	K-1-U	103,800	137,700	4.5	11	Weld and heat-affected zone
	K-1-L	106,500	134,500	4.4	12	Weld and heat-affected zone
Welded and aged at 875° F, 1 hr, air cooled to room temperature	G-U	[c]	43,100	1.4	0.1	Weld
	G-L	119,200	132,500	2.5	6	Weld
	K-2-U	115,000	141,100	4.0	16	Weld and heat-affected zone
	K-2-L	115,500	139,800	5.5	26	Weld and heat-affected zone
Welded and aged at 1100° F, 1 hr, air cooled to room temperature	H-U	109,500	122,200	9.4	35	Weld, heat-affected zone, and base metal
	H-L	106,500	116,200	8.5	34	Weld, heat-affected zone, and base metal
	K-3-U	106,500	121,600	8.5	22	Weld
	K-3-L	111,500	125,500	7.0	28	Heat-affected zone and base metal
Welded and solution treated at 1900° F, 1 hr, air cooled to room temperature, water cooled to below 60° F; aged at 875° F, 1 hr, air cooled to room temperature	I-U	[d]	113,000	..	..	Weld
	I-L	123,200	161,000	3.5	7	Weld
	K-4-U	129,200	161,000	4.0	2	.....
	K-4-L	126,000	169,800	4.5	8	.....
Welded and solution treated at 1900° F, 1 hr, air cooled to room temperature, water cooled to below 60° F; aged at 1100° F, 1 hr, air cooled to room temperature	J-U	115,200	131,000	3.5	[b]	Weld
	J-L	122,500	134,250	7.5	26	Heat-affected zone and base metal
	K-5-U	112,500	120,750	9.5	31	Weld
	K-5-L	118,800	128,800	7.0	8	Weld and heat-affected zone
Welded and solution treated at 1900° F, 1 hr, air cooled to room temperature, water cooled to below 60° F; aged at 1200° F, 1 hr, air cooled to room temperature	K-6-U	101,000	109,500	9.0	32	Weld
	K-6-L	103,200	115,500	13.0	36	.....

[a] U and L represent specimens machined from upper and lower portions of the weldment, respectively.
[b] Reduction of area was not measurable because of type of fracture.
[c] Specimen was cracked.
[d] Specimen broke at 0.005 in. strain on rising load.

treatment to 46 Rc after the heat treatment.

The results of tension tests at 800° F on as-welded and on welded and heat-treated samples are reported in Table 9.

Weldments in AMS 5528 have rather low strengths in the as-welded condition. Heat treatment is required to develop high strengths. The properties of AMS 5528 weldments should be compared with the properties of weldments in AMS 5643, where yield strengths greater than 100,000 psi were obtained in as-welded specimens.

Welding Tests of AMS 5735 Stainless Steel

At the start of the investigation, AMS 5735 was considered to be one of the most promising alloys because of its high strength at elevated temperatures. However, other investigators had found that the alloy was susceptible to heat affected-zone cracking.

Tests with AMS 5735 Filler Metal

Preliminary welding studies of this alloy were started using a double-U joint machined in turbine-disk sections. The argon-shielded tungsten-arc process was used with 280-amp straight-polarity direct current and no filler metal. The root bead on the first side contained both porosity and an 8-in.-long longitudinal crack. Welding on the other side of the joint produced a longitudinal crack the length of the weld. This crack is shown in Fig. 7. A weld was made in 2-in.-thick AMS 5735 plate with AMS 5735 filler metal and high restraint. All four passes were cracked; the cracks appeared to follow the dendritic pattern.

A test was made in a 2-in.-thick joint of AMS 5735 to determine whether a sound root pass could be obtained under conditions of low restraint. The root pass was made in a single-U joint using no restraint on the plates, a $^1/_{32}$-in. root clearance, and 250-amp straight-polarity direct current. The root pass, to visual observation, was crack free. However, cracking occurred in all subsequent passes.

In an attempt to minimize the high

Table 8—Results of Tension Tests at 800° F on Specimens Machined from 24-in.-Long Weldment of 2-in.-Thick AMS 5643 Stainless Steel

Condition	Specimen[a]	0.2% offset yield strength, psi	Tensile strength, psi	Elongation,[b] %	Reduction of area, %
Welded and heat treated at 1700° F, 1 hr, cooled to room temperature with an air blast; aged at 1100° F, 2 hr, air cooled to room temperature	LA-2U	103,000	113,700	9.8	25.0
	LA-2L	104,500	114,600	7.2	9.9[c]
	LB-2U	101,900	111,500	9.7	14.7
	LB-2L	106,500	115,200	10.2	21.0[d]
	LC-2U	105,300	113,500	11.7	35.6
	LC-2L	104,300	112,300	12.9	38.5
	LD-2U	103,800	112,000	10.9	34.5
	LD-2L	106,200	114,300	9.4	30.0

[a] U and L represent samples from the upper and lower portions of the weld, respectively.
[b] Transverse tension specimens had 3-in. gage length; remaining specimens had 2-in. gage length.
[c] Defect found at fractured surfaces.
[d] Failed outside of weld.

Table 9—Results of Tension Tests at 800° F on Weldments of 2-in.-Thick AMS 5528 Stainless Steel

Condition	Designation[a]	0.2% offset yield strength, psi	Tensile strength, psi	Elongation in 2 in., %	Reduction of area, %	Location of fracture
As-welded	U	64,500	85,500	5.5	45.0	Base metal
	L	47,800	75,500	16.0	58.0	Base metal
Welded and heat treated at 1400° F, 1½ hr, air cooled to room temperature, water cooled to below 60° F; aged at 1050° F, 1½ hr, air cooled to room temperature	U	136,000	144,000	1.5	1.8[b]	Weld
	L	131,500	141,300	3.7	7.2	Weld

[a] U and L represent specimens from upper and lower portions of the weldment, respectively.

[b] Defect found at fractured surfaces.

shrinkage stresses obtained during the welding of 2-in.-thick plates, the weld bead was peened immediately after deposition in another test. Although cracking was not eliminated by this procedure, the amount of cracking decreased.

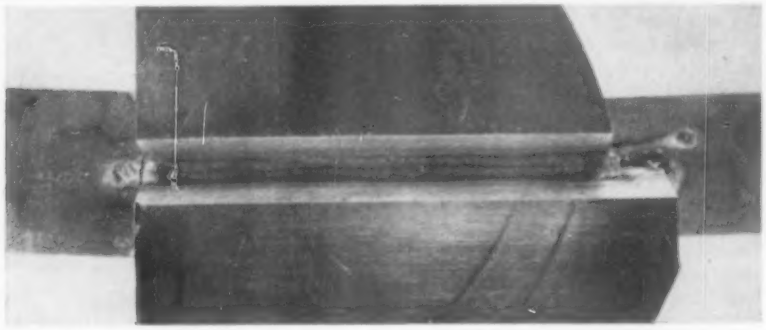

As-welded

Fig. 7 Longitudinal crack in root pass of 2-in.-thick AMS 5735 stainless steel

Metallographic and X-ray diffraction studies were made of AMS 5735 weldments and base materials to try to find the causes of cracking. The metallographic studies were made of AMS 5735 plate in various heat-treated conditions. The specimens were in the solution-treated, aged, overaged, and overheated conditions. Figs. 8 through 11 show the structures of AMS 5735 after various heat treatments. The specimen in the overheated condition contained intergranular cracks, as shown in Fig. 12.

The most important feature of these photomicrographs is the secondary phase in the grain boundaries of the overheated specimen (Fig. 11). It was believed that the grain-boundary constituent which appeared in the overheated specimen might be the cause of the hot shortness. An attempt was made to determine the composition of this grain-boundary phase.

X-ray diffraction examination of the polished and etched surfaces of specimens in the various heat-treated conditions showed only the diffraction lines of the base metal. Therefore, it was necessary to extract the grain-boundary phase or phases for X-ray examination by mechanical removal after deep etching. Attempts to extract the grain-boundary phase mechanically were successful only for the specimen overheated at 2450° F. An X-ray sample obtained by probe removal of the grain-boundary material of this specimen showed a strong pattern of $TiFe_2$.

The observed incipient melting in the grain boundaries could not have occurred with $TiFe_2$, which has a melting point of 2786° F. However, there is a eutectic between iron and $TiTe_2$ at approximately 86 w/o iron. The eutectic

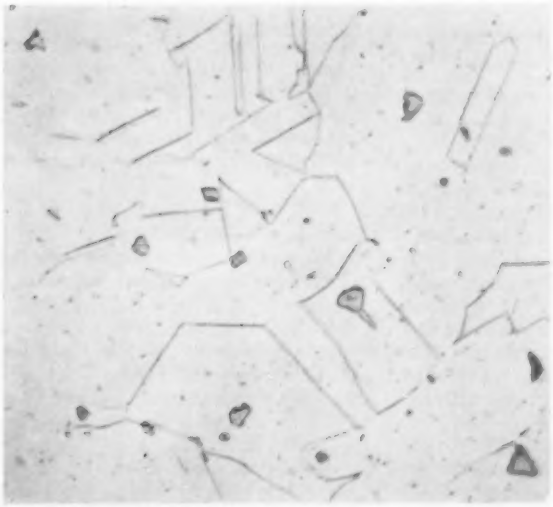

4 HCl:1 HNO_3 etch; X500

Fig. 8 AMS 5735, solution treated at 1800° F, 1 hr, oil quenched

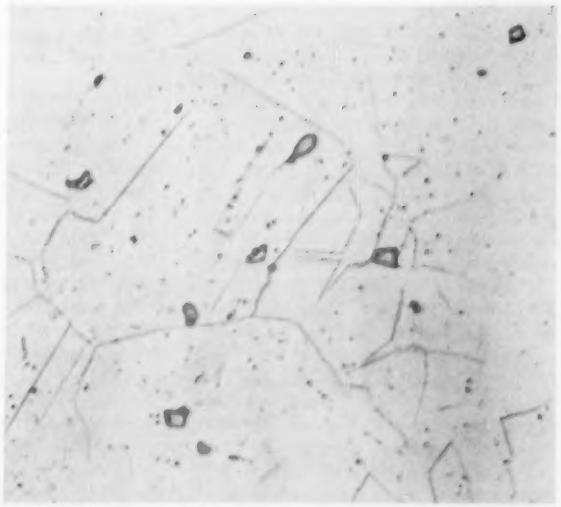

4 HCl:1 HNO_3 etch; X500

Fig. 9 AMS 5735, aged at 1325° F, 8 hr, air cooled

4 HCl: 1 HNO_3 etch; X500

Fig. 10 AMS 5735, overaged at 1500° F, 8 hr, air cooled

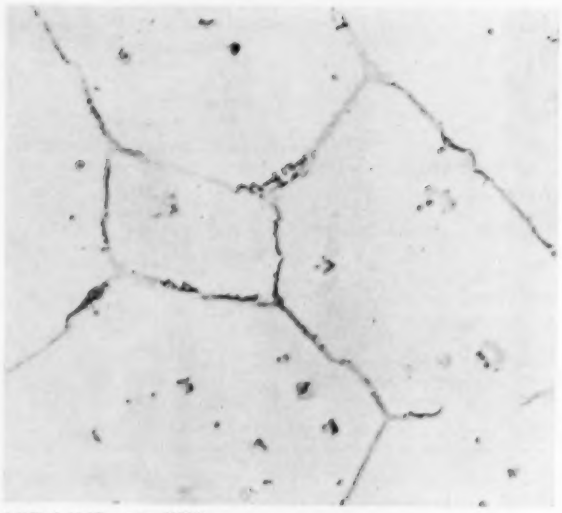

4 HCl: 1 HNO_3 etch; X500

Fig. 11 AMS 5735, overheated at 2450° F, 15 min, water quenched

temperature is 2390° F. This temperature is probably low enough to cause hot shortness.

It would appear from these results that the cracking of restrained weldment in AMS 5735 may be due to the presence of $TiFe_2$. As the presence of titanium is essential for age hardening in this alloy, it would appear that crack-free weldments cannot be obtained when high restraint and AMS 5735 filler metal are used. The only possibility appears to be the use of another alloy for filler metal.

Tests with AMS 5528 Filler Metal

As cracking was obtained in every test in which 2-in.-thick AMS 5735 was welded using AMS 5735 filler metal, tests were made using AMS 5528 filler metal. This alloy was used because it was thought that a hardening heat treatment could be found which would work for both weld metal and base metal. The initial tests indicated lower susceptibility to cracking with AMS 5528 filler metal, but cracking was not eliminated. A test was made using peening immediately after deposition of each weld bead. This hot-peening procedure appeared to eliminate cracking. Therefore, a weldment was made in 2-in.-thick AMS 5735 using AMS 5528 filler metal and hot peening.

The conditions used to weld this specimen were similar to those used for AMS 5616. A single-U joint was used. Argon shielding was provided, 50 cfh to the underbead area during the first pass and 30 cfh through the torch. No preheat was used, and a maximum interpass temperature of 250° F was maintained. Starting with the second pass, peening was done immediately following the weld pool.

The only cracking recorded was in the root pass, $^1/_8$ in. from the beginning of the pass and $^9/_{16}$ in. long. In all, 45 passes were used to fill the joint.

After welding, four $^7/_8$-in.-thick specimens and three $^1/_2$-in.-thick specimens were cut from the weldment transverse to the weld. An inspection using a dye penetrant was made on the cut samples machined from the weldment. The inspection showed porosity in the weld metal and cracks along the fusion line.

These tests showed that it was possible, using AMS 5528 as filler metal, to deposit a sound weld in AMS 5735. However, the cracking in the heat-affected zone was still severe, and, until this can be overcome, there appears to be little hope that sound thick-plate weldments can be obtained in this alloy.

Discussion of Results of Welding Investigation

Results now available on the welding characteristics of the stainless steels investigated indicate that highly restrained thick plates of both AMS 5643 and AMS 5616 stainless can be welded satisfactorily using the conditions outlined in previous sections. Although the welds were peened, the exact effect of peening was not determined. It was found that the strengths of weld joints in the AMS 5643 alloy and in the AMS 5616 stainless steel could be improved by post-welding heat treatment.

From the small amount of work done with AMS 5528, this alloy also appears to show promise in its ability to be welded in heavy sections under high restraint.

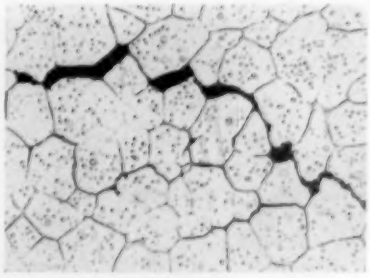

Aqua regia etch; X100

Fig. 12 Crack in overheated AMS 5735 stainless steel. (Reduced by $^1/_2$ upon reproduction)

The AMS 5735 alloy did not appear to be promising in the welding tests. Several weldments were made in $^3/_8$-in.-thick plate and appeared to be satisfactory. However, in heavy plate, highly restrained, attempts to weld the AMS 5735 alloy were entirely unsuccessful.

Acknowledgments

The authors wish to acknowledge the valuable discussions and suggestions made by P. J. Rieppel and C. B. Voldrich under whose supervision this work was conducted. We wish to thank Dr. H. W. Russell and Vernon Thompson for their technical assistance, and John Dethloff, who made the weldments described in this paper.

Acknowledgment is due to Arthur Levy and Michael Kycia, Pratt and Whitney Aircraft, for their interest and assistance.

CONTROLLED LOW-TEMPERATURE STRESS RELIEVING OF PRESSURE VESSELS

Tests indicate that controlled low-temperature stress-relieving process is a practical method of stress-relieving large structures, field erected tanks and final assembly welds of pressure vessels

BY T. W. GREENE AND C. R. McKINSEY

ABSTRACT. Controlled low-temperature stress relieving is accomplished by progressively and simultaneously heating two 6-in. wide bands, one on each side of the weld, to 350–400° F while keeping the weld relatively cool. The longitudinal expansion of the heated bands stretches the weld plastically, and when temperature equilibrium is again established, weld stresses have been reduced. This process was applied to three large propane storage tanks constructed of ASTM A-212 steel. Stress measurements were made before and after stress relieving. The results showed that use of this process reduced the residual welding stresses to very low values on all seams without significant distortion. Even the high residual tensile stresses in welded plugs were reduced to negligible values.

Introduction

It is well known that residual tensile stresses of high magnitude are normally present in welded joints in both the weld metal and the immediately adjacent base metal. The need for reducing these stresses to low levels for certain welded structures is also well established, and thermal stress relieving is specified for certain unfired pressure vessels constructed according to the ASME Boiler and Pressure Vessel Code.[1] However, many welded structures, because of size and shape or due to field assembly or erection, cannot be stress relieved in furnaces. For such structures, stress relief is sometimes attempted by heating a band containing the weld to 1100° F or higher. However, this so-called "local stress relieving" can be dangerous if misapplied, since it is possible to increase, rather than decrease, the residual stress or even to cause fracture in complex, rigid structures.[2]

During World War II, a method of stress relieving was developed that is not only applicable directly to welded joints that otherwise could not be stress relieved, but which also accomplishes the desired result at moderate temperatures, so that problems associated with distortion are not encountered. This method became known as the controlled low-temperature stress-relieving process. The name is somewhat misleading, however, because the temperature is not low in the sense that the words "low temperature" are normally used, but only low in relation to the temperatures used in furnace stress relieving. Furthermore, the heat introduced does not relieve the stresses, but is only a means of causing local expansion. As described by Greene and Holzbaur,[3] the stress reduction is accomplished by simultaneously heating two 6-in. wide bands, one on each side of the weld, to 350–400° F, while keeping the weld relatively cool. The force thus developed by the thermal expansion of the heated bands mechanically stretches the weld metal. Since the residual stress in the weld is at or near yield strength magnitude in tension, the weld is forced to flow plastically while the stress in the heated base metal remains in the elastic range. Upon cooling, equilibrium conditons are reached at a new and lower stress level.

In order to understand the principles of the low-temperature stress-relieving process, it is necessary to consider the following questions:

1. How does mechanical straining reduce residual stresses?
2. Is it possible to achieve the required amount of strain by heating

T. W. Greene, now deceased, was formerly Welding Engineer, Linde Air Products Co., New York, and C. R. McKinsey is Research Metallurgist, Metals Research Labs., Niagara Falls, N. Y.

This paper, based on a more detailed unpublished report by Mr. Greene, is the first publication of the data obtained under Mr. Greene's direction in 1945.

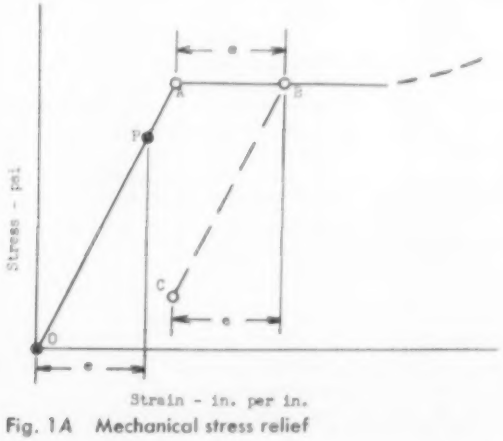

Fig. 1A Mechanical stress relief

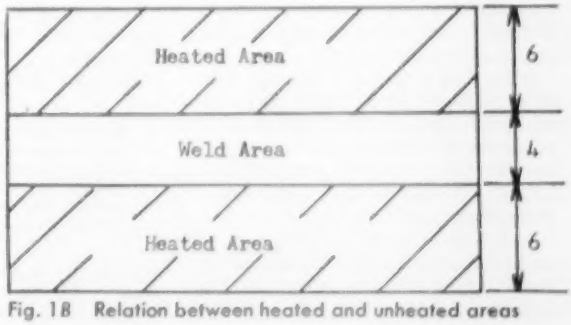

Fig. 1B Relation between heated and unheated areas

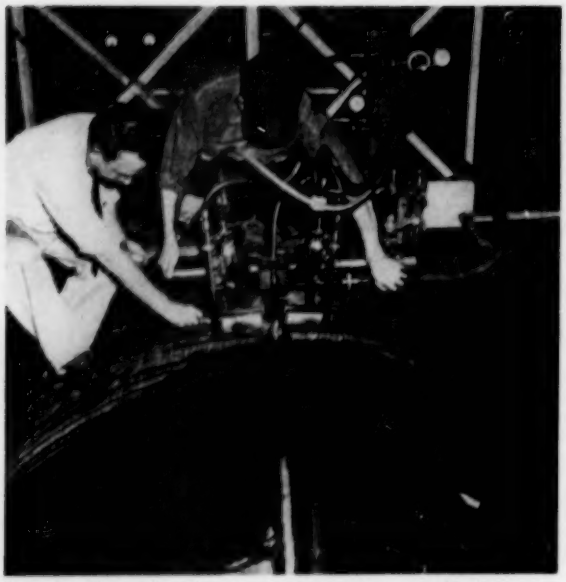

Fig. 2 Controlled low-temperature stress-relieving equipment in operation on longitudinal weld

Fig. 3 Photograph of the temperature-indicating marks on the inside of the tank three days after stress-relieving treatment

bands on each side of the weld to a relatively low temperature?

The reduction of residual stress by mechanical straining is illustrated schematically in Fig. 1*A*. It is assumed that the weld metal contains longitudinal residual stresses of yield strength magnitude, represented by point *A*. It is also assumed that the stress in the base plate on either side of the weld is zero, represented by point *O*. (Actually, the base metal contains residual tensile stresses immediately adjacent to the weld and relatively low residual compressive stresses farther from the weld. At a point approximately 3 to 5 in. from the weld centerline, the residual stress is zero.)

If the weldment is placed in a tensile machine and a longitudinal tensile force of the proper magnitude is applied, the weldment will be elongated "*e*" inch per inch. The base metal is stretched to point *P*, but the applied force is not sufficient to cause plastic flow, since the stress is less than the yield strength. The weld metal is strained the same amount, but the strain is in the plastic range, since the weld metal initially contained residual stresses of yield strength magnitude. Therefore, the weld is stretched to point *B*.

If the load is then released, the base metal relaxes to point *O*, since the strain was purely elastic. The weld metal is an integral part of the structure, and it also contracts "*e*" inch per inch and reaches equilibrium at a lower stress level, represented by point *C*.

In this illustration, the reduction in residual stress is numerically equivalent to the applied tensile stress. If the weld metal initially contains residual

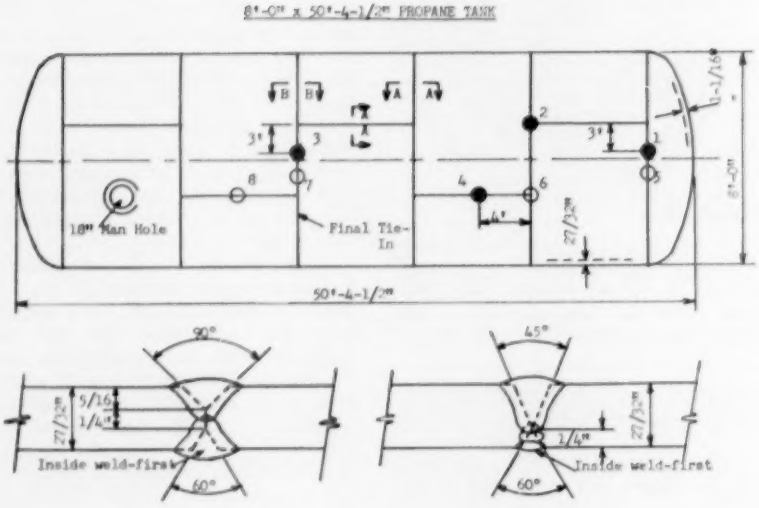

Fig. 4

Section A-A

Submerged arc welds

$^1/_4$-in. diam rod

20- x 200-mesh granular material

Inside weld (first)

1020 amp, 37 v, 12–14 in. per min

Outside weld

1100 amp, 37 v, 10–12 in. per min

Section B-B (Tie-In Weld)

Inside weld-manual (first)

First pass $^5/_{16}$-in. diam electrode

Second and third pass $^1/_4$-in. diam electrode

Outside weld-submerged arc

$^1/_4$-in. diam rod

20- x 200-mesh granular material

1250 amp, 37 v, 6–7 in. per min

Welding Sequence

1. Inside longitudinal seams of the two sections of tank
2. Inside circular seams of the two sections of tank
3. Outside longitudinal seams of the two sections of tank
4. Outside circular seams of the two sections of tank
5. Inside manual weld joining the two sections of tank
6. Outside submerged arc weld joining the two sections of tank

Identification of Plugs for Stress Measurements

Plugs ● 1, 2, 3 and 4 (as-welded) drilled from seams before stress-relieving

Plugs ○ 5, 6, 7 and 8 (stress-relieved) drilled from seams after stress-relieving

Plugs ○ 5 and 7 drilled approx. 180° from plugs ● 1 and 3

Table 1—Optimum Conditions for Low-Temperature Stress-Relieving Butt Welds*

Plate thickness, in.	Approximate travel speed, ipm	Width of heat bands, in. 350° F	400° F	450° F	Distance between flame heads and cooling spray, in.
1/2	24	4–5	None	None	6
5/8	20	5–5 1/2	None	None	6
3/4	16	5–6	Trace	None	6–8
7/8	12	5–6	Trace	None	6–8
1	10	5–6	1–3	None	6–8
1 1/4	9	5–6	1–3	None	6–8

NOTE 1: Two 6-in. wide flame-priming heads are used, and are spaced symmetrically on each side of the weld. The distance between the head centers is 10 in. (see Fig. 2).
NOTE 2: The tip-to-plate distance may vary from 5/16 to 1 1/8 in.

* From Greene and Holzbaur.[3]

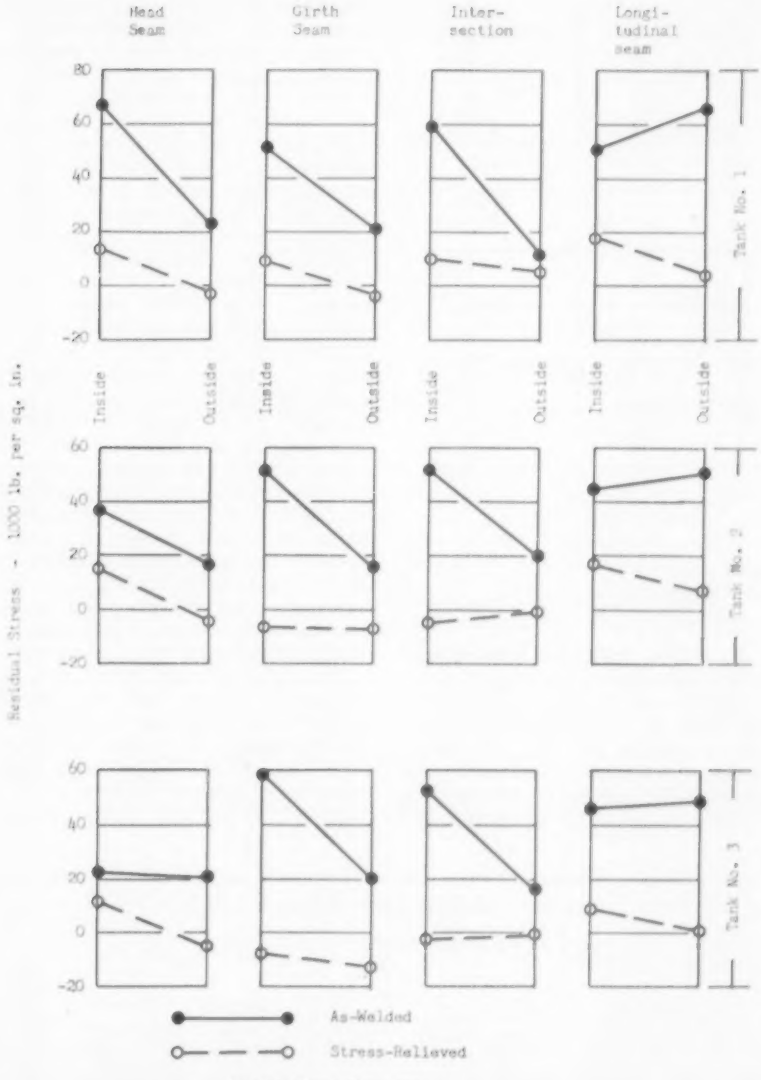

Fig. 5 Residual stresses in direction longitudinal to welds

tensile stresses somewhat lower than the yield strength, a portion of the applied load will be used to raise the stress to the yield strength and the remaining applied load will cause plastic deformation and subsequent stress relief.

It may be questioned whether the above analysis is applicable to weldments because of the stress gradients involved, but it has been demonstrated experimentally that residual stresses can be reduced by mechanically stretching a weldment in a tensile testing machine and that the numerical reduction in residual stress is approximately equal to the applied tensile stress.[4]

It then remains to be determined whether the necessary increment of strain can be obtained under the conditions used in low-temperature stress relieving. As stated before, in applying this process, a 6-in. wide band on each side of the weld is heated to 350–400° F. The heating torches are spaced as shown in Fig. 1*B*, so that a 4-in. wide area containing the weld is not directly heated by the torches.

For purpose of analysis, it is assumed that the 4-in. wide weld area contains a uniform residual tensile stress of 45,000 psi, which is equal to the yield strength, and that the heated area contains no residual stress, thus implying an infinite stress gradient at the boundaries. It is also assumed that the reduction in residual stress is numerically equivalent to the applied stress.

Suppose it is desired to reduce the residual stress in the weld area, A_1, to zero. Since the reduction in residual stress is equal to the applied stress, the weld must be strained

$$\epsilon = \frac{S}{E} = \frac{45{,}000}{30 \times 10^6} = 0.0015 \text{ in. per inch}$$

The force required to strain the weld area 0.0015 inch per inch is obtained by heating an area on each side of the weld. The total heated area, A_2, is three times the weld area ($A_2 = 3A_1$). Since the entire area, $A_1 + A_2$, must behave as a unit, the total force must be sufficient to strain the entire area 0.0015 inch per inch. The stress required to obtain this strain is 45,000 psi. However, this stress must be developed by heating area A_2, which is 3/4 of the total area. Therefore, the force which must be developed is equivalent to a stress in A_2 of

$$4/3 \times 45{,}000 = 60{,}000 \text{ psi}$$

The unit strain developed by thermal expansion is

$$\epsilon = \alpha T$$

where

ϵ = strain, inch per inch.
α = coefficient of thermal expansion, inch per inch per ° F.
T = temperature, ° F.

Since $\epsilon = S/E$, then $S/E = \alpha T$, and $T = S/E\alpha$. Therefore, the tempera-

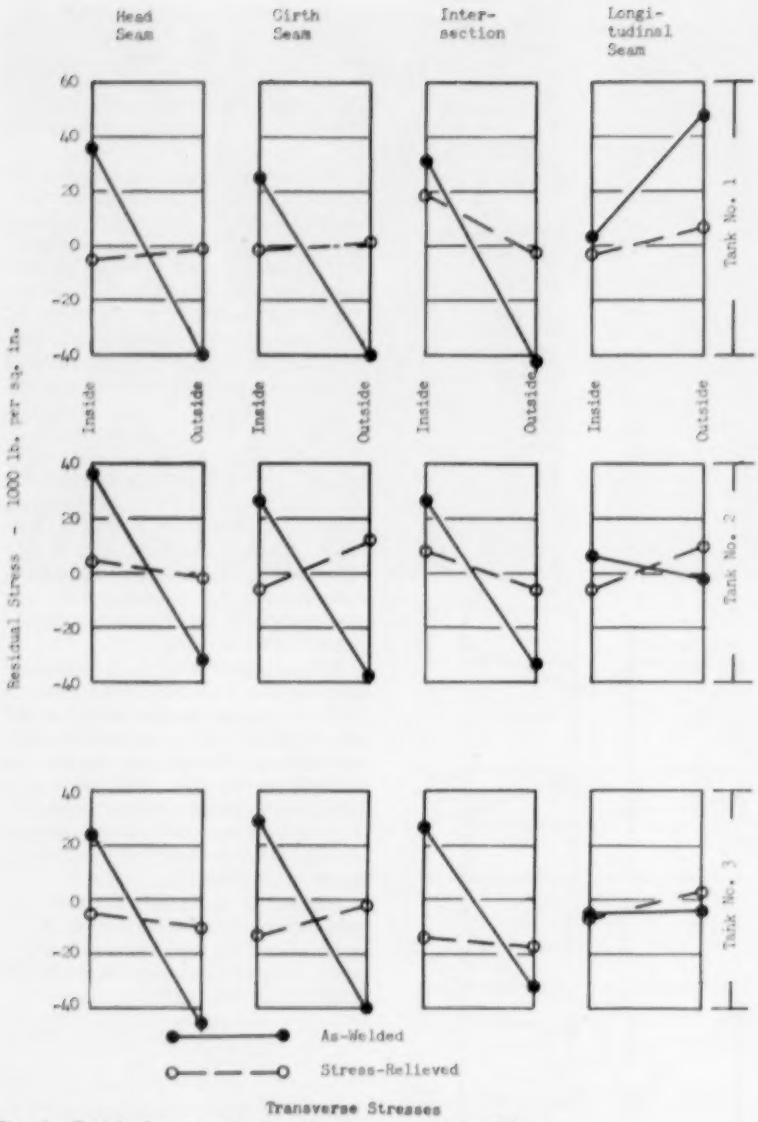

Fig. 6 Residual stresses in direction transverse to welds

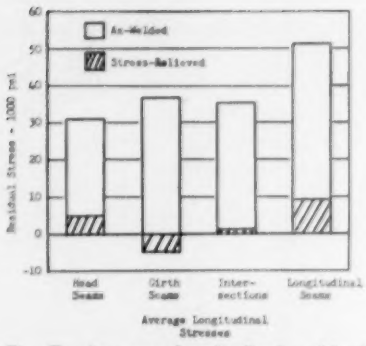

Fig. 7 Average longitudinal residual stresses in three tanks

ture T, to which area A_2 must be heated to stretch the total area 0.0015 inch per inch is

$$T = \frac{S}{E\alpha} = \frac{60{,}000}{30 \times 10^6 \times 6.5 \times 10^{-6}} = 308^\circ \text{ F}$$

Thus, the area in the base metal must be heated to 308° F above the ambient temperature to completely eliminate the residual stress in the weld.

Again, it may be questioned whether this simplified analysis is applicable because of the complex stress and temperature gradients involved during application of the process. However, it has been demonstrated experimentally that temperatures of 350 to 400° F are sufficient to achieve almost complete elimination of residual stress in weldments.[3]

In practice, controlled low-temperature stress relieving is accomplished by simultaneously and progressively heating two 6-in. wide bands, one on each side of the weld, with 6-in. wide multiflame oxyacetylene stress-relieving heads. The middle of each band is about 5 in. away from the centerline of the weld, leaving about 2 in. each side of the weld centerline unheated. The speed of travel is dependent upon the plate thickness and is regulated to give the proper width and temperature of heated bands. Uniformly low residual stresses are obtained when the heating conditions are controlled to produce a 5- to 6-in. wide band heated to 350° F and a narrower band heated to 400° F. The plate should not be heated to 450° F, as this results in excessive residual compressive stresses in the weld, with residual tensile stresses imposed in the plate outside the weld. The heated areas should be cooled with water or an air-water mixture 6 to 8 in. behind the advancing flames. This prevents the accumulation of heat which might cause distortion in the structure, and facilitates the expansion of each successive heated increment by removing the bucking thermal expansion force of the area just passed. The weld may be cooled between the advancing flames, but this is of much less importance than cooling the heated area at a proper distance behind the flames. A photograph of the equipment in operation is shown in Fig. 2, and the optimum conditions for stress relieving butt welds in ordinary steel plate are given in Table 1[3] for plate thicknesses from $^1/_2$ to $1^1/_4$ in.

The inspection and control of low-temperature stress relief are simple, since the only important variable during the operation is the speed of travel. The application of temperature-indicating crayons or lacquers to the underside of the joint before heating

Table 2—Mill Test Report

Firebox Quality ASTM A-212 Steel

	Thickness, in.	Lb per sq in. Yield strength	Lb per sq in. Tensile strength	% Elongation in 8 in.	C, %	Mn, %	Si, %	P, %	S, %
Shell plate	$^{27}/_{32}$	43,600	74,500	24.7	0.28	0.68	0.21	0.018	0.028
Head plate	$1^1/_{16}$	41,700	78,700	27.7	0.26	0.75	0.21	0.022	0.03

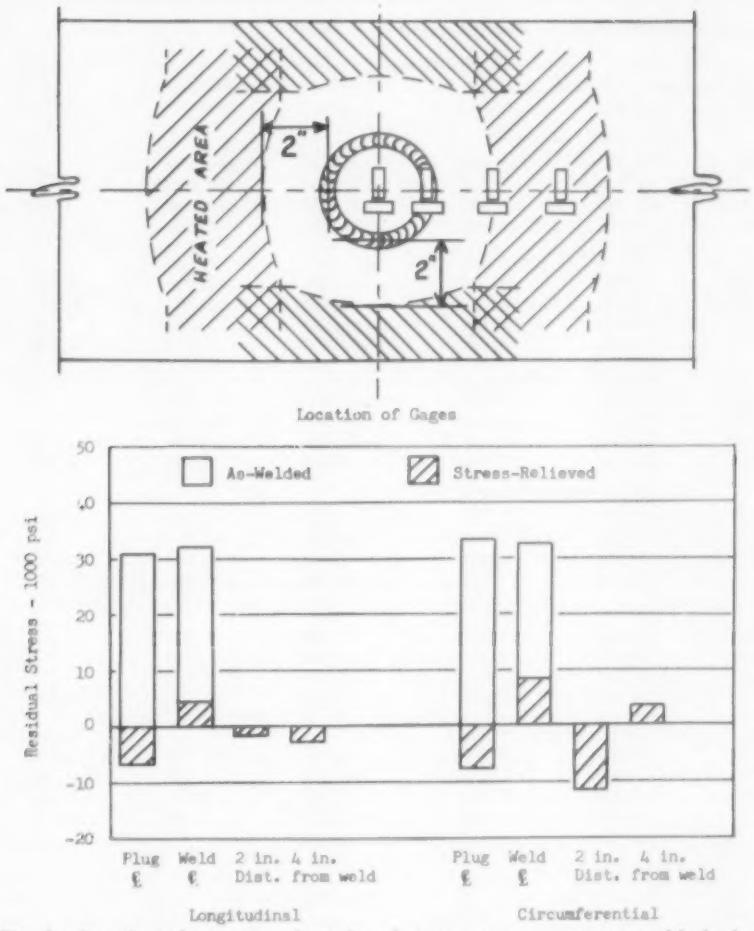

Fig. 8 Location of gages and results of stress measurements on welded plug

enables the inspector to note the width and temperature of the heat band after the operation is completed, as shown in Fig. 3. The descaled steel in the path of the stress-relieving torches serves to show whether a seam has been treated.

The suitability of controlled low-temperature stress relieving for welded ships has been demonstrated,[1] but its application to large welded pressure vessels had not been completely explored. Therefore, it was decided to apply the process experimentally to three large propane tanks during construction. The results of these tests are presented in this paper.

The material has been separated into three parts dealing with (A) stress relieving the major welded seams, (B) measurement of distortion and (C) stress relieving welded plugs.

PART A—LOW-TEMPERATURE STRESS-RELIEVING BUTT WELDS

Experimental Procedure

The propane tanks were 8 ft in diameter and 50 ft 4 1/2 in. in over-all length. The wall thickness was 21/32 in., and the heads were 1 1/16 in. thick. These tanks were designed for 200-lb working pressure and were constructed of ASTM A-212 steel, having a minimum tensile strength of 70,000 psi. The design of the vessels, welding conditions, and sequence of welding are shown in Fig. 4. Typical mill test reports of the shell and head plates are given in Table 2.

In order to determine the efficiency of the process, the residual welding stresses were measured before and after stress relieving, using SR-4 electric resistance strain gages, at four typical points: (1) head seam, (2) girth seam, (3) longitudinal seam and (4) intersection of girth and longitudinal seams. One gage was applied longitudinally to the weld and another transversely, and in all cases, gages were applied to the inner and outer surfaces directly opposite each other. Small plugs containing the gages were then removed from the tank by carefully drilling a ring of overlapping holes to avoid increasing the temperature of the plug. The amount of relaxation was measured with a commercial strain indicator, and the corresponding stress was calculated using the equations of elasticity for a two-dimensional stress system.

After initial measurements in the as-welded condition were completed, the plugs were rewelded into the tank, and all seams were then low-temperature stress relieved. The stresses remaining were determined by the same procedure at four similar locations. The head and girth seam plugs were taken from the same seams as before, 180 deg from the original plugs. The location and identification of the plugs are shown in Fig. 4.

In this investigation, 3-in. diam plugs were selected to minimize the danger of injuring the gages during trepanning. Since the size of the trepanned plug might have affected the results, two of the 3-in. diam plugs were machined to 1 1/2-in. diam, the smallest size permissible without damaging the gages, and the additional relaxation was measured. The results are shown in Table 3 and it is apparent that the stresses were of the same order of magnitude in plugs of both sizes.

Discussion of Results

The residual stress measurements for each tank are listed in Table 4, and the average values for all three tanks are shown in Table 5. The results are shown graphically in Figs. 5, 6 and 7.

The residual stresses in the as-welded condition were quite consistent and were highest in the longitudinal direction. The stresses were higher for the longitudinal tank seams than for the circumferential seams, averaging about 51,000 psi for the former and about 35,000 psi for the latter. The stresses at the intersections were not significantly different from other points on the circumferential seams remote from the intersections. It should be noted that the data are presented in relation to the

Table 3—Effect of Plug Size on Residual Stress Measurements, Tank No. 1

		Average stress,* lb per sq in.					
		Longitudinal to weld			Transverse to weld		
Plug No.	Condition	3 in. diam	1 1/2 in. Diam	Change	3 in. diam	1 1/2 in. diam	Change
1	As-welded	44,800	44,300	−500	−2000	−650	1350
5	Stress relieved	5,300	7,200	1900	−3250	−2850	1200

* Positive stress indicates tension; negative stress indicates compression.

Table 4—Residual Stress Measurements

Plug No.	Location	Residual stress,* psi: Longitudinal to weld — Inside	Longitudinal to weld — Outside	Longitudinal to weld — Avg	Transverse to weld — Inside	Transverse to weld — Outside	Transverse to weld — Avg
		Tank No. 1, as-welded					
1	Head seam†	66,600	23,000	44,800	36,000	−40,000	‡
2	Intersection†	59,800	11,700	35,750	31,400	−42,500	‡
3	Girth seam†	51,800	20,900	36,350	24,700	−40,000	‡
4	Longitudinal seam	51,000	66,000	58,500	3,300	47,500	25,400
		Tank No. 1, stress-relieved					
5	Head seam	13,500	−2,900	5,300	−5,300	−1,200	−3,250
6	Intersection	9,900	5,200	7,550	19,300	−2,600	8,350
7	Girth seam	9,500	−4,200	2,650	−1,350	2,000	325
8	Longitudinal seam	18,200	4,000	11,100	−2,800	7,150	2,125
		Tank No. 2, as-welded					
1	Head seam	36,600	16,800	26,700	36,200	−31,800	‡
2	Intersection	51,700	20,000	35,850	26,400	−33,500	‡
3	Girth seam	51,700	16,000	33,850	26,400	−37,900	‡
4	Longitudinal seam	45,100	50,400	47,750	6,600	−2,300	2,150
		Tank No. 2, stress-relieved					
5	Head seam	15,300	−4,100	5,600	4,450	−1,700	1,375
6	Intersection	−4,800	−900	−2,850	8,200	−6,000	1,100
7	Girth seam	−6,500	−7,100	−6,800	−5,700	12,500	3,400
8	Longitudinal seam	16,700	7,100	11,900	−6,400	10,300	1,950
		Tank No. 3, as-welded					
1	Head seam	22,600	21,000	21,800	23,800	−45,000	‡
2	Intersection	52,600	16,300	34,450	26,700	−31,700	‡
3	Girth seam	59,300	20,500	39,900	29,000	−40,200	‡
4	Longitudinal seam	46,400	48,800	47,600	−4,700	−3,700	−4,200
		Tank No. 3, stress-relieved					
5	Head seam	12,300	−5,200	3,550	−4,600	−10,300	−7,450
6	Intersection	−2,400	−400	−1,400	−14,100	−17,400	−15,750
7	Girth seam	−7,900	−13,300	−10,600	−12,900	−2,200	−7,550
8	Longitudinal seam	9,300	1,000	5,150	−5,600	3,100	−1,250

* Positive stress indicates tension; negative stress indicates compression.
† Stresses longitudinal to weld are circumferential to tank.
‡ No average, since measurements indicate bending.

direction of the weld, so that longitudinal stresses in the girth seams would be circumferential to the tank.

The stresses transverse to the longitudinal weld seams were generally quite low, and in some cases were residual compression. There was evidence of bending at the circumferential joints, since the transverse stresses were in tension on the inside of the tank and surprisingly high in compression on the outside. This may be explained by considering the circumferential welds as shrinking bands which tended to deform the tanks inward and thus imposed a bending stress transverse to the weld and longitudinal to the tank.

After stress relieving, all the residual stresses were reduced to low values. As shown in Fig. 5, the longitudinal stresses were not only reduced in magnitude but the stress gradient between the inside and outside surfaces was also significantly reduced. This is even more apparent in Fig. 6, where it is shown that the high stress gradient caused by the bending stresses transverse to the welds was essentially eliminated, and that the magnitude of the remaining stresses approached zero.

The results were quite consistent among the three tanks, as indicated by the data in Table 5, and the average values for the longitudinal stresses are depicted in the bar chart in Fig. 7. These results thoroughly demonstrate the applicability of the stress-relieving process to structures of this type.

PART B—MEASUREMENT OF DISTORTION

In conjunction with the stress measurements on tank No. 3, an attempt was made to measure any distortion produced by the low-temperature stress-relieving process. Since measurements of changes in the diameter or circumference would obviously be inadequate, a pattern of gage marks, made with a No. 55 drill, was laid out on the welds and in the adjacent plate. Measurements were made with a 2-in. mechanical strain gage, accurate to less than 0.0001

Table 5—Summary of Results from Three Tanks

Location	Average residual stress,* psi: Longitudinal to weld — Min	Longitudinal to weld — Max	Longitudinal to weld — Avg	Transverse to weld — Min	Transverse to weld — Max	Transverse to weld — Avg
	As-welded					
Head seam†	21,800	44,800	31,100	‡	‡	‡
Intersection†	34,450	35,850	35,350	‡	‡	‡
Girth seam†	33,850	39,900	36,700	‡	‡	‡
Longitudinal seam	47,600	58,500	51,283	−4,200	25,400	7783
	Stress relieved					
Head seam	3,550	5,600	4,817	−7,450	1,375	−3108
Intersection	−2,850	7,550	1,100	−15,750	8,350	−2100
Girth seam	−10,600	2,650	−4,917	−7,550	3,400	−1275
Longitudinal seam	5,150	11,100	9,383	−1,250	2,125	942

* Positive stress indicates tension; negative stress indicates compression.
† Stresses longitudinal to weld are circumferential to tank.
‡ No averages; see Table 4.

Table 6—Distortion in Welds and Adjacent Heated Areas During Low-Temperature Stress-Relieving Treatment

Distance from weld, in.	Longitudinal to weld: Inside surface, in./in.	Longitudinal to weld: Outside surface, in./in.	Longitudinal to weld: Avg, in./in.	Distance from weld, in.	Transverse to weld: Inside surface, in./in.	Transverse to weld: Outside surface, in./in.	Transverse to weld: Avg, in./in.
			Longitudinal seam				
0	−0.0001*	+0.0000	0	Across weld	−0.0010	+0.0001	−0.0004
2	+0.0001	+0.0005	+0.0003	1–3	−0.0002	−0.0008	−0.0005
4	+0.0003	+0.0005	+0.0004	3–5	+0.0002	−0.0010	−0.0004
6	+0.0001	+0.0004	+0.0002	5–7	+0.0003	−0.0011	−0.0004
8	+0.0003	+0.0004	+0.0003	7–9	+0.0001	+0.0001	+0.0001
10	+0.0002	+0.0004	+0.0003	9–11	−0.0003	+0.0006	+0.0001
12	+0.0002	+0.0004	+0.0003	11–13	−0.0002	+0.0005	+0.0001
			Girth seam				
0	+0.0003†	+0.0009†	+0.0006†	Across weld	−0.0028	+0.0005	−0.0011
2	+0.0002	+0.0006	+0.0004	1–3	−0.0011	−0.0009	−0.0010
4	−0.0001	+0.0005	+0.0002	3–5	−0.0005	−0.0010	−0.0007
6	−0.0003	+0.0004	0	5–7	−0.0004	−0.0011	−0.0007
8	−0.0001	+0.0003	+0.0001	7–9	+0.0003	−0.0003	0
10	−0.0001	+0.0005	+0.0002	9–11	0	+0.0004	+0.0002
12	−0.0007	+0.0002	−0.0002	11–13	0	+0.0004	+0.0002

* + Indicates elongation, − indicates contraction.
† Longitudinal to girth seam is circumferential to tank.

inch per inch. Readings were taken before and after stress relieving, both longitudinally and transversely to the welds.

The results are shown in Table 6, and it is apparent that no significant distortion was produced by stress relieving. In fact, the measured strains were generally less than one-third those that would accompany the application of the working pressure. Thus, relief of residual stress was accomplished, as discussed earlier, without accompanying distortion.

PART C—STRESS RELIEVING WELDED PLUGS

A brief experiment was made to determine the effectiveness of low-temperature stress relieving when applied to plugs, such as those welded into the 3-in. diam openings drilled for stress measurements. These tests were made on a smaller tank, 4 ft 6 in. in diameter and 10 ft long, with a wall thickness of $^3/_4$ in. A 36-in. diam opening was to be cut into this tank, and the experiments were made in the center of the material which was subsequently to be removed. The steel plate had the following tensile properties:

Yield strength, psi	35,800
Tensile strength, psi	58,100
Per cent elongation in 8 in.	27

A circular plug, $2^1/_2$ in. in diameter, was first torch-cut out of the $^3/_4$-in. thick plate. The plug and opening were beveled, and the plug was rewelded into the plate and then X-rayed. Strain gages were applied both inside and outside to measure the residual stresses in both the longitudinal and circumferential directions. Gages were located both at the center of the plug and on the weld. After original strain readings were taken, a $3^1/_4$-in. diam plug was drilled out and subdivided, by handsawing, into elements containing the sets of gages. The residual stresses in the as-welded state were thus determined.

A $3^1/_4$-in. diam plug was then rewelded into the opening, X-rayed and low-temperature stress relieved. The stress relieving was accomplished by making first a longitudinal and then a circumferential pass around the plug as shown in Fig. 8, using manually operated stress-relieving equipment. The two 6-in. wide torches were positioned so that the edges of the heat bands were about 2 in. outside the weld. The speed of travel was about 15 ipm for the $^3/_4$-in. thick plate, and produced 6-in. wide bands of 350° F and 4-in. wide bands of 400° F, with no indication of 450° F. The residual stresses after stress relieving were then measured at the center of the plug and in the weld, as before, and also in the area under the heating torches to determine whether any additional stresses had been introduced.

The results are listed in Table 7 and are shown graphically in Fig. 8, together with the layout of the gages. They illustrate that the residual welding stresses, which had approached yield strength tension in all directions, were reduced to very low values. Moreover, no stresses of significant magnitude were introduced into the plate area heated by the stress-relieving torches.

Table 7—Stress Measurements on Welded Plugs

Location	Residual stress,* psi: Longitudinal to tank: Inside	Longitudinal to tank: Outside	Longitudinal to tank: Avg	Circumferential to tank: Inside	Circumferential to tank: Outside	Circumferential to tank: Avg
			As-welded			
Center of plug	39,400	22,400	30,900	38,200	28,900	33,550
Center of weld	38,800	25,500	32,150	39,300	26,000	32,650
			Stress-relieved			
Center of plug	−7,500	−6,200	−6,850	−8,800	−6,700	−7,750
Center of weld	6,800	2,200	4,500	13,100	4,200	8,650
Heated area, 2 in. from weld	−1,600	—	−1,600	−17,300	−5,300	−11,300
Heated area, 4 in. from weld	0	−5,600	−2,800	900	6,800	3,850

* Positive stress indicates tension; negative stress indicates compression.

Summary and Conclusions

Residual tensile welding stresses having a magnitude approaching the yield strength of the material were measured in head seams, girth seams, longitudinal seams, and intersections of girth and longitudinal seams in three pressure

vessels constructed of ASTM A-212 steel. The results were consistent among the three tanks.

The residual welding stresses were reduced to low values in all welds by the controlled low-temperature stress-relieving process, and the results were consistent among the three tanks.

No significant distortion was introduced by the controlled low-temperature stress-relieving treatment, and no significant residual stresses were introduced into the heated zone in the base plate.

The high residual tensile stresses in welded plugs were reduced to negligible values by application of this process.

Based on these and other tests, it is apparent that the controlled low-temperature stress-relieving process is a practical method of stress relieving large structures, field-erected tanks, and final assembly welds of pressure vessels.

Acknowledgments

Appreciation is expressed for the cooperation and help extended by the officials and personnel of the Hamler Boiler and Tank Co. who made this investigation possible. Acknowledgment is also given to engineers and representatives of the Boiler Code Committee, insurance companies, inspection agencies and others for their interest and constructive suggestions.

References

1. Rules for Construction of Unfired Pressure Vessels, Section VIII, ASME Boiler and Pressure Vessel Code, American Society of Mechanical Engineers, New York (1952).

2. The Welding Handbook, Third Edition, American Welding Society, New York, p. 1095 (1950).

3. Greene, T. W., and Holzbaur, A. A., "Controlled Low-Temperature Stress Relieving," The Welding Journal, **25** (3), Research Suppl., 171-s to 185-s (1946).

4. Meriam, J., *et al.*, "Redistribution of Residual Welding Stresses by Tensile Loading Along a Unionmelt Weld Joining Two 3-Ft by 12-Ft by 1-In. Plates," *Ibid.*, **25** (10), Research Suppl., 697-s to 699-s (1946).

INTERNATIONAL INSTITUTE OF WELDING MEETINGS

The American Council of the International Institute of Welding announced that the next two annual meetings of the Institute will be held in Madrid, Spain, July 1–8, 1956, and in Essen, Germany, June 29–July 6, 1957.

The open public session of the Madrid meeting will be on the general subject of "Welding as an Aid to Productivity." The open session of the German meeting has not yet been determined. It will probably be on some phase of metallurgical developments in welding.

The official business of the International Institute of Welding is handled through a number of Commissions of which there are 15. Although the United States has official representatives on these Commissions, it is possible to appoint "experts" to attend any particular Commission meeting and participate in the discussions. Any member of the American Welding Society or the Welding Research Council who desires to participate in these activities should communicate with the secretary of the American Council of the I.I.W., W. Spraragen, 29 W. 39th St., New York 18, N. Y.

A list of the Commissions and the official United States representatives are:

Commission	
I	Gas Welding and Allied Processes—J. H. Zimmerman
II	Arc Welding—John J. Chyle
III	Resistance Welding—T. Embury Jones
IV	Documentation
V	Testing, Measurement and Control of Welds—A. Gobus
VI	Terminology—M. A. Cordovi
VII	Standardization—A. N. Kugler
VIII	Hygiene and Safety—H. F. Reinhard
IX	Behavior of Metals Subjected to Welding—R. D. Stout and D. P. Brown
X	Residual Stresses and Stress Relieving—T. McLean Jasper, W. Spraragen, *Alternate*
XI	Pressure Vessels, Boilers and Pipelines—Arthur R. Gatewood, H. C. Boardman, *Alternate*
XII	Special Arc Welding Processes—C. J. Sullivan
XIII	Fatigue Testing—A. M. Freudenthal, Expert—LaMotte Grover
XIV	Welding Instruction—Prof. Harry Udin
XV	Fundamentals of Design and Fabrication for Welding—A. Amirikian

ANALYSIS OF THE DIRECT-CURRENT ARC

Mechanism of power transfer to the anode, the formation and extent of the cathode region and the power dispersal in the arc are some of the phenomena which are evaluated and discussed

BY ALAN D. MORRIS AND WILLIS C. GORE

SUMMARY. An analysis of the thermionic electric arc, based primarily upon interpretation of calorimetric data, is presented. Phenomena within the arc which are evaluated and discussed include the mechanism of power transfer to the anode, the formation and extent of the cathode region, the power dispersal in the arc and the effect of cathode electrode variations upon the arc. Data are representative of the test configuration only when a steady flow state is obtained, and it is shown that many prior investigations of the electric arc were hindered by nonequilibrium conditions.

Introduction

Although the electric arc has been subjected to numerous investigations, no integrated explanation of the arc mechanism is available. Current trends in arc research are typified by the work of spectroscopists[1-4] and others.[5-9] A calorimetric approach, while not new,[10,5] was used in this work to obtain data whose interpretation led to an understanding of the arc behavior.

A direct-current shielded-welding arc was the configuration utilized. However, present-day interest in the arc is not solely derived from commonplace applications in welding, electron tubes, lighting and rectification, but also from new uses that are being found. The low-current carbon arc is a standard means for spectroscopic sample volatilization[11] and the anode crater of such an arc provides an excellent source for infra-red absorption spectroscopy.[12] Inert-gas arcs are used by biologists[13-15] and metallurgists.[16]

The arc analyzed was unique in that it could be made to burn at voltages below the ionization potential of the ambient gas. As Finkelnburg[1] points out, these low voltages are not due to the presence of electrode metal vapor in the discharge carrier, whose ionization potential lies between that of the metal and that of the ambient gas. Contrary to the criterion proposed by Compton (Reference 17, p. 463), the "cathode fall of potential" for this arc may be considerably less than the ionization potential of the gas.

Alan D. Morris and Willis C. Gore are associated with the School of Engineering, The Johns Hopkins University, Baltimore, Md.

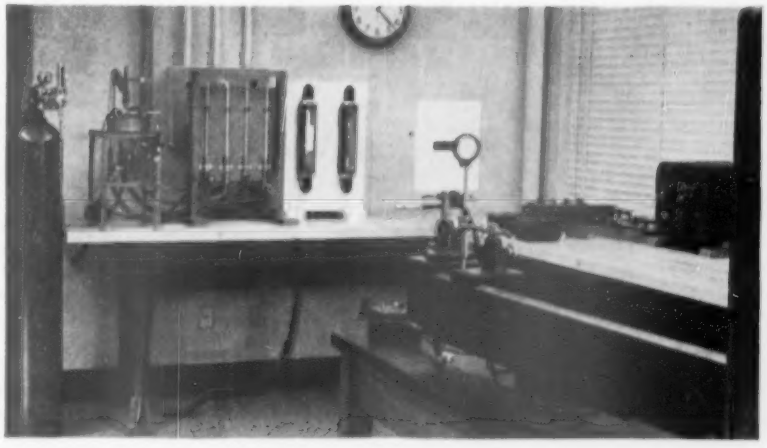

Fig. 1 Over-all view of experimental apparatus

Instrumentation

The prime effort in this investigation was directed toward the determination of the power evolved at the electrodes of an arc as a function of the voltage applied, electrode separation, electrode material, and the ambient gas. It was hoped that these quantities, when found would furnish an important clue to understanding the arc mechanism.

To procure these results, a calorimetric apparatus was conceived and instrumented as shown in Figs. 1, 2 and 3. For convenience and in order to serve a practical turn, a gas-shielded welding torch was employed as the cathode mount. This torch provided in a compact assembly the facilities for gas shielding, electrode support, water cooling and a current path. Interchangeable collets allowed the use of 0.04-, $^1/_{16}$-, $^3/_{32}$-, and $^1/_8$-in. diam cathode rods, and gas cups were furnished in sizes appropriate to each electrode size and were made of either nickel-plated copper or of ceramic. Accompanying the torch was a gas flowmeter-regulator, calibrated for the commercial flow-rate range, which maintained constant flow despite variations in cylinder pressure.

Surmounted by the torch was a specially constructed well-cooled copper block in whose center was a tapered, removable plug—the anode. The configuration was then closely akin to welding conditions on a flat surface where direct-current straight polarity nonconsumable electrode methods are employed.

Figure 1, an over-all view, shows the entire calorimetric apparatus to the immediate right of the argon cylinder. Centrally located are the optical bench and riders of the Baird grating spectrograph; on the table past the spectrograph are the electrical meters, welding generator and controls and a high-frequency arc starter. Seen from the rear on the front bench rider is a cali-

brated projection screen upon which a 10X arc image was placed to facilitate separation adjustments. Since the image could be racked vertically across the screen, any desired portion of the arc was selected for a spectrogram by placing the portion selected over a "pinhole" in the screen center, which served as the source for the spectrograph. A mercury-vapor discharge tube was mounted just forward of the screen and could be moved into position over the pinhole to provide a calibrating exposure.

The water system is detailed in Fig. 2. Ever-occurring transients in supply pressure were filtered by the air chamber shown above the pressure gage. From the filter the water passed through the two control valves on the thermometer stand, through the two input thermometer wells, into the torch and the block, to the output wells and finally through the flowmeters on the right.

Regulator, torch, block and plug, projection lens and a miniature spotlight are depicted in Fig. 3. Electrical connection to the block was by means of a clamp to the inlet water copper tube, seen below the steel stand. The exact surface position of the anode on the projection screen could be found by touching a sharp point to the plug surface and employing the spotlight. When in operation, the arc obscured the anode surface, and it was thus located prior to arc initiation.

A check run on a known heat source indicated a system accuracy of five percent. Under conditions later described, all results derived from the arc were reproducible to within six percent. Reproducibility is a doubtful quality where the arc is concerned and thus the incompatibility of the above percentages.

Technique

The gas flow was first started. Although the flow rate has a marked effect upon the arc behavior and although rates both higher and lower would have been satisfactory, a standard flow of 15 cfh of helium or argon was used.

The arc was then started by closing the generator contactor and momentarily applying the high-frequency voltage, the latter being a decided convenience rather than a necessity. Care was exercised to make the arc burn symmetrically from the cathode since the resultant tip shape is important not only in achieving reproducibility but also constitutes an intimate factor in the arc mechanism.

Data were taken while progressing from the lower range of separation and current and working toward the higher. At each setting of current and separation adequate time was allowed for the arc system to come to equilibrium although intermediate values of data were recorded so that the factors having to do with equilibrium could be evaluated. From five to ten minutes was required to achieve equilibrium and thus a complete set of data took many hours to obtain. It was absolutely essential that any one run be an entirety so that the data would faithfully represent the configuration under test. (Equilibrium here refers to a steady flow state and not to thermodynamic equilibrium.)

Values of power evolved at the anode are termed anode watts on the figures and represent the total power transferred to the anode by the arc. However, cathode watts is not the total power evolved at the cathode but the values given in the figures are corrected for losses originating in the torch from the collet grip point on the electrode to the water-cooled cable termination. Thus cathode watts is the power absorbed by the cooling water at the cathode electrode itself. All voltages are corrected for the drop in the torch body and leads. Power is computed in this manner: power = $(T_{out} - T_{in}) \times 4.19$ joules/calorie $\times$ flow rate. Power, for the electrode considered, is in watts. $(T_{out} - T_{in})$ is the corrected temperature differential of the cooling water in degrees centigrade. Flow rate is the reading of the appropriate flowmeter in cubic centimeters/second.

Variations

Comparative runs were made using helium instead of argon as the shield gas. The shielding is so perfect and the gases so pure that if a small percentage of another gas is desired in a particular weld situation it must be premixed in the cylinder prior to use.

The diameter of the tungsten cathode was varied to evaluate the effect upon the arc of the heat conduction and generation within the electrode. Nickel was substituted for the copper plug as an anode to verify a hypothesis concerning the transferral of power to the anode and the independence of the arc mechanism of the anode metal.

Anode Phenomena

The total energy, kinetic and potential, of an electron striking the anode is transferred to the anode metal. Thus power is transferred to the anode in an electric arc by virtue of the two components of the inpinging electrons' energy; one portion is the thermal kinetic energy corresponding to electron temperature and the other is the potential energy of the electrons.

Two metals of differing work functions, when brought into contact at a junction where thermal equilibrium exists, will have an electron flow between them until their Fermi levels coincide. High-energy electrons will cross the contact boundary into the higher work function metal from the lower work function metal. This flow continues until there are enough higher energy electrons in the high work function metal so that no electron in either metal can, by crossing the boundary, find a quantum level lower than its present one (Reference 17, p. 253). The flow of electrons is not sufficient to change the absolute density of the electrons in the metals and therefore does not alter the values of E_m, which is a function of electron density, but it does vary the electrical potential of the metals. The fact that E_w is different for each metal is responsible for the contact po-

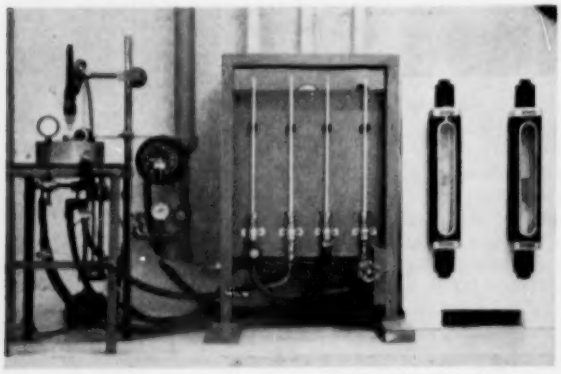

Fig. 2 The water cooling system

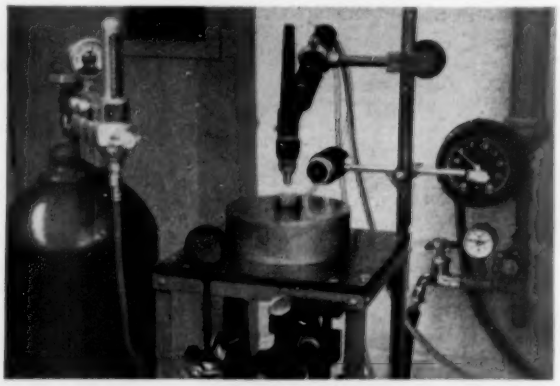

Fig. 3 Gas regulator, torch, and anode assembly

tential between exposed faces of metals in contact. Because the Fermi levels will all coincide, intermediate metals will not affect the value of contact potential between the end metals.

What bearing does the static situation described above have upon the electric arc? The anode plays no part in the arc mechanism except to serve as the positive electrode, and there is no reason why the arc mechanism should vary with a change in the anode material. Electrons which constitute the current flow must travel through the external circuit, into the cathode where they are emitted or neutralized, through the discharge where they are continually subject to the processes of ionization and recombination, and finally into the anode and external circuit.

Every electron active in the discharge between the electrodes must have a potential energy equal to its kinetic energy as a free conduction electron in the external circuit. Assuming that, since the cathode is the seat of the all-important arc phenomena, the potential energy under consideration is the electron-volt equivalent of the cathode work function, then the potential energy which every electron possesses upon arriving at the anode is the value of E_w for the cathode.

If the anode metal has a higher work function than the cathode metal, then the external circuit must furnish a component of voltage which will decrease the potential energy requirement at the anode surface to that of the cathode work function. This voltage serves to depress the Fermi level of the anode below that of the cathode so that the surface barriers are equal in height, thereby allowing the lower energy cathode region electrons to satisfy the potential requirements at the anode. With the arc in operation the anode is as many volts above the cathode in potential as is read on an electromagnetic voltmeter. But the potential difference indicated by the meter is that of the Fermi levels; the arc potential difference is the voltage read less the difference of the electrode work functions.

Consider now the situation opposite to the one just described where the anode work function is less than that of the cathode. To satisfy constant cathode potential requirements, the cathode Fermi level will be depressed, and thus, the electromagnetically measured voltage across the arc will be less than that which actually appears. The power source does not supply all the power needed by the arc, since the potential energy of the cathode electrons is in excess of that required when they arrive at the anode. This energy is available as kinetic energy throughout the discharge, and thus the source need supply less power than in the previous case. Therefore, the power evolved at the anode of an arc due to the incoming electrons is independent of the anode material.

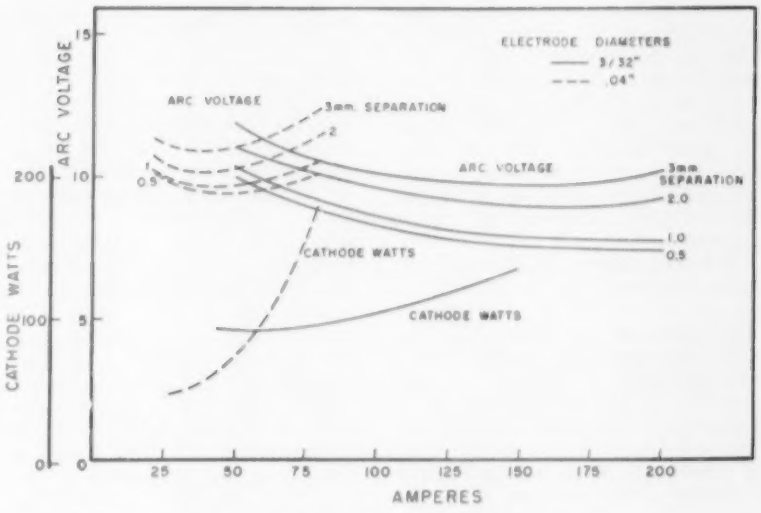

Fig. 4 Effect of cathode diameter on arc characteristics

Table 1—Work Functions

Metal	*Thermionic*	*Photoelectric*	*Reference*
Copper	4.33	...	21
	4.1	...	22
Nickel	5.03	...	24
	5.24	5.05–5.20	21
	5.0	...	22
Tungsten	4.52	...	21

To verify the hypothesis that the power evolved at the anode in an arc is independent of the anode work function, a critical experiment was performed using a nickel insert press fitted into the original copper plug. A small insert $^3/_4$ in. in diameter was used instead of an entire plug to obviate errors introduced by the low thermal and electrical conductivities of the nickel. Copper was originally chosen because of its excellent properties in this regard, and the copper plug easily withstood a 300-amp argon arc without surface destruction of consequence. Even at low currents, the nickel melted in a small area, not because its melting point is lower than that of copper, but due to its low thermal conductivity. This melting created a raised surface which invalidated small separation data. As can be seen from Table 1, the work function of nickel is different from that of copper by an amount, which when multiplied by a high current value would result in an "anode watts" difference, if one existed, detectable by the experimental apparatus.

From a survey of the data in Table 2 an estimate of both the experimental accuracy and the arc reproducibility may be obtained. Within both these limitations the results are that the power delivered to the anode is independent of the anode metal. Although the nickel arc burned at voltages higher than the copper arc by an amount approximately equal to the work function difference of the metals, despite the apparent increase of power for the nickel anode arc, none of the increase was reflected at the anode.

Cathode Phenomena

Tungsten was chosen for a cathode in these experiments not only because it is the material used in actual welding but because its extremely high melting point would permit copious thermionic emission and heavy currents without marked attrition of the tip. The melting and boiling temperatures of tungsten 3655 K and 6970 K, respectively, are the highest of all metals.[30] Yet it is very probable that under certain conditions the electron emission from the tungsten cathode is limited.

Table 2—Comparative Test—3 mm Separation

	Nickel		*Copper, Run 1*		*Copper, Run 2*	
Amperes	*V*	*Anode watts*	*V*	*Anode watts*	*V*	*Anode watts*
50	11.6	415	11.0	400	10.9	391
75	11.5	595	10.6	580	10.5	565
100	11.3	780	10.7	790	10.7	790
120	11.8	960	11.0	950	11.1	945

Figure 4 illustrates the marked effect of a variation in cathode diameter. The arc characteristic, including the negative and positive "resistance" values of the arc discharge, can be altered significantly by varying nothing but the cathode diameter. Thus, this same characteristic could be obtained and advantageously studied in the milliampere current range if the cathode diameter were small enough.

The heat conduction capabilities, resistive losses and radius of curvature of the tip of the cathode are intimate factors in the arc operation. From Fig. 4 one will note that at 40 amps the arc voltage is higher for the $^3/_{32}$ in. electrode than for the 0.04-in. electrode despite the fact that the resistive drop for the former is about $^1/_4$ that of the latter. For the $^3/_{32}$-in. electrode almost all the measured voltage appears across the arc since the voltage drop in this electrode may be neglected while several volts are lost along the 0.04-in. rod. At this current the 0.04-in. electrode is molten on the tip and the $^3/_{32}$-in. electrode is hardly incandescent. The higher voltage is attributable to the limited thermionic capabilities and the smaller curvature of the larger electrode as compared to the smaller one.

Any direct attempt to measure the cathode resistance destroys the major part of the resistance located at the tip. The resistance drop may be properly included in the total arc voltage and the accompanying losses considered as a part of the arc operation.

Although a rough estimate of the actual cathode resistance was computed from the relative extension observed for varying currents, no further attempt was made to measure the resistance since this quantity is to be included with every other indeterminable factor which concerns the cathode. With the aid of the tables in (Reference 32, Table 3 was derived.

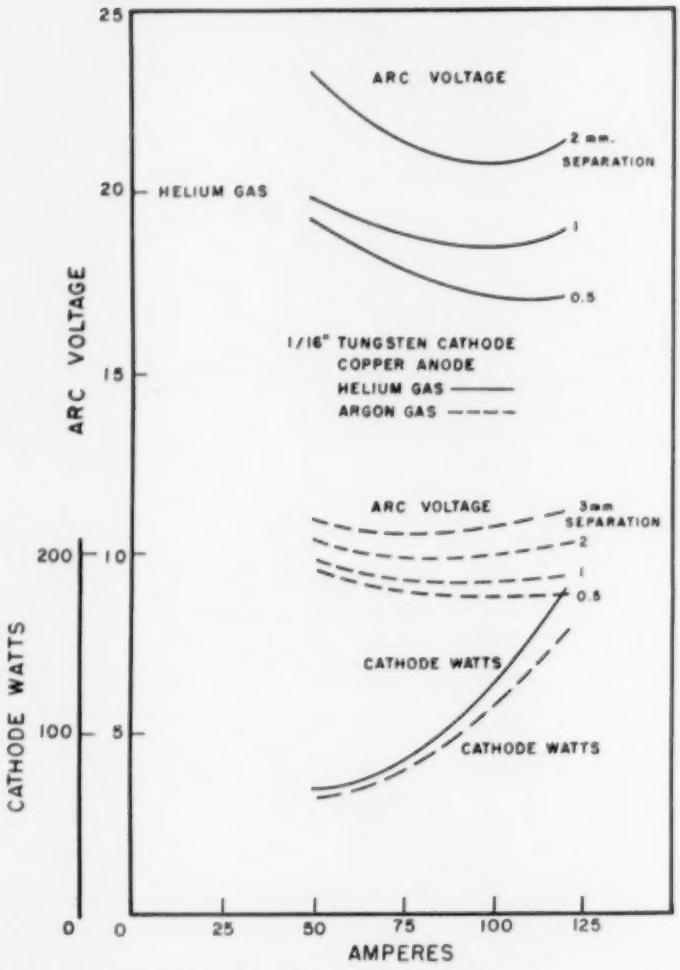

Fig. 5 Effect of shielding gas on arc characteristics

Table 3—$^3/_{32}$-in. Tungsten Cathode, Cold Length to Collet Jaw = 26.7 Mm

Amperes	*Extension*	*Resistance*	*IR drop*	*Average T*	*Tip T (K)*
20	0.0076	0.003	0.06	1800	3300
50	0.013	0.0047	0.25	2600	4900
100	0.018	0.0058	0.58	3100	5900
150	0.021	0.0065	0.97	3400	6500
200	0.023	0.0067	1.3	3500	6700

The upper current limit for each electrode was determined when bubbles formed at the tip and the arc was seen to wander over the cathode surface. These limits were:

0.04 in.	80 amp
$^1/_{16}$ in.	120 amp
$^3/_{32}$ in.	200 amp

As noted under "Experiment," times ranging from five to ten minutes were required to reach equilibrium at a new current setting; anode equilibrium simply depended upon the absorption of varying quantities of power by the anode plug and block. The process of establishing the cathode equilibrium was responsible for the greater part of the time lag, and the times could be extended by using a porcelain cup instead of the usual metal one. After equilibrium was established, the cathode tip resembled that in the first photograph of Fig. 6. The second photograph is the tip shape immediately after the current was adjusted to that of the first picture from a current of lower value, and the third shows the tip shape resulting from a change in current from a higher value to the first one. Figure 7 represents the cathode watts and the arc voltage as a function of cathode tip shape, for constant current.

The arc voltage is dependent upon the temperature, shape, and resultant electric field at the cathode. Equilibrium cannot be quickly established unless definite sinks are supplied for the electrode power. Arc characteristics, such as reported[16–18] are not indicative of the configuration used because no sinks were provided, and the experiments were short time, and in one case, instantaneous.

The power absorbed by the water at the cathode, called "cathode watts" can only be used to determine equilibrium and to set an upper limit for the I^2R loss in the electrode. Others working to evaluate thermionic emission constants found that long time variations in emission accompanied current changes in the test cathode.[32]

In Fig. 4, note that the total arc voltages for the two electrode diameters coincide at a current where the "cathode watts" curves intersect. All the electrode sizes have an intersection current when compared; these are:

$^1/_{32}$–0.04 in.	60 amp
$^3/_{32}$–$^1/_{16}$ in.	85 amp
$^1/_{16}$–0.04 in.	50 amp

Because everything other than the cathode diameter was maintained constant for the tests represented by the figures mentioned, these intersections must be more than mere coincidence. When the power absorbed by the water at the cathode is identical for two electrodes, different in diameter, the total arc voltage is the same for the same separation. This in spite of the fact that the voltage actually appearing between the electrode surfaces, the heat conduction ability of the cathode, the radiation, the numbers of electrons emitted and of the ions impinging and the conduction to the gas are all different.

When a certain power is absorbed by the cathode sink at a given separation from the "cathode region," the current through the arc and the total power input to the arc will be identical regardless of cathode diameter.

Motion of the "cathode spot" over the cathode surface has been observed by many, particularly for the lower boiling point metals such as copper. Some have attempted to arrest this motion by pointing the cathode or employing magnetic fields in order to improve the reproducibility of their data.[16] This motion occurs on a tungsten cathode when its surface reaches the boiling temperature so the phenomenon is not limited to the low-boiling point metals.

When the cathode spot wanders, it was observed that the arc characteristic has already assumed a positive slope. If the arc operates in a column whose cross-sectional area is on the order of 0.1 mm, then at a current corresponding to the boiling point of the cathode tip all the electrons are emitted into the discharges that are available from that area. The electron current must be limited for all higher values of arc current. Sputtering of the cathode is pronounced when it boils, and the authors believe that the spot wanders because the arc strips a small area not only of electrons but also of material so that a subsurface layer at lower temperature is exposed. This layer is not capable of the required emission and thus the spot moves on to anchor elsewhere for a short time. Wandering of the cathode spot also has been observed at lower currents where some believe thermionic emission has not started. An explanation of this action might be that thermionic emission does start with a resultant fall in the total arc voltage because of the more plentiful supply of electrons. Since the current is low, the cathode will not have stored up enough heat, and the thermionic emission at the active spot will decrease when less power is delivered by the fewer incoming ions. The discharge will then revert to its former state and seek a new anchoring spot which is at a higher temperature than the spot just vacated.

What happens when copper is used as a cathode? Apparently thermionic emission is limited by the low temperatures available, poor heat storage of the metal, and small heat generation due to resistive losses. As a result, a high voltage is required to supply the necessary anode electrons by means of increased ionization. If the source can supply this voltage, then the copper is quickly raised locally to its boiling point, and the cathode spot will wander.

When the cathode is of large size, or if it is an infinite sink, then the initiation and subsequent maintenance of a thermionic arc might prove impossible. Thus, low-current stability can be achieved by pointing the cathode.[18] The electric field intensity is increased and the heat transfer ability is limited, thereby allowing the cathode tip to reach the requisite temperature. To test this, a $^1/_8$-in. cathode was pointed sharply, and it was found to operate successfully at 30 amp or less, a current much lower than that required for stable operation when naturally rounded. Upon raising the current slightly, the tip easily boiled and bright pieces of tungsten were shot out. These could be seen to condense on the cathode at a relatively cold portion of the electrode behind the active tip. The tungsten condenses in the form of jagged spires. Although this effect is easily obtained in argon, it was thought to be restricted to the higher voltage helium arc and that the deposited material originated at the anode, which of course it does not.

Apparently the sputtered tungsten acquires a charge upon leaving the cathode, and the field turns the particles back toward the cathode, thus explaining why, especially at currents lower than those which produce boiling, no tungsten is present in the discharge. The electrodes in this test were allowed to assume a tip shape, as shown in the figures, which at equilibrium must be such as to satisfy the resultant of surface tension, gravity, and field forces. Then the electrodes gave results indicative of their individual diameters, and the artificiality of prepointing, which would have obscured the desired effect, was not employed.

Arc Mechanism

The purpose here is not to detail the fundamental processes of discharges such as ionization, excitation, recombination or plasma maintenance since excellent accounts of gas-discharge theory are to be found in many books and papers. Theories are ever-changing, as witness the failure of the Townsend Spark Breakdown in certain instances and the subsequent development of streamer theory. Current information and numerous references will be found in Meek and Craggs[21] and Dow.[17] This portion of the paper is devoted to an explanation of the characteristics of this particular electric arc based upon experimental data.

When considering the arc and its gaseous column, it is important to realize that a steady flow, equilibrium state does not imply thermal equilibrium. Energy is flowing at all times from the arc to its cool surroundings at the electrodes and into the flowing shield gas. Of course this energy flow is accompanied by a temperature gradient and under equilibrium conditions a temperature difference cannot exist. Certain atomic processes are, however, approximated closely, when they occur in steady-flow situations, by relations derived for strict thermodynamic equilibrium.

The perfect gas laws assume that the particles exert no forces upon one another except when collisions occur, and at sufficiently high temperatures and low densities all gases tend toward "perfection." Although the interactions between the charged particles of an ionized gas produce deviations from the perfect gas law, the corrections amount to only a few percent, and thus the important relationships of statistical mechanics can be advantageously employed.[35]

The spectroscope is the primary means for analysis of matter in its gaseous state; temperature distribution and relative particle densities of electric arcs can be determined with the aid of quantitative spectroscopic data. These exacting analyses, however, are made for a *particular* arc configuration and do not generally apply, but the results obtained are of interest to the field of high-temperature physics.[36] Herewith will be presented a gross mechanism which may well fit all thermionic emission arcs.

All the essential arc processes are included in the region which involves not only the gas adjacent to the cathode but the cathode electrode itself. This "cathode region" is responsible for the production of the total electron current at the anode, and once the region is fully developed, its losses are fixed. The reader can arrive at the same conclusion by noting, in Figs. 4 and 5 that cathode watts is independent of separation. As was previously remarked, cathode watts is not the power evolved at the cathode, but it is a direct indication of cathode equilibrium. When the cathode is separated from the anode, the cathode region in its entirety accompanies the

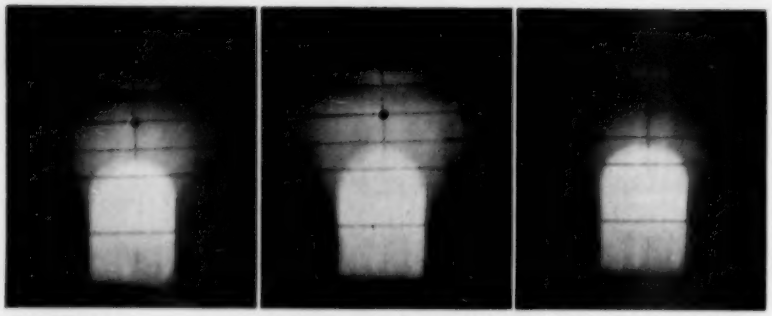

I at equilibrium | II voltage greater than equilibrium voltage | III voltage less than equilibrium voltage

Fig. 6 Cathode tip shape

cathode, and a plasma is created to fill the gap. An important exception to these statements occurs when the separation is so small that the anode enters the cathode region and thereby introduces to that region an additional loss. Those familiar with probe theory will recognize this action as being the same as the reaction of any discharge to the insertion of a probe. On closing the separation at a constant current the arc voltage reaches a minimum and then rises to supply the additional losses demanded by the anode intrusion (Fig. 8). Thus the traditional procedure of extrapolating the voltage-separation curves in Fig. 8 to the voltage axis does not give the correct arc voltage for small separation.[1,7,8,21]

When fully established, the cathode region of an electric arc is independent of separation. Once the separation has progressed to a value larger than the "minimum" and the anode no longer affects the cathode region, a plasma region is created to fill the gap. Since the plasma need only supply the electrons lost from the cathode region while traversing the gap to the anode, its temperatures are much lower than those of the cathode region and a small voltage gradient appears in it. Thus, the greater part of the measured arc voltage, for small separations at least, is developed across the cathode region. An excellent discussion of plasma energy requirements, equilibrium and cross section can be found in Dow.[17] The plasma potential gradient is just large enough to cause a power introduction into the plasma sufficient to raise the gas temperature to a point where there will be enough ionizing collisions to replace the charged particles lost at the plasma lateral boundaries. At a certain value of plasma diameter the losses are minimum; when the diameter is less, losses are more because of an increase in diffusion, and for larger diameter, losses increase because more area is available for thermal conduction (Reference 13, p. 377). Detailed consideration of arc diameter must include the constricting action of the charged particles when they represent parallel strands of current.

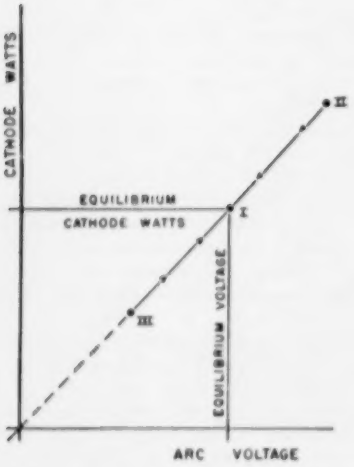

Fig. 7 Representation of cathode watts as a function of arc voltage while equilibrium is being obtained. (Roman numerals refer to cathode shapes in Fig. 6)

To illustrate the use of the figures, a complete rundown on a particular situation is presented, based on the data given in Fig. 4. The total arc voltage is that read by an electromagnetic voltmeter and is not a corrected voltage to take into account the electrode work functions as explained under "Anode Phenomena." Such a correction would only alter the values of the total power and the undistributed power loss in the cathode region; it would constitute an additive (or subtractive) correction. Since the values of the electrode work functions are only known (approximately) at temperatures below melting, then the actual voltage between the electrodes cannot be computed for the arc because the cathode is nearly always molten if not boiling. The numbers shown in the analysis of Fig. 9 are obtained directly from the data curves.

Figure 9 is the key to the whole mechanism. At the top of the page, the cathode and anode of the arc are shown at the "minimum" separation, 0.5 mm. The total measured arc voltage and the total arc input power are then expended in the cathode region, which includes the cathode electrode. Experimentally, it is found that 380 w of the total 570 w are evolved at the anode by means of the processes previously discussed; a known 98 w are absorbed by the cathode water. Therefore, 92 w are the unaccounted cathode region losses, and a portion of these 92 w is expended in ionizing the gas, the remainder being losses to the surrounding gas by thermal conduction and radiation. In the second diagram on Fig. 9, the separation has been doubled, thus introducing a plasma region. The cathode region remains as before, but the increase in arc voltage, 0.4 v, appears across the plasma. Power consumption in the plasma is then $0.4 \times 60 \cong 25$ w. Of these 25 w, 20 are found as an increase of power evolved at the anode, and the rest are the plasma losses. The last two diagrams illustrate the same trends.

Although it may appear that the plasma temperature increases without limit, the reader will note that the proportion of plasma power delivered to the anode decreases as the separation grows larger, indicating that the plasma losses rise rapidly as it lengthens. The values on Fig. 9 are only approximate, but they fall well within the range given by experimental error. According to the figure, the real cathode region length is not 0.5 mm but 0.4 mm, as the following proportion indicates:

$$\frac{0.6 \text{ mm}}{25 \text{ w}} = \frac{1.6 \text{ mm}}{65 \text{ w}} = \frac{2.6 \text{ mm}}{110 \text{ w}}$$

In the first diagram of Fig. 9, then, some plasma exists, and the minimum separation is closely 0.4 mm.

Figure 8 shows that the minimum voltage for lower currents is less pronounced than for higher ones, probably because losses introduced by the insertion of the anode into the cathode region are proportionately less; a further inspection of this figure will indicate that the higher current arcs have proportionately more losses with increase of separation than the lower current arcs as evidenced by the curve intersections. This effect is also shown in Fig. 4. Note that the volt-ampere curves in these figures are essentially parallel at low currents and that they separate at higher currents, the larger separation curves upturning before the small separation curves. Therefore, plasma losses are one of the factors which shape the arc characteristic, and since the cathode region remains constant at a given current, the plasma losses dominate the arc operation at large separations.

A comparison of the curves for anode watts in Fig. 10 shows that the power transferred to the anode is dependent only upon the current and the separation. This implies that the plasma temperature at the anode surface depends only upon the current and separation, and is independent of the cathode diameter and the accompanying arc voltage. For example at 75 amp and 3 mm separation:

Electrode diam	*Anode watts*	*Total power*	*Arc voltage*
0.04 in.	580	950	12.0
1/16 in.	580	795	10.6
5/32 in.	600	790	10.5

When in this experiment the flow rate of the shield gas was varied, different arc characteristics were obtained, necessitating a choice of a standard flow rate, as previously explained. The gas cools the electrodes and the discharge gas electrode—copper anode, 100 amp, 2-mm separation column, and thus the quantity flowing determines how much power the gas removes. As is to be expected, an increased flow at constant current will result in a higher arc voltage, as can be seen from Table 4.

Table 4

Argon gas—1/32-in. tungsten

Flow rate, cfh	*Arc voltage*	*Arc power*	*Anode watts*	*Cathode heat*
15	9.24	924	695	97
30	9.39	939	700	90
45	9.44	944	690	86

Ions charged singly and perhaps doubly are impinging at the cathode surface. Their arrival rates depend upon their temperature and the active cathode area. But the total external circuit current is electronic, while at the cathode a balance is obtained between the emitted electrons and the incoming ions. Evidently this balance is one of those factors in the arc which determines the voltage appearing across the arc for a given current flow. Compare two cathode diameters for the same current, as in Fig. 4. The smaller one is at a higher temperature and can emit more electrons than the larger electrode. Therefore, the current of the larger cathode is composed of more ions than that of the smaller electrode. The larger electrode arc voltage is higher than the smaller electrode arc voltage because more electrons must be supplied by ionization in the former situation than in the latter.

Thus, the cathode emission possibilities play a most important role in shaping the arc characteristic. At the low currents a higher voltage is necessary to effect the requisite ionization. As the current increases and the cathode temperature increases, more thermionic electrons are available and the voltage drops. What happens when the electrode melts and then boils? It must be that the emission becomes limited once again, and the voltage rises on a positive slope. Of course other factors are involved. The cathode surface condition is the predominant one. The cathode region produces sufficient charges to supply the anode electronic current and to accommodate its losses. If the separation is more than the minimum, then a plasma region, which constitutes a conduction path only, is formed. Since power is lost and charges diffused out, additional power must be supplied to the plasma to retain the total electron anode current. Every process within the arc must have a limitation. At high currents, then, the arc becomes a linear circuit element of positive resistance.

Thus, within the arc are numerous factors interacting in a most intricate way to achieve the final balance that is indicated on ammeter and voltmeter.

Those who have attempted to write equations for arc characteristics have failed to produce a relation which covers the entire range of operation or which has any bearing on the particular configuration used.[5,15,26] If an equation *could* be found, it would refer only to a certain arc and would not be of general application. All one need do to alter the arc characteristics would be to change the component materials, or merely to vary the cathode diameter or shape or length, change the cooling at the electrode supports, or change the gas flow rate.

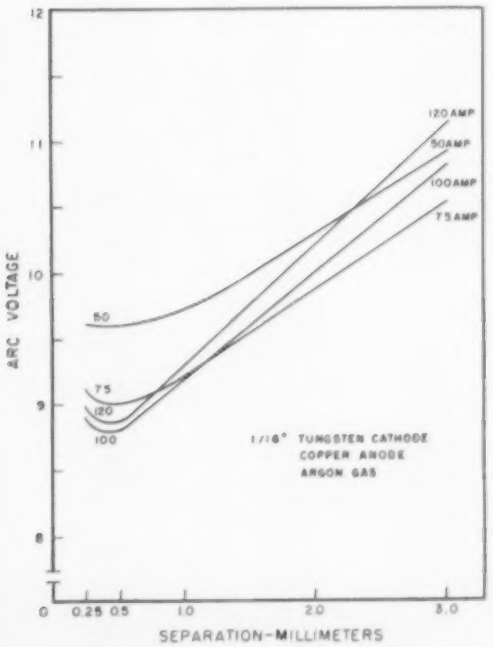

Fig. 8 Effect of separation on arc voltage

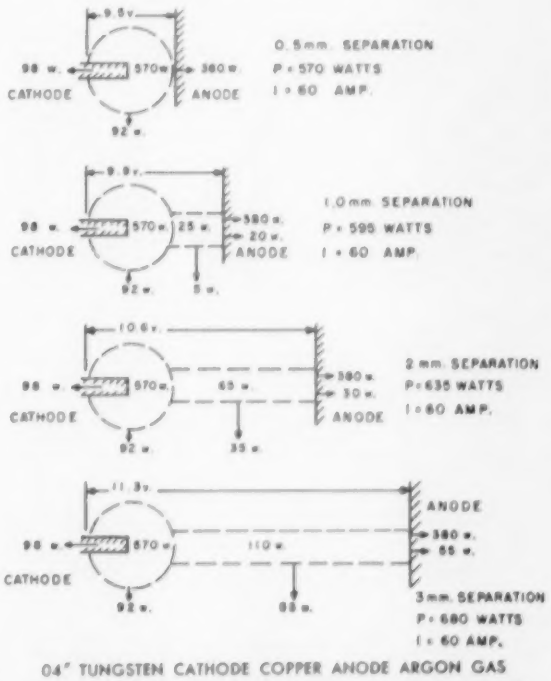

Fig. 9 Formation of the plasma region and the resulting power flow

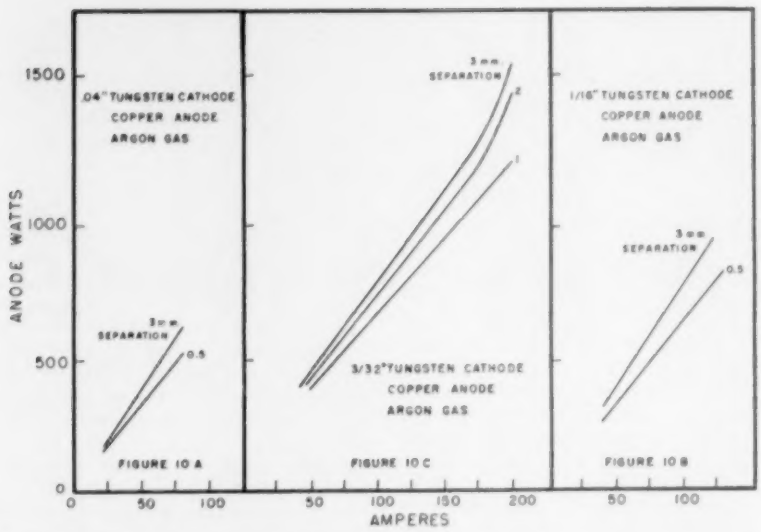

Fig. 10 Results of the measurement of anode watts for various separations cathode diameters, and arc currents

Applications to Welding

Metals and alloys that are welded by means of the arc described in this paper are stainless steel, brass alloys, silicon and dioxidized copper, silver, cast iron, low- and high-carbon steels, and nickel. The inert-gas-shielded arc produces a weld which sometimes needs no finishing.

If the weld efficiency were defined as the ratio of the power supplied to the arc to the power delivered to the workpiece, then for all practical purposes the efficiency remains constant, independent of separation. The efficiency has a value of approximately 74% for argon shielding and 85% for helium shielding. The total power input to a helium arc is twice that for a comparable argon arc and the power to the anode is proportionately more than double that of the argon arc. One of the main objections to the helium arc is its relative sensitivity to separation variations, making hand welding difficult.

An automatic welding procedure might well utilize the minimum separation if maximum economy is desired. The melting rate of the workpiece is, for a given current, dependent only upon the thickness of the metal and its thermal conductivity, while the arc delivers the same power to the work regardless of the work metal.

If the weld is to have no tungsten inclusions, the maximum current for each electrode size must be carefully ascertained so that the electrode will suffer no attrition due to boiling and sputtering.

References

1. Finkelnburg, W., and Busz, G., "Über einen Hochstrombogen sehr hoher Temperatur und extrem kleiner Brennspannung," *Die Naturwissenschaften*, **40** (21), 550 (1953).
2. Finkelnburg, W., and Busz, G., *Zeitschrift für Physik*, **138**, 212 (1954).
3. Maecker, H., "Elektronendichte und Temperatur in der Saule des Hochstromkohlebogens," *Ibid.*, **136**, 119 (1953).
4. Elenbaas, W., *The High Pressure Mercury Vapour Discharge*, Interscience Publishers, New York (1951).
5. Gillette, R., and Breymeier, R., "Some Research Techniques for Studying Arcs in Inert Gases," THE WELDING JOURNAL, Research Suppl., **30** (3), 146-s (1951).
6. Skeats and Schuck, "Measurement of Current Density in the High Current Arc," *AIEE Trans.*, **73**, part 3, 848 (August 1954).
7. Kouwenhoven, W. B., and Jones, T., "Arc Phenomena with Electrodes Moving at High Speed," *Ibid.*, Research Suppl., **30** (3), 146-s (1951).
8. Skolnik, M., and Jones, T., "Characteristics of the High Current Tungsten Arc in Argon, Helium, and Their Mixtures," *J. Appl. Phys.*, **23** (6), 643 (1952).
9. Dzimianski, J., and Jones, T., "Characteristics of the High Current Argon Arc with Various Electrode Materials," *AIEE Trans.*, 665 (January 1955).
10. Alexander, P., "The Calorimetric Study of the Arc," *J. AIEE*, 138 (February 1930).
11. Ahrens, L. H., "Spectrochemical Analysis," Addison-Wesley Press, Cambridge, Mass. (1950).
12. Rupert, C. S., *J. Op. Soc.*, **42**, (9) 684 (1952).
13. Vallee, B., and Adelstein, S., "The Effects of Argon and Argon-Helium Mixtures on the Direct Current Arc," *J. Opt. Soc.*, **42** (5), 295 (1952).
14. Vallee, B., and Peattie, R., "Volatilization Rates of Elements in the Helium Direct Current Arc," *Anal. Chem.*, **24** (March 1952).
15. Vallee, Reimer, and Loofbourow, "The Influence of Argon, Helium, Oxygen and Carbon Dioxide on Emission Spectra in the D. C. Arc," *J. Opt. Soc.*, **40** (11), 803 (1950).
16. Stephens, W., Gilbert, H., and Beall, R., "Consumable Electrode Arc Melting of Zirconium Metal." Paper presented before the Eighth Western Metal Congress, Los Angeles, Calif., March 23, 1953.
17. Dow, W. G., Fundamentals of Engineering Electronics, John Wiley & Sons, Inc., New York, 2nd ed. (1952).
18. Becker, J. A., "Thermionic Emission and Adsorption," *Rev. Mod. Phys.* **7**, (2) 95 (1935).
19. Millman and Seely, Electronics, McGraw-Hill Book Co., New York (1951).
20. Beck, A. H. W., Thermionic Valves, Cambridge Univ. Press (1953).
21. Loeb, L. B., Fundamental Process of Electrical Discharge in Gases, John Wiley & Sons, Inc., New York (1939).
22. Zeluff, V., and Markus, J., Electronics Manual for Radio Engineers, McGraw-Hill Book Co., New York, 665 (1949).
23. Maxfield and Benedict, Theory of Gaseous Conduction and Electronics, McGraw-Hill Book Co., New York (1941).
24. Aller, L. H., Astrophysics, Ronald Press, New York (1953).
25. Chaffee, E. L., Theory of Thermionic Vacuum Tubes, McGraw-Hill Book Co., New York (1933).
26. Mayer and Mayer, Statistical Mechanics, John Wiley & Sons, Inc., New York (1940).
27. Cobine, J. D., Gaseous Conductors, McGraw-Hill Book Co., New York (1941).
28. Davisson and Germer, *Phys. Rev.*, **24**, 666 (1924).
29. Compton, K. T., "On the Theory of the Mercury Arc," *Ibid.*, **37**, 1077 (1931).
30. Doan, G. E., "Cathode Energy of the Iron Arc," *Jour. AIEE*, **49**, 453 (1930).
31. Bol'shov and Bobretsov, "Thermionic Emission from Copper at the Melting Point," *Compt. Rend. Acad. Sci. (URSS)*, **98**, 193 (1954).
32. Smithells, C. J., Tungsten, Chemical Publishing Co., New York (1953).
33. vanVoorhis, C. C., *Phys. Rev.*, **30**, 318 (1927).
34. Meek and Craggs, Electrical Breakdown of Gases, Oxford, Clarendon Press (1953).
35. Finkelnburg, W., *J. Appl. Phys.*, **20**, 468 (1949).
36. Nottingham, W. B., *Phys. Rev.*, **28**, 764 (1926).
37. Ayrton, H., The Electric Arc, D. Van Nostrand Co., New York (1902).
38. Bowie, R. M., "This Matter of Contact Potential," *Proc. I.R.E.*, **24**, 1501 (1936).